5-2005

A Method to Calculate the Femoro-Polyethylene Contact Pressures in Total Knee Arthroplasty In-Vivo

Adrija Sharma
University of Tennessee - Knoxville

To the Graduate Council:

I am submitting herewith a thesis written by Adrija Sharma entitled "A Method to Calculate the Femoro-Polyethylene Contact Pressures in Total Knee Arthroplasty In-Vivo." I have examined the final electronic copy of this thesis for form and content and recommend that it be accepted in partial fulfillment of the requirements for the degree of Master of Science, with a major in Engineering Science.

Richard D. Komistek, Major Professor

We have read this thesis and recommend its acceptance:

Mohamed R. Mahfouz, William R. Hamel

Accepted for the Council:
Carolyn R. Hodges

Vice Provost and Dean of the Graduate School

(Original signatures are on file with official student records.)

To The Graduate Council:

I am submitting herewith a thesis written by Adrija Sharma entitled "A method to Calculate the Femoro-polyethylene Contact Pressures in Total Knee Arthroplasty In-Vivo." I have examined the final electronic copy of the thesis for form and content and recommend that it be accepted in partial fulfillment of the requirements for the degree of Master of Science, with a major in Engineering Science.

Richard D. Komistek

Major Professor

We have read this thesis and

recommend its acceptance:

Mohamed R. Mahfouz

William R. Hamel

Accepted for the Council:

Anne Mayhew

Vice Chancellor and Dean of
Graduate Studies

(Original signatures are on file with official student records.)

A METHOD TO CALCULATE THE FEMORO-POLYETHYLENE CONTACT PRESSURES IN TOTAL KNEE ARTHROPLASTY IN-VIVO

A Thesis
Presentation for the
Master of Science Degree
The University of Tennessee, Knoxville

Adrija Sharma
May 2005

Dedication

This thesis is dedicated to my parents Kamal Sharma and Debjani Sharma, great role models and friends, and my brother, Nirmalya Sharma, and the rest of the family, for always believing in me, inspiring me, and encouraging me to reach higher in order to achieve my goals.

Acknowledgements

I would like to thank all those who helped me in the pursuit of this Master of Science Degree in Engineering Science. I would like to thank Dr. Komistek for educating me and guiding me throughout this entire endeavor. I would also like to thank Dr. Mahfouz and Dr. Hamel for giving me invaluable insights and also serving as members on my committee. A special thanks to Dr. Ranawat and the Knee Society for funding this project without which this would not have been possible. I would also like to thank Dr. Dennis for letting me use the data on his patients.

Finally, I would like to thank my colleagues and other lab members, whose suggestions and help has been invaluable in completing this task.

Abstract

This study deals with the development of a computational method that generates the in-vivo contact pressures on the superior side of the polyethylene in total knee arthroplasty (TKA) based on in-vivo kinematic data. Ten clinically successful subjects (five fixed and five mobile bearing TKA), having Hospital for Special Surgery (HSS) knee scores greater than 90, were analyzed under fluoroscopic surveillance while performing a weight-bearing deep knee bend. 3D in-vivo contact positions and kinematics, determined using a 2D to 3D registration technique, and soft tissue locations derived from literature were entered into a 3D inverse dynamics mathematical model to determine the in-vivo bearing contact forces. The contact areas were obtained by assembling the 3D CAD models of the components and measuring the interference area between them. The contact pressure was calculated by dividing the contact forces with the contact areas. For subjects with the mobile bearing TKA the average lateral contact forces varied from 0.34BW to 0.91BW and the average medial contact forces varied from 0.5BW to 2.7BW from full extension to full flexion. In subjects with the fixed bearing TKA the average contact forces ranged from 0.43BW to 0.92BW and from 1.04BW to 2.73BW on the lateral and medial sides respectively from full extension to full flexion. The contact areas for the mobile bearing TKA was always higher than the fixed bearing TKA. The average medial contact pressures ranged from 5.49MPa to 25.7MPa and from 12.8MPa to 34.38MPa for the mobile and fixed bearing TKA respectively. The average lateral contact pressures varied 3.08MPa to 18.83MPa and from 3.71MPa to 18.36MPa for the mobile and fixed bearing TKA respectively. This study reveals that the in-vivo contact forces and pressures are greater for the medial condyle than the lateral condyle, which is similar to polyethylene retrievals that demonstrate greater posterior-medial wear. Also the ability of the polyethylene insert, in mobile bearing TKA, to rotate helps in maintaining higher femoro-polyethylene contact areas resulting in lesser contact pressures compared to the fixed bearing TKA.

Table of Contents

List of Tables

List of Figures

CHAPTER 6 DISCUSSION - ANALYSIS OF RESULTS

APPENDIX A

APPENDIX C

APPENDIX D

APPENDIX E

Abbreviations and Acronyms

ACL	=	Anterior Cruciate Ligament
PCL	=	Posterior Cruciate Ligament
TKA	=	Total Knee Arthroplasty
TKAs	=	Total Knee Arthroplasties
BW	=	Body Weight
AP	=	Antero-Posterior
ML	=	Medio-Lateral
SI	=	Superior-Inferior
CR	=	Cruciate Retaining
PCR	=	PCL Retaining
PCS	=	PCL Sacrificing
PS	=	Posterior Stabilized
RSA	=	Roentgen Stereophotogrammetric Analysis
FEA	=	Finite Element Analysis
UHMWPE	=	Ultra High Molecular Weight Polyethylene

Chapter 1

Background

1.1 Anatomy of the Knee

The knee is the largest and the most complex joint in the human body, serving as the connection between the upper and the lower leg and controlling the relative motion between the two structures. It is defined as a diarthrodial or synovial joint. This means that it is a freely moving joint, lubricated by synovial fluid and the whole structure is enclosed in a joint capsule.

1.1.1 Bone Structure

The knee joint is made up of three bones – the femur (thigh bone), the tibia (shin bone) and the patella (knee cap) (Figure 1-1). There is one more bone in the lower leg, the fibula, but it does not form a part of the knee joint. However, it does serve as an attachment site for soft tissues associated with the knee.

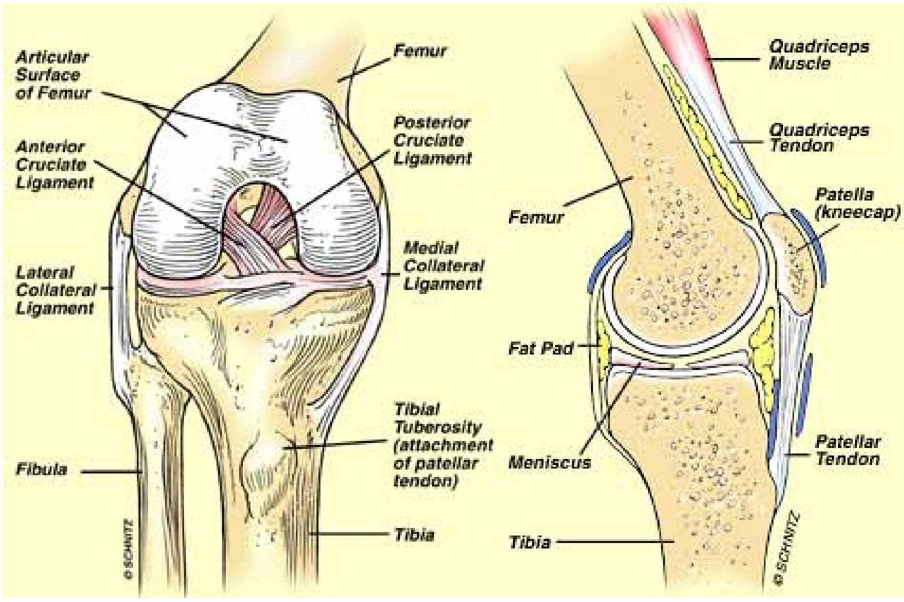

Figure 1-1: (Left) Anterior View, (Right) Medial View of the Normal Knee (Ahlfeld Sports Medicine Orthopaedic Centre, 2005).

The femur and the tibia are the two longest bones in the body and form the femoro-tibial articulation. The inferior end of the femur has two convex shaped condyles which are positioned medially and laterally and are separated by the intercondylar notch in the posterior direction and the trochlear groove in the anterior direction. The condyles have varying radii of curvatures when moving in the antero-posterior direction. Femoro-tibial articulation is achieved by the contact of the femoral condyles with shallow concave shaped condyles present in the tibia. The femoro-tibial articulation carries the maximum load passing through the knee joint. To accommodate this, the femur and tibia is made of hard cortical bone on the outside and soft and more compressible cancellous bone on the inside.

The patella is a sesamoid bone (formed completely within the structure of a tendon). The patello-femoral articulation is achieved by the contact of the patella on the medial and lateral condyles of the femur just adjacent to the trochlear groove, the place where the patella is located. The function of the patella is to increase the lever arm of the quadriceps extensor mechanism and to provide antero-posterior constraint for the femur.

1.1.2 Articular Cartilage and Meniscus

Cartilage is a collagen based soft viscoelastic material and is attached to the end of the knee joint bones where articulation occurs (Figure 1-1). This makes the mating surfaces almost frictionless and helps in smooth motion in the knee with less wear and tear. This is also facilitated by the viscous, protein filled, synovial fluid which is filled up in the joint capsule and acts as the natural lubricant.

Between the articular cartilage coated ends of the femur and tibia are two crescent shaped pieces of fibrocartilage, called the meniscus (Figure 1-1). Due to their wedge-like shape, which deepens to cup-shape for the femur to articulate and move, they increase the contact area of the bones. Thus they serve to cushion the joint against impact type loads and distribute the compressive and shear loads across vulnerable articular cartilage surfaces. They also contribute in overall joint stability.

1.1.3 Ligamentous Structures

Ligaments are fibrous tissues, carrying only tensile loads, connected from bone to bone which help in stabilization of the joint. There are two main groups of ligaments that play a significant role in the control and stabilization of the knee joint – the collateral ligaments and the cruciate ligaments (Figure 1-1).

The collateral ligaments attach at the sides of the joint laterally and medially. The lateral collateral ligament is a round cord-like ligament that attaches on the outer side of the lateral femoral condyles and on the superior end of the fibula. The medial collateral ligament is a flat band like ligament attached to the outer side of the medial condyle of the femur and extends downwards to attach on the tibia on the antero-medial aspect. The medial and lateral collateral ligaments assist in supporting the knee during abduction-adduction (valgus-varus) motion.

The cruciate ligaments are found at the centre of the knee within the joint space and are so named because the two ligaments in this group cross each other. The anterior cruciate ligament (ACL) inserts on the anterior end between the tibial condyles and on the medial side of the femoral lateral condyle. The posterior cruciate ligament (PCL) is attached more laterally on the tibia compared to the ACL and inserts on the medial side of the medial femoral condyle. The PCL is located posteriorly compared to the ACL. These ligaments are flat in cross-section and are twisted between their insertion points. These ligaments stabilize the knee against antero-posterior translations as well as the medial and lateral rotations of the tibia relative to the femur. The ACL restrains anterior subluxation while the PCL restrains posterior subluxation of the tibia.

1.1.4 Muscle Structures

Muscles are the motion generators in the human body and connect to the bone through the tendons. Force is generated in them during the extension of the fibers. The major muscle groups in the upper leg are the quadriceps and the hamstrings. In the lower leg the largest muscle group is the gastrocnemius (Figure 1-2). All these muscles are biarticulate, that is, they work on more than one joint. However, the level of activity for one joint is much more than the other joint.

The quadriceps, technically known as, the quadriceps femoris muscle group is made up of four muscles located anteriorly in the upper leg - rectus femoris, vastus laterlis, vastus medialis and vastus intermedius. Except for the rectus femoris, which inserts in the ilium (one of the bones making the pelvis), all the muscles insert on the femur. All the four muscles coalesce to form the quadriceps tendon. The quadriceps tendon, containing the patella bone, attaches the quadriceps muscle group to the anterior tibial bone and is known as the patellar tendon in the region between the patella and the tibia. The quadriceps muscles are the primary extensors of the knee.

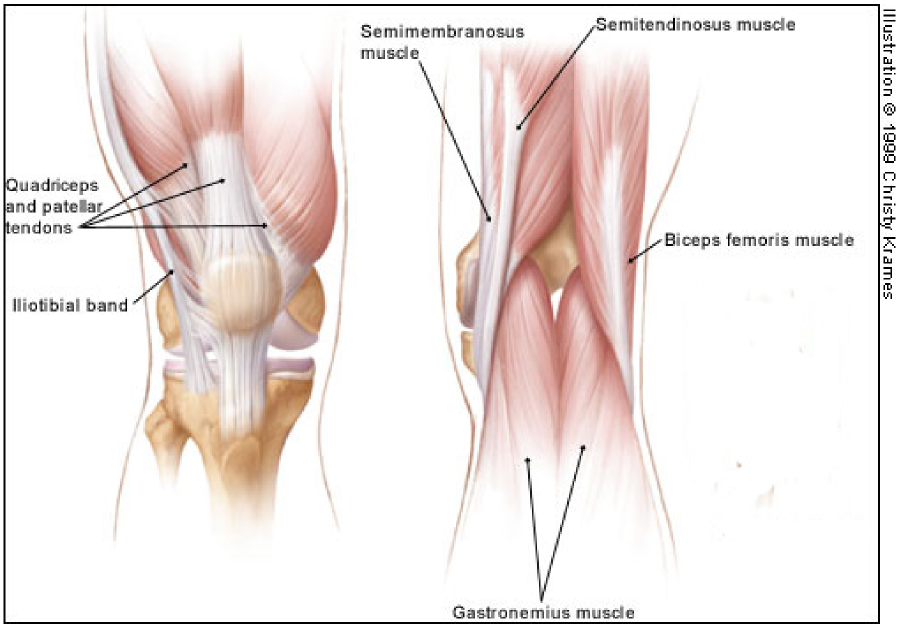

Figure 1-2: Major Muscles used in the Flexion and Extension of the Knee (Modified from American Academy of Family Physicians, 2005).

The hamstring muscle group is situated posteriorly on the upper leg and is made up of three separate muscles – biceps femoris (lateral side), semitendinosus and semimembranosus (medial side). Other medial thigh muscles, the gracilis, the pectinius and the adductor longus/ brevis/ magnus are not technically part of the hamstring group. All the hamstring muscles have one of their insertion points on the ischium (one of the bones making the pelvis) while the other insertion points lie on the fibula and femur (for biceps femoris) and on the tibia (for semitendinosus and semimembranosus). The hamstring muscles are the primary flexors of the leg.

The gastrocnemius muscle group, commonly known as the calf muscles, is located posteriorly in the lower leg and is made of three muscles - soleus, medial gastrocnemius and lateral gastrocnemius. While the soleus inserts in the fibula and the tibia, the medial and lateral gastrocnemius muscles insert on the posterior aspect of the femoral condyles. All the three muscles coalesce to from the Archilles tendon, which is attached to the back of the heel. Though these muscles primarily function in extending the heel, they also assist in the flexion of the leg.

1.2 Osteoarthritis in the Knee

Osteoarthritis is a degenerative joint disease caused due to the break down of the articular cartilage. Over a period of time, as the articular cartilages are worn away, bone to bone contact sets in. This leads to excessive joint pain and causes roughening and even wearing away of the bone articulation. Bony protrusions, known as osteophytes may also appear at the edge of the bone (Figure 1-3). This results in significant pain, inflammation and a loss of function and mobility. Though ideally osteoarthritis should develop during old age, however, early onset of the disease is accelerated by injuries, trauma and bone deformities. Treatments such as weight loss, braces, orthotics, steroid injections and physical therapy can alleviate the symptoms associated with mild to medium level of osteoarthritis.

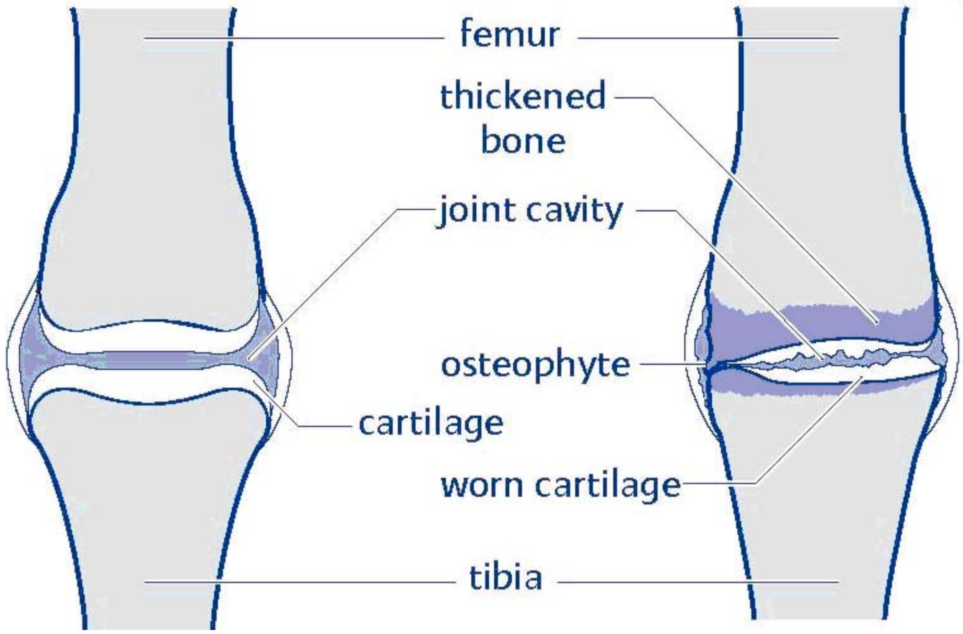

Figure 1-3: Deterioration in the Knee caused by Osteoarthritis (Modified from New York Online Access to Health, BUPA, 2005).

However, in severe cases the only choice remains is to undergo a knee.replacement surgery. Knee replacement surgery consists of the replacing the degenerated contact surfaces at the knee. If the arthritis affects only one side of the joint then it is replaced with a unicondylar knee replacement which resurfaces only the single damaged femoral and tibial condyle. If the arthritis affects the whole joint then a total knee arthroplasty (TKA) is used. Apart from restructuring both the femoral and tibial condyles, this type of replacement also has a component that fits with the patella.

1.3 Total Knee Replacements

Osteoarthritis can be extremely disabling, leading to discomfort and often excruciating pain. The artificial orthopedic implants are designed so as to provide pain relief and allow a subject with severe osteoarthritis to return to a normal daily life. The first attempt to design a total knee arthroplasty (Figure 1-4) was around 60 years ago. With more studies concentrating in this area and with greater knowledge about normal knee kinematics, TKA designs have transformed from highly constrained hinged type and highly conforming designs to moderately conforming designs.

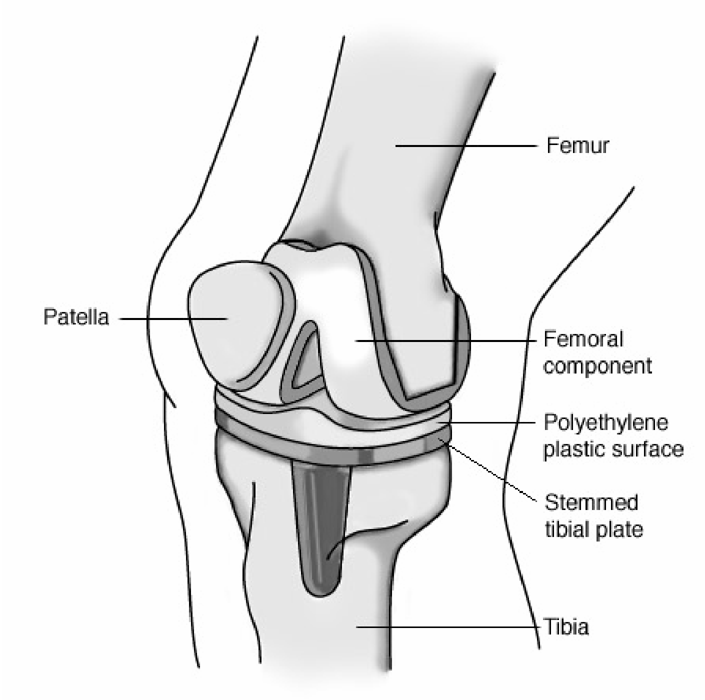

Figure 1-4: Simplified Image of TKA (New York Online Access to Health, AAOS, 2005).

A modern TKA design consists of four components. Two components, attached separately to the femur and the tibia, are made of high strength, wear resistant and biocompatible titanium or cobalt chromium alloys. The other two components are made of biocompatible and wear resistant crosslinked ultra high molecular weight polyethylene (UHMWPE). One of this components attach on the patella and the other acts as the bearing material between the femoral and tibial components. Though different TKA designs use different dimensions, however among comparable designs, they all have a similar shape at the contact surface. The patellar component articulates in a groove made on the anterior aspect of the femoral component and resembles the articulation of the patella on the trochlear groove in the femur of the normal knee. The contact surface between the polyethylene insert and the tibia is generally flat with modifications with respect to the fixing mechanism between the two. The contact surface between the femoral and polyethylene bearing is elliptic having radii both in the sagittal and the coronal planes. Though there is no fixed pattern of the radius on the tibial component, the sagittal radius on the femoral component decreases from the anterior to the posterior direction (DesJardins, 2000).

Modern TKA designs can be classified with respect to their attachments of the components to the bone, the rigidity between the tibial component and the polyethylene component and the surgical technique.

The femoral, the tibial and the patellar components can be attached to the bone with the use of bone cement, or can be fixated without cement, using the concept of inference fit. A hybrid approach, where some of the components are fitted with cement while the others are fitted without cement, can also be used. Most non-cement approaches use a porous coating for the bone to grow into the metal leading to a more secure fixation. The polyethylene insert for TKA designs can be of fixed type or mobile type depending on its attachment with the tibial component. Fixed bearing designs rigidly fix the two components, with grooves, notches, etc., thus preventing relative motion between them. Mobile bearings, however, allow relative motion between the two components and can be of rotating type (where only rotational motion is allowed) or of meniscal type (where both rotation and translation is allowed). Modern TKAs can also be PCL retaining (PCR), PCL sacrificing (PCS) or posterior stabilized (PS). PS designs differ from other designs by having an additional cam-spine (also called cam-post) contact between the femoral component and the polyethylene bearing in order to initiate posterior femoral rollback. This is required in order to prevent the impingement of the femur on the tibia during high values of flexion. The spine (post) is located on the polyethylene bearing and the cam is provided on the femoral component in between the two condyles. PCR designs do not have this mechanism as the PCL is believed to be the one that causes posterior femoral rollback in the normal knee.

Chapter 2

Literature Review

2.1 Introduction

Experimental studies in humans are difficult and often restrictive due to the exclusion of any measuring device that would require invasive techniques. Since cadaveric studies fail to simulate in-vivo conditions adequately (Komistek, 2005), biomechanical researches have strived for new and unique methods for indirect measurements. This chapter aims at providing the reader with some background related to this thesis, and deals with:

- Analysis of motion in TKA.
- Analysis of forces in TKA.
- TKA failure mechanisms.
- Analysis of wear in TKA.
- Stress in the polyethylene bearings in TKA.

2.2 Motion Studies

Previous methods that have been used to determine in-vivo motions can be categorized as either invasive or non-invasive techniques. Some of invasive techniques include the use of fracture fixation devices (Cappozzo, 1993), bone pins (LaFortune, 1992), minimally invasive 'halo ring' pin attachments (Holden, 1994) and Roentgen Stereophotogrammetric Analysis (RSA) (Karrholm 1989; Nilsson, 1995). Though they probably generate very accurate results, they haven't received a wide scale approval due to their invasive nature.

Some of the non-invasive techniques include the use of skin markers (Antonsson, 1989), externally worn goniometric devices (Chao, 1980), single plane fluoroscopic techniques (Banks, 1996; Hoff, 1998) and non-invasive RSA technique (Valstar, 2001).

Since, the skin based marker systems have been found to generate substantial error due to undesired motion between the markers and the underlying bones (Murphy, 1990; Sati, 1996; Holden 1997), modifications have been made to reduce the errors associated with it. Some of these methods include artifact assessment (Lucchetti, 1998), Point Cluster Technique (Andriacchi, 1998; Alexander, 2001) and optimization using minimization techniques (Spoor, 1988; Lu 1999).

Though fluoroscopic techniques have been accused of exposing patients to radiation (Andriacchi, 2000), the amount of risk to the patient due to radiation is minimal and have been found to generate more accurate results, errors within 0.4° and 0.1mm, under dynamic load bearing conditions (Mahfouz, 2003).

It has now been accepted that knee motion can be described in terms of 6 degrees of freedom (DOF), though they are not necessarily mutually perpendicular (Bull, 1998).

Flexion -Extension

This is the rotation of the knee as viewed in the sagittal plane and represents the largest motion of the knee. In the normal knee this range of motion has been found to vary from 0° -140° with a little bit of hyperextension in some cases.

Internal- External Rotation

This is the rotation of the knee in the transverse plane. This motion is influenced by the position of the joint in sagittal plane. During flexion, the tibia is found to rotate internally with respect to the femur and during extension, the tibia is found to rotate externally with respect to the femur. At full extension, rotation is completely restricted by the interlocking of the femoral and tibial condyles. This happens because the medial condyle is longer than the lateral condyle (Nordin, 2001).

Abduction-Adduction

This is the rotational motion in the knee as viewed from the frontal plane and is also dependant on the flexion-extension motion in the knee joint. This motion is also known as valgus-varus movement and causes one of the condyles (generally the lateral condyle) to lift off. Passive abduction and adduction increases with increase in knee flexion to about 30°, but only to small values, after which it decreases due to the effect of soft tissues (Nordin, 2001).

Medial-Lateral Shift

This is the sliding motion experienced by the knee in the medial and lateral directions. This type of motion is very small compared to the other movements in the knee. Since the tibial plateau is not flat in the medial lateral direction, so medial-lateral shifts are accompanied by a coupled abduction/ adduction and vice-versa.

Anterior-Posterior Translation

This is the second largest motion in the human body and is the movement in the anterior and posterior directions. This motion arises due to slipping of the femur while rotating in the sagittal plane. With increasing knee flexion, the femoral condyles move in the posterior direction on the tibial plateau. This happens due to the tension exerted by the posterior cruciate ligament and helps in allowing the knee to go into high flexion without causing the femur to impinge on the tibia.

Superior-Inferior Translation

This motion refers to the movement of the femur in the superior-inferior direction with respect to the tibia. Since the sagittal contour of the condyles are not exactly circular and also since the medial condyle is larger than the lateral condyle, so the flexion and extension motion is coupled with compression distraction causing an unequal load sharing between the two condyles.

Knees implanted with TKAs have been found to be experience variable kinematic patterns compared to the patterns demonstrated by normal, non-implanted knees. Primary among those derived differences are restricted range of flexion, decreased normal axial rotation and increased occurrences of reverse axial rotation and condylar lift off (Dennis, 2003, 2005a; Oakeshott, 2003). The causes for such variations are believed to be the effects of TKA geometry and implantation procedure. This is due to the fact that the TKA fails to replicate the condylar and contact geometries and also causes a change in the operating environment at the knee by the removal or alteration of the soft tissues within the knee which act as secondary stabilizers (Dennis, 2005b).

2.3 Force Studies

The in-vivo force studies related to the knee joint can be divided into two broad categories – telemetry and mathematical modeling.

Studies using telemetry utilize force sensors, fitted to the prosthetic components, which are implanted directly inside the human body. This is the method which generates the best results because it directly derives in-vivo measurements. However, it is restricted in its use because of the high amount of costs involved in developing a telemetric implant, making it unsuitable for mass scale production and use. Telemetry is a developing art and though there are quite a number of telemetric studies for the hip, its use in the knee has been pretty restricted to date (Komistek, 2005). Previous attempts to incorporate telemetry for the knee have either used special femoral prosthesis (non TKA) fitted with strain gauges (Taylor, 1998, 2001; Burny, 2000) or have used a modified tibial tray of the TKA fitted with load cells (Kauffman 1996, Morris 2001). While the first set of studies have generated in-vivo data for weight bearing conditions, the second set was tested in-vitro. Recently a telemetric TKA has been designed (D'Lima 2005) and implanted. This also incorporates the principle of using load cells in the tibial tray. However, only preliminary data, up to 6 weeks of follow up, for this implant has been published (Colwell, 2005).

Unlike the experimental telemetric approach, mathematical modeling techniques provide a theoretical approach, which can be used on a large scale to predict in-vivo forces both for the normal and the implanted knee using the principles of inverse dynamics. In this principle, kinematics of a system is input to the mathematical model to derive the kinetics of the system. Due to a large number of muscles and soft tissues, the number of unknowns in the human body is large. Therefore mathematical modeling of the human body is a challenging task and relies on two techniques – optimization and reduction, to resolve this issue. In the optimization technique, the number of unknowns is greater than the number equations that be generated for the solution. Therefore, the process deals with the solution generated by the minimization of a suitably chosen objective function (Seireg, 1973; Brand, 1982; Anderson 2001; Piazza 2001). The reduction technique, however, uses simplifying assumptions to reduce the complexity of the system. In this case the system is always kept determinate i.e. the number of unknowns is always made equal to the number of equations that can be generated to solve them (Paul, 1965, 1976; Wimmer, 1997; Lu, 1997, 1998; Komistek, 1998, 2005).

There are variances in the force data generated by the studies (Table 1). This is because data collected by telemetry and the data input to the mathematical models for the same type of activity are collected at different speeds. The interactive forces increase as the speed of the activity is increased. However, it is now a well accepted fact that the contact forces increase with the increase in the angle of flexion (Komistek, 2005).

Table 1: Knee Contact Forces from Previous Studies (Modified from Komistek, 2005).

Authors	***Technique***	***Activity***	***Knee Force***
Taylor et. al.	Telemetry	Normal gait	2.2 – 2.8 BW
		Treadmill gait	2.75 BW
		Stair descent	3.1 BW
		Stair ascent	3.8 BW
		Jogging	3.6 BW
Colwell et. al.	Telemetry	Walking	2.4 BW
		Stair ascent	3.3 BW
Seireg et. al.	Optimization	Walking	7.1 BW
Paul	Reduction	Walking	2.7 – 4.3 BW
		Stair descent	4.9 BW
		Stair ascent	4.4 BW
		Up ramp	3.7 BW
		Down ramp	4.4 BW
Wimmer et. al.	Reduction	Walking	3.3 BW
Komistek et. al.	Reduction	Walking	2.1 – 3.4 BW
		Deep knee bend	1.8 – 3.0 BW

2.4 TKA Failure Studies

The nature of failure in TKAs has been the main guideline in its development. The major reasons for failure of TKAs leading to revision surgery were loosening of the components, instability in the joint due to incorrect surgery, mechanical failure of the components and infection (Hood, 1983; Fehring 2001, Sharkley, 2002). Infection being a non-engineering issue has been neglected in this review. Modern day TKAs have been found to have survival rates of more than 90% at ten years and 84% at fifteen years (Godest, 2000; Rand, 2003).

2.4.1 Component Loosening

In earlier implant designs, tibial component loosening was the main cause of TKA failure with cemented fixation (Scuderi, 1989; Windsor, 1989). The main reason for this type of failure was believed to be:

- **Malalignment:** Due to incorrect valgus-varus alignment of the component, the implant experiences off centered loading which can result in the lift off the tibial baseplate (Windsor, 1989).

- **Poor Initial Fixation:** For cemented implants, an adequate amount of bone cement must be used to ensure proper intrusion of the cement into the bone and the porous surface of the implants. Too much intrusion of the bone cement into the bone, for cemented designs, can lead to the necrosis of the bone and consequent loosening of the components (Moreland, 1988). For cementless designs too little stress on the trabecular bone holding the prosthesis components, due to disuse or stress shielding, can result in atrophy of the bone causing the prosthesis to loosen (Matthews, 1985).

- **Impact Loading and Implant Design:** The amount of resistance generated in the implant for displacement and rotation of the femoral component on the tibia is a measure of the constraint in the implant (Thatcher, 1987; Heim, 2001). For a given tibial sagittal radius, the larger the femoral radius in the sagittal plane, the larger is the translation constraint. The rotational constraint depends both on the sagittal radius and the coronal radius of the components (Haider, 2005). Higher the constraint, higher is the force required for movement and higher is the force at the bone joint interface. Moreover, use of the implant for which it is not designed such as running and jumping, leads to higher forces and stresses which can be more than the bonding strength thereby causing loosening. This can also lead to the fractures of the surrounding bone (Pugh, 1973).

2.4.2 Joint Instability

TKA implantation requires loosening, and alteration of the medial and collateral ligaments and the removal of the ACL and the PCL (PS designs). Since the surrounding ligaments are the secondary stabilizers for the knee joint, a successful implantation requires correct ligament balancing and proper alignment of the components. Instabilities can be caused by excessive bone resection, improper balancing of the ligaments leading to improper flexion gaps, mismatch and incorrect alignment of the prosthetic components (Gebhard, 1990; Fehring, 1994). Malalignment is believed to be the major reason leading to joint instability. If alignment is correct then mild instability can be tolerated but if alignment is incorrect then even mild instability can lead to severe disfunctionality (Moreland, 1988).

2.4.3 Mechanical Failure of Components

Earlier designs using metal on metal articulations and highly constrained hinged-type designs had severe wear and high rate of fracture caused due to fatigue (Wright, 1985). The problems associated with the failure of the metallic components have been eliminated with the use of ultra high molecular weight polyethylene (UHMWPE) as the bearing material between the femoral and tibial component (Hood, 1983). The main cause of TKA failure nowadays is due to the wear of the UHMWPE insert (Collier, 1991). The wear in the polyethylene insert can cause the implant to fail in a number of ways. The particles generated during wear may cause synovitis (joint swelling), osteolysis (bone resorption) and in extreme cases, necrosis (bone death). This would cause the components to loosen and even cause fractures in the bones due to weakening. Wear would increase the roughness of the contact surfaces in the polyethylene insert. This would result in an increase in the frictional force between the femur and the polyethylene. Thus there would be an increase of the constraints in the implants. Moreover, due to imperfections and irregularities on the surface, the femoral component won't rest properly on the polyethylene. The ultimate effect would be reflected in poorer kinematics, malalignment and instability of the joint which would ultimately lead to component loosening, more wear and failure (Walker, 2000a).

2.5 Wear Studies

Wear of UHMWPE has been found to be the major limiting factor in the longevity of the modern TKA implants (Collier, 1991; Jacobs, 1994; Sharkley, 2002). Therefore, the major focus of biomechanical engineers and orthopedic surgeons has switched to the understanding of the mechanism associated with polyethylene wear and ways to prevent it. The study of wear can be divided into two broad groups – results obtained from simulators and the results obtained from retrieval studies. In case of simulators, the cause is input and the effect is studied. For retrieval studies, on the other hand, the final effect is analyzed and the cause for wear is hypothesized and estimated.

Speaking in broad terms two types of simulators are used in wear studies – the knee simulators and the wear simulators, Knee simulators are complex and expensive equipments that test actual knee prosthesis. These are extensively used by TKA manufactures and provide physiological loading in at least four degrees of freedom – flexion-extension, AP sliding, tibial rotation and abduction-adduction (Thompson, 2001). Wear simulators are simplified testing devices which have lesser degrees of freedom and makes use of circular metallic discs (to simulate the femur) which rotate and slide of flat or curved UHMWPE blocks (to simulate the polyethylene insert).

Thus wear simulators basically focus on the effect of the rolling and sliding motion of the femoral component on the contact fatigue failure mechanism in polyethylene (Blunn, 1991; Walker, 1996; Wang, 1999; Kennedy, 2000). Apart from studying the effect of contact fatigue failure, knee simulators can also help in the quantification of surface area of wear and the volume of wear in actual polyethylene inserts (Harman, 2001; Bell, 2003; Laurent, 2003; Muratoglu, 2003).

Retrieval studies on the other hand examine the wear patterns in the polyethylene inserts which have been obtained directly from patients (Collier, 1991; Wasielewski, 1994; Wang, 1998) and tries to correlate the reasons which might have resulted in such a pattern. The implant is divided into zones and the amount of wear in each of the regions is identified (Wasielewski, 1994; Currier, 2005).

2.5.1 UHMWPE Wear Models

Among the many reasons which can cause wear, fatigue related wear and wear due to abrasion adhesion have been found to be prevalent in UHMWPE. Seven types of damage modes affecting wear have been identified for polyethylene inserts (Hood, 1983):

- **Burnishing**: This is caused by the constant rubbing of the femoral component on the polyethylene, thereby smoothening out surface roughness and creating a polishing effect.
- **Abrasion**: This causes severe shredding of the material due to the small particles on the surface, generally generated by the exposed bone and the cement around the femoral component. Wear particles generated in the polyethylene also aid in this process.
- **Delamination**: This causes the top layers of the polyethylene to break away. The process of delamination starts at regions of high stress, caused by micro-cracks or defects in the material (Blunn, 1991). Under cyclic loading these cracks, assisted by tensile and shear stresses (Bartel, 1986), propagate parallel to the articulating surface and results in sheets of material breaking away (Walker, 1993).
- **Pitting:** These are small holes generated in the articulation surface from similar fatigue mechanisms as delamination.

- **Surface Deformation:** This is the permanent deformation of the material caused by cold flow and creep.
- **Scratching:** These are small wear tracks that are caused on the surface of the polyethylene. This is a mild version of abrasion caused due entrapment of small particles between the articulating surfaces.
- **Embedded Debris:** This is caused due to the embedment of hard particles like bone and bone cement on the soft polyethylene material.

2.5.2 Factors Influencing UHMWPE Wear

As a material UHMWPE exhibits low wear rates when compared to metals and other polymers, previously used as tibial inserts, like polytetrafluoroethylene (PTFE) and high density polyethylene (HDP) (Fisher, 1991). This is because polyethylene has very long chains of hydrocarbons which are bonded strongly and so does not break due to mechanical stresses. If the material property is neglected, the performance of UHMWPE as used in TKAs is affected by the process of manufacture and the geometrical design of the components.

2.5.2.1 *Manufacturing Process*

Polyethylene inserts used in TKAs are manufactured in one of the three ways (Bellare, 1996):

- Machined from sheets created by compression moulding of resin.
- Machined from bars created by extrusion of the resin.
- Direct compression moulding of the resin to the required shape.

Fusion defects are caused when the UHMWPE resin is polymerized into bar and sheet stock. These are microscopic defect areas of unconsolidated resin remaining in the material either due to the quality of the resin or the manufacturing process. Moreover, the machining of the raw stock to the final shape causes strain hardening and work hardening in certain areas. These act as the main causes related to polyethylene wear (Wrona, 1994; Bankston, 1995). Polyethylene inserts that are directly made from the compression moulding of the resin have been found to be significantly stiffer in the outer layer in comparison to machined components which can lead to surface cracking and delamination (Tanner, 1995).

After manufacturing, the components are sterilized before packaging. Previously sterilization methods used gamma radiation in the presence of air or used ethylene oxide. This is was found to oxidize the material reducing its fatigue resistance (Baker, 2000) and increasing wear rates and contact stresses (White, 1996; Heim, 1996). Moreover, shelf life was also found to be a major cause of polyethylene oxidation thereby increasing its tendency to wear (Heim, 1996).

Orthopedic companies have addresses this issue by now using gamma sterilization in the absence of air – either in vacuum or in an inert atmosphere of nitrogen. This prevents oxidation of the outer layer of the polyethylene and has been found to dramatically improve fatigue related wear like delamination and pitting (Li, 1994; Williams, 1998). The use of gamma rays has also helped in increasing the abrasion-adhesion wear resistance of polyethylene (McKellop, 1999; Wroblewski, 1999). This happens by a mechanism called cross-linking where the gamma radiation knocks of atoms from a molecular chain and the two such chains join together forming a cross-linked structure.

2.5.2.2 *Geometrical Design*

The stresses produced in the polyethylene insert under loading have been found to have a direct influence on the wear and damage associated with it (Collier, 1991; Kuster, 2002). The critical factor that is associated with stresses developed is the contact area. The contact stresses have been found to decrease almost exponentially with an increase in the contact area (Rullkoeter, 1999). Increasing the polyethylene thickness has been found to increase the contact areas at the femoro-polyethylene interface and reduce contact stresses (Bartel, 1985, 1986; Collier, 1991, Heim, 1996). Using the same reasoning it can be said that highly conforming designs would also have larger contact areas leading to lower stresses. This is certainly true in the neutral position where studies have shown that high conformity reduces contact stresses compared to low conforming designs (Bartel, 1995; Kuster, 2002; Liau, 2002). However, when the position is not neutral higher conforming designs have been found to generate higher stresses than low conforming designs (Heim, 1996; D'Lima, 2001, Liau, 2002). This is because for highly conforming designs a slight change in alignment due to flexion, internal-external rotation and AP translations causes the conformity to reduce drastically. Low conforming designs on the other hand maintain a similar kind of conformity for most orientations thereby experiencing lower stresses.

Incidence of wear on the tibio-polyethylene interface and its contribution to the generation of microscopic particles, leading to osteolysis, has also been found in fixed bearing polyethylene inserts (Wasielewski, 1997; Rao, 2002; Conditt, 2005). This has been attributed to backside micromotion caused to inadequate locking in the modular fixed bearing polyethylene inserts. Interestingly enough retrieval studies of rotating mobile bearing TKA inserts have reported no evidence of significant backside wear (Huang 2002a, 2002b). This has been ascribed to the decoupling effect on motion mobile bearing TKAs have (Bell, 2003; McEwen, 2005). Both the surfaces of the mobile bearing experienced unidirectional motion. For the fixed bearing both surfaces experience multidirectional motion arising due to rotation and translation of the components. Thus is can be concluded that polyethylene wear depends on the type of motion its experiences. Unidirectional motion causes the grain to orient along the direction of motion, thereby, increasing wear resistance. For multidirectional motion, the grains of the polyethylene are randomly oriented, thus experiencing higher wear rates.

2.6 UHMWPE Stress Studies

The study of stresses in polyethylene inserts can be divided into two broad groups – experimental methods and analytical methods.

Experimental methods are used to calculate the contact stresses/ pressures and basically work on the principle of dividing the normal force generated/ assumed with the measured area of contact. The main advantages of these methods lie in the rapid generation of data and therefore are used extensively by orthopedic companies. Some experimental techniques used previously include stereophotogrammetric methods (Ateshian, 1994), dye injection methods (Greenwald, 1971; Black, 1981), silicone rubber methods (Kurosawa, 1980), 3S technique (Yao, 1991), Fuji pressure sensitive film (Stewart, 1995), resistive ink sensors (K-Scan^{TM}) (Ochoa, 1993), ultrasound (Zdero, 2001), piezoelectric transducers (Mikosz, 1988; Buechel, 1991) and micro-indentation transducers (Ahmed, 1983). All of these experimental methods, however, are in vitro techniques that either assumes the contact forces and/or the orientation of the implanted components. Also, the differences between these various techniques and loading conditions make direct data comparisons difficult. Finally, these methods do not calculate sub-surface stresses which are important in determining potential wear and failure (Harris, 1999).

Previous studies using analytical methods involve the use of "Hertzian Contact Stress" analysis (Hertz, 1881) or Finite Element Modeling. Using Hertzian analysis is probably the quickest method in calculating the contact stresses as it does not involve time consuming calibration and positioning of the components and also does not require extensive calculations. Though this method has been used previously to calculate the stresses in polyethylene inserts (Bartel, 1985; Walker, 1988), the accuracy of this method is limited due to the simplifying assumptions on which the theory is based (Lewis, 1998). As a result, it is used more as a tool for comparison rather than for the actual generation of data.

Finite Element Analysis (FEA) is a well proven method that is used in CAD-CAM (computer aided design and computer aided manufacture) as a virtual prototyping tool. In this method, complex structures, whose exact solution is not possible, is broken down into smaller elements that can be solved independently. The results of the individual elements are summed up to predict the behavior of the entire complex structure. Along with the ability to perform analysis for complex structures, it can work on non-linear materials and can also compute sub-surface stresses. Past finite element studies have either used two dimensional plane strain models (Bartel, 1986; Morra, 1998; Walker, 2000b) or have used three dimensional models but with simplified material properties (Sathasivam, 1998) or have been static and quasi-static models (Rawlinson, 2001; Machan, 2004). In more recent studies, explicit dynamic models have also been developed (Godest, 2002; Halloran, 2005). Though FEA provides the best capability to model the polyethylene accurately and calculate stresses in it, however, the greatest disadvantage of this method lies in the high amount of effort, time and computational infrastructure required for the analysis. Thus most studies, using FEA have used simplifying assumptions to reduce the complexity of the method.

As with most types of studies in this field, the stress and contact area data generated by the various methods have a lot of variability in them (Table 2).

Table 2: Summary of some Previous Contact Area and Contact Stress Studies (Thompson, 2001).

Method	Reference	Load	Average Contact Area	Maximum Contact Stress
Elasticity	Bartel et. al.	1.5 KN	N/A	18.0 MPa
FEA	Bartel et. al.	1.5 KN	N/A	20.0 MPa
Fuji film	Collier et. al.	2.8 KN	N/A	23.5 MPa
Fuji film	Collier et. al.	0.7 KN	0.3 cm^2	N/A
K-scan sensor	Harris et. al.	3.6 KN	3.5 cm^2	N/A
Fuji film	Harris et. al.	3.6 KN	2.3 cm^2	N/A

Chapter 3

Research Aims

While TKA procedure is found to be very successful in treating severe osteoarthritis, failure, especially in the form of polyethylene wear limits its longevity (Howling, 2001; Currier, 2005). Efforts to address this issue have mainly concentrated on improving the manufacturing process and the material properties. Some of these efforts include improvement of the sterilization techniques to reduce oxidation and therefore reduce fatigue related delamination and pitting of the polyethylene (Li, 1994; Williams, 1998), and development of highly crosslinked polyethylene (Marathon^{TM}, Depuy; Longevity^{TM} and Durasul^{TM,}, Zimmer; Crossfire^{TM}, Stryker) and scratch resistance femoral components (Oximium^{TM}, Smith and Nephew, Ceramics) to reduce abrasive wear mechanisms (Wroblewski, 1999; Heimke, 2002).

Wear is ideally a function of kinematics, kinetics and the material properties (Wimmer, 1997). Interestingly enough, all the various types of TKA available today use similar kind of materials but have wide differences in the design and the dimension of the components. This suggests that the correlation of kinetics, kinematics and wear hasn't been developed (Sathasivam, 2001; Fregly, 2005). With modern TKA designs aiming at higher degree of flexion, which generates higher forces (Komistek, 2005), and also TKAs being implanted in younger and more active patients a perfecting understanding of the relation of kinematics, kinetics and wear has become increasingly important (Walker, 1999).

Methods to study wear behavior in UHMWPE have been limited to the use of simulators or retrieval studies. The greatest drawback with using simulators is the fact that it works on in-vitro conditions. Comparison between wear generated by simulators and that obtained from retrieval studies, for the same bearing designs and for similar cycles, have indicated greater amount of wear in the retrieved inserts (Harman, 2001). On the other hand retrieval studies involve a backward approach and can only give us an idea about what 'might have caused' such wear rather can pinpointing as to 'this is the cause'. Thus the correct approach would be to go in the forward direction and predict wear from the in-vivo kinematics and kinetics. At present there has been just one study attempting to do this (Fregly, 2005). However, this study is limited due to the fact that it assumes a linear material model, does not incorporate friction and assumes an axial force distribution.

Previously, fluoroscopy has been successfully used in our lab to determine the in-vivo kinematics of TKA, allowing for the determination of antero-posterior translation, axial rotation, femoral condylar lift-off and weight-bearing range-of-motion (Komistek, 2000, 2004; Dennis, 2003). The objective of this research is to devise a new computational methodology which would extend this capability to the calculation of in-vivo contact forces and torques, contact stresses and sub-surface stresses and ultimately serve as reliable predictor for potential polyethylene wear.

This thesis describes the initial process that has been derived. This process is currently restricted in its complexity and can calculate only the contact pressures at the femoro-polyethylene interface. We intend to increase the accuracy and the capability in the future by continuation of this work. In order to test the method we have come up with so far, this methodology was applied on subjects having either a fixed or a mobile bearing PFC Sigma Posterior Stabilized (PS) TKA (Depuy, Warsaw, IN). The femoro-polyethylene contact geometry of the components for the two types of implants is similar in the sagittal plane but the mobile bearing has greater conformity in the coronal plane than the fixed bearing. We therefore hypothesize that subjects implanted with a mobile bearing TKA will have larger contact areas and lower contact pressures at the superior surface of the polyethylene bearing.

Chapter 4

Materials and Methods

4.1 Test Group

The data used in this study is a subset from a previous study in our lab, which was conducted to analyze the in-vivo kinematics for the PFC Sigma PS^{TM} fixed bearing and the PFC Sigma PS^{TM} RP mobile bearing (Depuy, Warsaw, IN) TKA patients, using fluoroscopy, while performing a deep knee bend (Komistek, 2004; Ranawat, 2004). Each groups consisted of five implants – three right TKA and two left TKA. Also, there was one subject in each group who had received bilateral TKA implants. This was chosen in order to analyze if there exists any patient related similarities. All the ten knee implants were judged clinically successful having Hospital for Special Surgery (HSS) knee scores greater than 90 (Insall, 1989) with no ligamentous laxity or pain. The five fixed bearing TKAs were implanted by one surgeon and all five mobile bearing TKAs were implanted by a second surgeon.

4.2 General Methodology

In order to calculate the in-vivo contact pressures, the method deals with two broad aspects – calculating the in-vivo contact forces and calculating the in-vivo contact areas (Figure 4-1). The in-vivo contact forces were calculated using an inverse dynamics mathematical model. In this technique the kinematics is inputted in order to predict the kinetics. The input to this model consisted of the implant kinematics, the dimensions of the bones and implant components and the ground foot interaction force. The implant kinematics was calculated by registering the 3D implant components on the 2D fluoroscopic image.

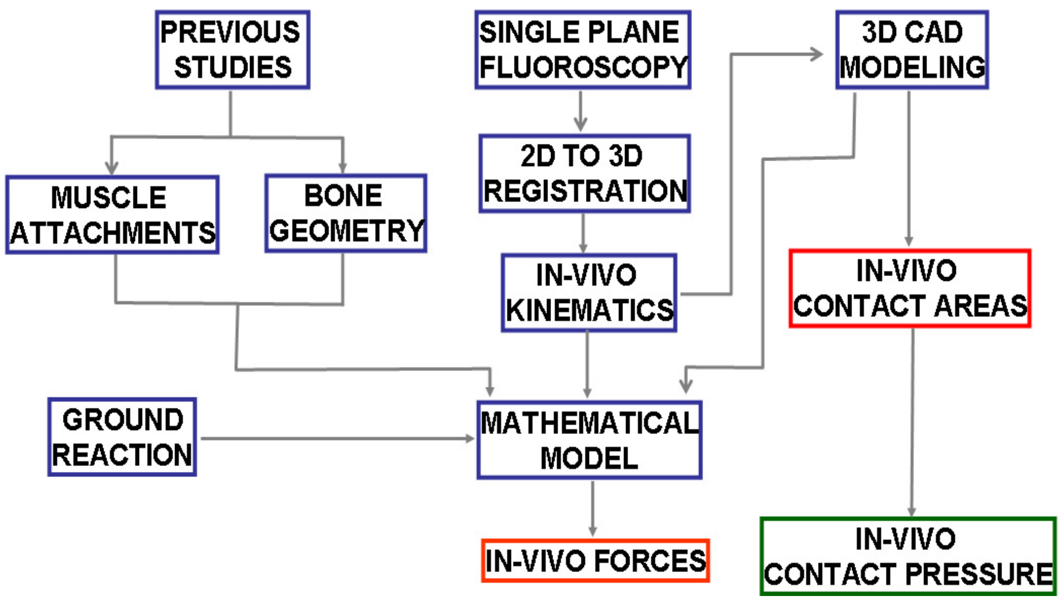

Figure 4-1: Flow Chart Describing the Method Followed in the Study.

Though this part was not performed during the course of this project, nonetheless it has been explained to allow the reader to understand the full process utilized in this methodology. The bone geometry and muscle attachment coordinates were obtained from the previously published anthropometric data. The required dimensions of the implant components were directly obtained from the CAD models of the components. The ground foot interaction force was obtained from force plate data.

In order to calculate the in-vivo contact areas, the implant models were loaded in a CAD package and were assembled based on the transformation matrices obtained previously from the 2D to 3D registration technique. Once the basic orientation of the components was achieved, the femoral component was re-oriented to interfere with the polyethylene. The amount of interference was calculated from the load versus deformation characteristics of polyethylene. The interference area was considered to be the contact area. The contact pressures were then calculated by the following relations:

$$\text{Average Contact Pressure (MPa)} = \frac{\text{Normal Force (N)}}{\text{Contact Area (mm}^2\text{)}}$$

$$\text{Maximum Contact Pressure (MPa)} = 1.5 \text{ x Average Contact Pressure (MPa)}$$

The relation between the maximum contact pressure and the average contact was an assumed one and was based on the Hertzian Contact Analysis which also uses the same relationship.

4.3 Fluoroscopy

The patients were fluoroscoped in the sagittal plane while performing the deep knee bend activity. There can be subtle variations in the way that a person performs a deep knee bend. So to maintain uniformity, the patients were asked to perform a deep knee bend from full extension to full flexion while always keeping their foot (of the fluoroscoped knee) fixed on the ground. While the leg which was fluoroscoped was placed forward, the patients had their other leg inclined backwards at an angle which was comfortable for them. Finally, they were asked to use their hands to support themselves against the frame of the fluoroscopy machine if needed (Figure 4-2).

The fluoroscopic videos were digitized using a frame grabber and were broken down into still images of size 640 x 480 and having 8 bits. For each patient, images from zero to maximum flexion at increments of 10° of flexion were used for the analysis. Some patients exhibited hyperextension. However, to maintain uniformity it was neglected from the study and only the image showing a zero angle of flexion between the femur and the tibia was used as the starting image. By keeping a record of the frames used in the study, the time elapsed for each frame was noted. (The time between each frame and the total time was used later while curve fitting the input data.)

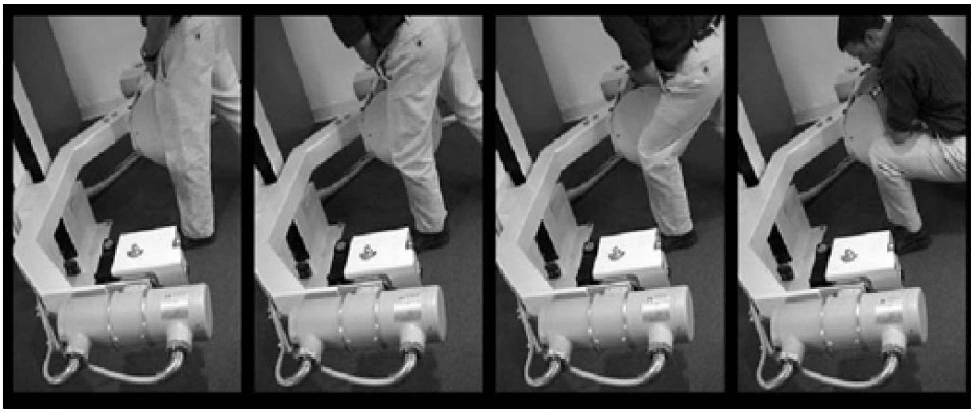

Figure 4-2: Fluoroscoping the Deep Knee Bend Activity (Mahfouz, 2003).

The individual fluoroscopic images are distorted due to the effects of pincushion and spiral distortion. Pincushion distortion is caused due to mapping of electrons from the input screen of the image intensifier, which is curved, to the flat output screen. This phenomenon is dependant on the distance between the X-ray source and the image intensifier and causes larger magnification at the periphery of the final image than at the centre of the image.

Spiral distortion, also known as S-distortion, is due to the effect of the magnetic field encompassing the image intensifier. The component of the magnetic field parallel to the image intensifier affects the radial electron velocity thereby causing a rotation of the image. The transverse component of the magnetic field affects the longitudinal electron velocity causing a translation of the final image. This generates the resultant image with a characteristic S-shape.

The distortion of the fluoroscopic images is corrected using the image of a board containing beads, at known positions, which act as control points (Figure 4-3). By comparing the known positions of the control points with it corresponding location in the distorted image, transformation coefficients for each pixel of the image can be determined (Mahfouz, 2003). By applying the obtained transformation coefficients on the distorted image, we can recover the true image. This final distortion free image is used for further analysis.

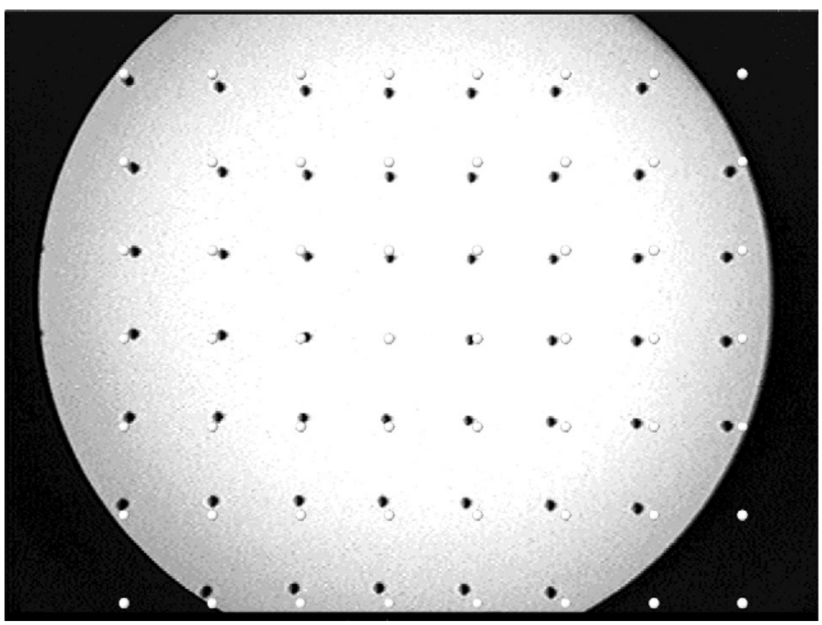

Figure 4-3: Image of a Bead Board. The white dots represent the actual location of the beads. The black dots represent the distorted images of the beads.

4.4 2D to 3D Registration

This technique has been developed in our lab and overlays the 3D models of the components on their projection in the 2D fluoroscopic image (Mahfouz, 2003). This is a semi-automated process that uses direct image to image similarity measure and works on the principle of recreation of the 3D scene in which the patient was fluoroscoped. This requires the calibration of the camera for the fluoroscopic unit. The CAD models are loaded in the software with their geometrical centre coinciding with the global origin of the system. The geometrical centre of the CAD models are found by drawing a 3D bounding box and then joining the diagonals. The common intersection of the diagonals is the geometrical centre. For the automated process to start, the user must orient the models (translate and rotate) to the pose they feel is the best estimate. Starting from this initial pose, the models are automatically oriented to their final position by the use of an automated optimization algorithm known as Simulated Annealing (SA). In its search for the global minimum, the SA algorithm searches the 6-dimensional space (3 rotational and 3 translational) and needs a metric for scoring how the pose of the model compares with that of the fluoroscopic image. This is done using the fluoroscopic image (input image) and a 2D projection image of the model (predicted image) which is generated in white against a black background. Using morphological operations, edge images are created for both the input and the predicted images. Also the input image is inverted to be similar in color with the predicted image (Figure 4-4).

The match between the input image and the predicted image is calculated by two metrics. The first metric compares the pixels of the predicted image and the inverted input image. The second metric evaluates the overlap of the contours in the edge images generated for both the input and the predicted image. The final matching score is obtained by multiplying the two images together, summing the result and then normalizing it with the sum of the predicted image. This method has been found to be robust and converges to the global minimum and is insensitive to image noise and occlusions. Also this method has been found to generate accurate results in the image plane with root mean square (RMS) errors of 0.4° in rotation and 0.1mm in translation. However, it is found to generate higher errors in along the axis perpendicular to the image plane (RMS errors of 0.65mm in translation and 1.5° in rotation) (Mahfouz, 2003).

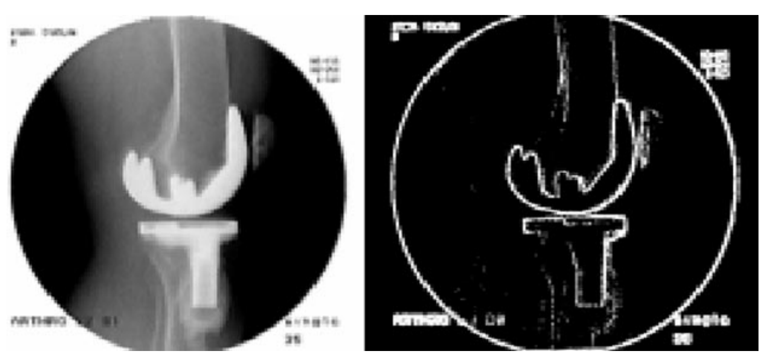

Figure 4-4: (Left) Inverted Image. (Right) Edge Image (Mahfouz, 2003).

4.5 Generating the Required Kinematics

4.5.1 Femoral and Tibial Components

The 2D to 3D registration process works effectively for components that are visible in the fluoroscopic images and outputs their transformation values (three rotational and three translational) based on the global origin defined in the system. Therefore, the transformations for the femoral and tibial components were directly obtained from this process. Once both the femoral and the tibial components have been overlayed this process also calculates the antero-posterior (AP) position of the femur with respect to the tibia. This is achieved by calculating the AP distance of the lowest point on each condyle of the femur measured from the centre of the tibial tray which is assumed to be flat. This is not necessarily the contact point between the femur and polyethylene component, which is curved both on the sagittal pane and the coronal plane (Figure 4-5). However, it serves as a good measure in studying the translational nature of the femur with respect to the tibia and was used in the mathematical model, details of which are explained later.

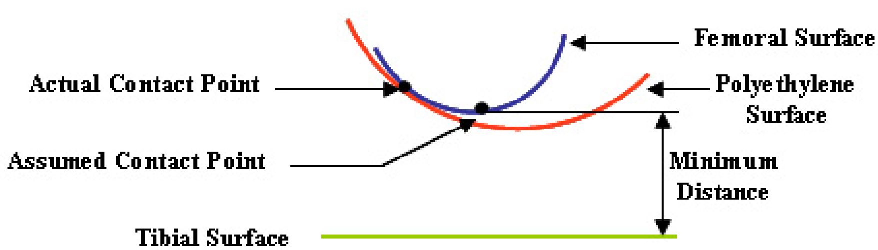

Figure 4-5: The Assumed Point of Contact to calculate AP Position of the Femur.

4.5.2 Polyethylene Insert

Since polyethylene is transparent to radiation, so it is rendered invisible in the fluoroscopic images. Therefore, the 2D to 3D registration technique cannot be directly applied to this component. To overcome this difficulty, for the fixed bearing TKA, the polyethylene was assumed to be rigidly fixed to the tibial component thus having the same kinematics as that of the tibial component. For the mobile bearing TKA, the polyethylene was specially prepared before implantation. Each insert was designed and manufactured with four tantalum beads strategically placed at locations offset with each other in all directions, so that they were always visible in the fluoroscopic images. The kinematics of the polyethylene was obtained by orienting the beads on it to the locations visible in the fluoroscopic images. Though the same 2D to 3D registration software interface was used to generate the transformation values, the matching of the four beads was done manually. To ensure correct alignment, the femoral and the tibial components were fit before the polyethylene insert (Figure 4-6). The final assembly was viewed in three mutually perpendicular planes to ensure correctness of the overlay process.

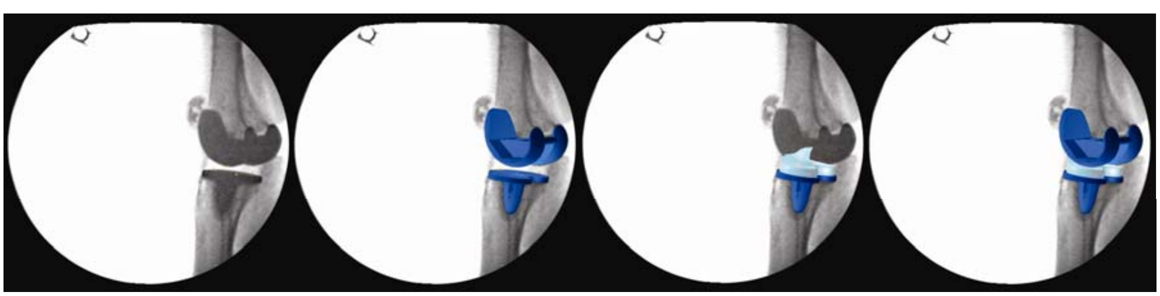

Figure 4-6: Process used to fit the Polyethylene Insert in the Mobile Bearing TKA.

4.5.3 Patella

For the patellar component, a similar problem, as with polyethylene insert, exists. However, the patellar bone is visible in the fluoroscopic images. Therefore, movements of the patellar component can be directly derived from the fluoroscopic images with the help of the patellar bone. The patella was assumed to rotate only in sagittal plane and the amount of tilt was calculated by measuring an axis of the patella (obtained by marking 4 points on the extremity of the patella, as visible in the fluoroscope image, and bisecting the lines joining them) with the axis of the tibia (Figure 4-7). The distance between the most anterior aspect of the femoral component and the most posterior aspect of the patella was defined as the patellar contact point. This method has been previously used in our lab to study patellofemoral kinematics (Komistek, 2000).

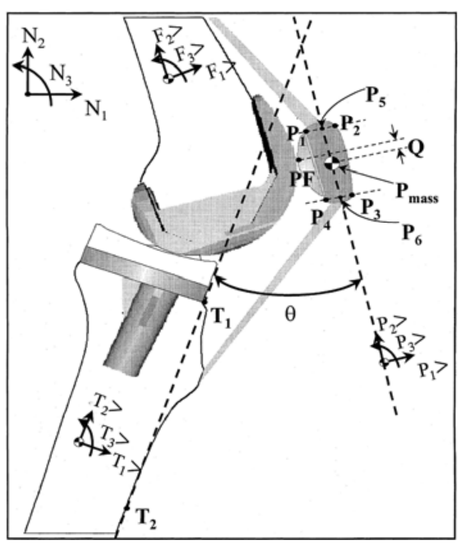

Figure 4-7: Method used to calculate the Patellar Tilt Angle from the Fluoroscopic Image (Komistek, 2000).

4.6 Mathematical Modeling

In order to predict the in-vivo forces during the deep knee bend activity, an inverse dynamics model was created. This model was based on the principle of rigid body dynamics and utilized the reduction technique, where, the system is always kept determinate by keeping the number of unknowns equal to the number of equations. The underlying assumption in this technique is that certain muscles, which do not influence the system significantly, are neglected. Moreover, the modeled muscles are grouped together and it is assumed that the force within the grouped muscles represents a good estimate of the force acting within each separate muscle. The model was developed using Autolev^{TM} (Online Dynamics Inc, Sunnyvale, CA), a symbolic manipulator based on Kane's dynamics (Kane, 1985; Komistek, 1998). Unlike classical methods in dynamics, Kane's method uses generalized multipliers, called partial velocities and partial angular velocities, to convert the actual forces and torques into what is known as generalized forces, based on which the equation for equilibrium is derived (Appendix B). Moreover the method is vector based, i.e., vector cross products and dot products are used to determine the velocities and accelerations rather than tedious calculus (Yamaguchi, 2001). Therefore, this method is extremely efficient and well suited for multibody systems having large degrees of freedom. This method allows for the solution of a maximum of six kinetic terms associated with each rigid body.

4.6.1 Inputs to the Model

Same amount of rotation between two different centers does not produce the same final orientation. Though the angle of body with respect to a reference line remains the same, the final position of the body is translated (Figure 4-8). The 2D to 3D registration process generates three rotational and three translational values for each component. However, these calculations are based on the geometrical centre of the model. In the constructed mathematical model, the rotational centre of the rigid bodies does not correspond to the geometrical centre of the implant components. Therefore, to take care of this effect, only the rotational values obtained from the registration process were considered. Before use in the model, the kinematic data was made continuous by interpolation using splines of at least the 3^{rd} order. This was done in order to make the acceleration, obtained by double differentiation of path of motion, continuous. Each data was fit with splines of order 3, 4, 5 and 6 respectively. The final selection was made based on the least sum square error generated by the splines when fitting the original data.

Ground reaction force, obtained from a force plate, was also used as an input to the model. However, this data was unavailable for each patient individually. Therefore, the data used in this study were that for a single healthy person. This data was scaled with respect to the patient weight and the time they took for the activity. Though this resulted in a variation in the magnitudes of the round reaction force for each patient, however, the variable nature of each curve with respect to flexion angle was similar.

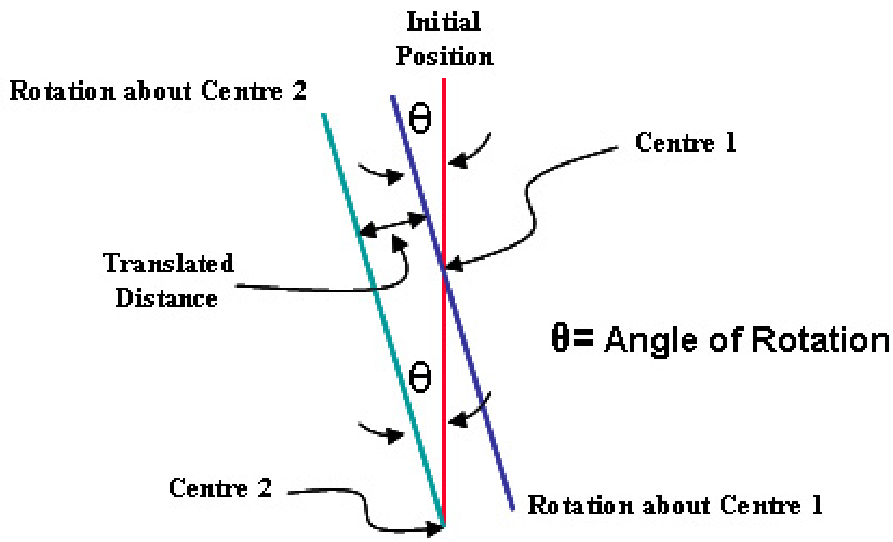

Figure 4-8: Effect of Rotation about different Centers.

The dimensions of the bones, location of prominences and their inertial parameters were obtained from previously published anthropometric data (Zatsiorski, 1983; White, 1989; deLeva, 1996). The attachments of the muscles were considered as points and were also obtained from previous studies (Yamaguchi, 2001). Since these studies use different axes systems, therefore, the data were transformed to the axis system in this study before being used. Also, these data were scaled with respect to the height and body weight of the patients. In this regard, the dimension of the patella was unavailable. So the patella was assumed to be a disc whose dimensions were measured directly from the fluoroscopic images at full extension. Finally, the relevant femoral, polyethylene and tibial component dimensions of the TKA were directly measured form the CAD models of the components.

4.6.2 Description of the Model

Initially, a free body diagram of the mathematical model, simulating the deep knee bend activity was derived in the sagittal plane (Figure 4-9). The anterior-posterior (AP) direction, superior-inferior (SI) direction, and the medial-lateral (ML) directions were denoted as unit vectors in the 1, 2, and 3 directions, respectively. This is the same set axes that the 2D to 3D registration technique uses. The system consisted of a kinematic chain starting from the foot-ground interaction through to the hip joint which was modeled as a fixed point corresponding to the superior most aspect of the femoral head.

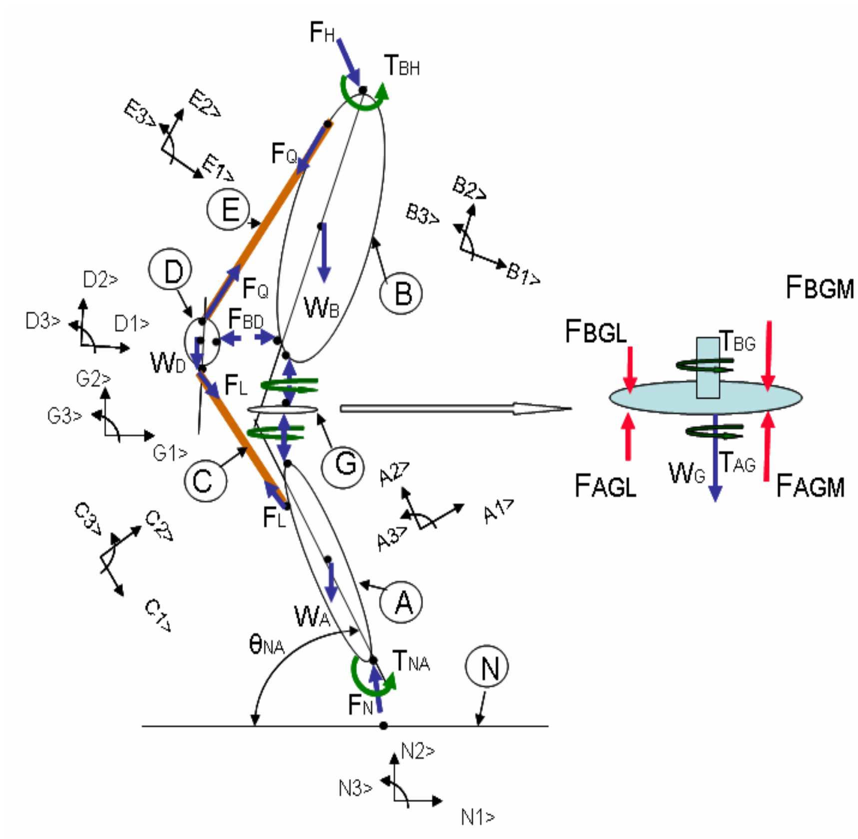

Figure 4-9: Simplified Free Body Diagram for the Mathematical Model used in the Study.

During this particular deep knee bend activity, the foot always remained firmly rooted to the ground. Therefore, it was removed from the analysis and the tibia was considered to have pure rotation in the sagittal plane about a point, corresponding to the ankle joint, which was fixed to the ground. The amount of rotation was the value that was obtained from the 2D to 3D registration process. This point was considered as the origin for the Newtonian and the tibial reference frames. Also since the patients did not do the deep knee bend activity bare footed, so the foot has a surface contact with the ground. The point of action of the original ground reaction was considered to be the midpoint of the foot. As the model starts from the ankle so the ground reaction force calculated from the force plate data was replaced by a force and moment acting at the ankle. The magnitude of this force was equal to the force plate value while the moment was calculated as the cross product of the position vector form the midpoint of the foot to the ankle and the magnitude of the force (Figure 4-10).

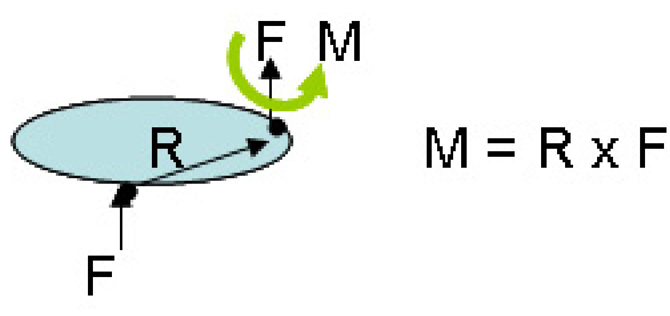

Figure 4-10: Transforming the Ground Reaction Force from the Foot to the Ankle.

The tibia, femur, patella and polyethylene were modeled as rigid bodies while the ground was chosen as the fixed Newtonian reference frame (referred to as ‘A’,’B’,’D’, ‘G’ and ‘N’ in the figure).

Subsequent transformation was then defined for the adjacent bodies. The mobile bearing polyethylene insert was assumed to have pure rotation with respect to the tibia in the transverse plane about the superior-inferior axis (A2>). The polyethylene coordinate system had its origin at the mass centre of the polyethylene. This point is aligned on the axis of rotation due to the symmetrical nature of the polyethylene insert. For the fixed bearing TKA, the polyethylene was assumed to be rigidly fixed to the tibial component, without having any motion relative to it, and the polyethylene axis system was similar to that of the mobile bearing. The femur was assumed to roll with slipping along the AP direction on the polyethylene insert. This was modeled as a cylinder rolling with slipping on a curved surface which had a curvature only in the sagittal plane. The cylinder had a radius equal to the radius of the femoral condyles in the sagittal plane and a length equal to the intercondylar distance of the femoral implant. The intercondylar distance was defined as the distance between the lowest points in the femoral condyles at full extension and this was assumed to be constant throughout flexion. Also, the effect due to the coronal curvature of the polyethylene was neglected. The femur was also assumed to rotate in the transverse plane with respect to the polyethylene about the superior-inferior axis (B2>) but rotation in the coronal plane, causing lift off, was neglected. The sagittal motion of the femur was the value obtained from the 2D to 3D registration transformation values. However, the translational effect and the axial rotation of the femur were obtained from the AP data, as previously specified. The slip factor for the motion was calculated as the ratio of the actual distance translated by the femur to the distance it would have moved had it been rolling without slipping in the antero-posterior direction (Figure 4-11).

The motion of the femur was finally depicted as rotations in the sagittal plane and the transverse plane about an instantaneous centre of rotation. This instantaneous centre was calculated as the line of intersection of the instantaneous axis of rotation in the sagittal plane and the axis of rotation in the transverse plane. Since, in the transverse plane, the rotation was calculated with respect to the bisector of the length of the cylinder, the axis of rotation for this case was always fixed.

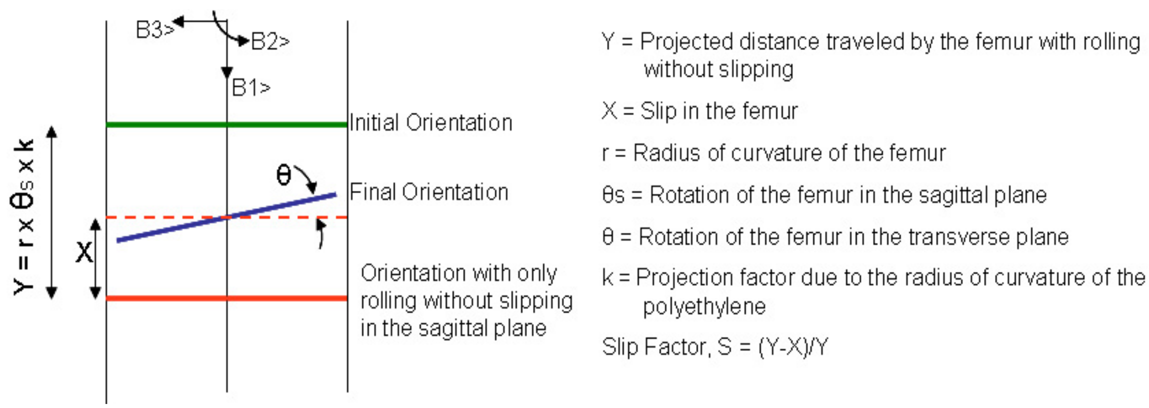

Figure 4-11: Calculating the Slip factor and the amount of Axial Rotation in the Femur.

The origin for the femoral coordinate system was defined at the intersection of the longitudinal axis and the transverse axis of the femur (considered to be a cylinder) (Figure 4-12). For the TKAs used in this study, the femoral component has three distinct radii in the sagittal plane and they contact with the polyethylene at around 0-60°, 60°-90° and 90° to maximum flexion. Similarly, the polyethylene also has two distinct radii in the sagittal plane and comes into action depending on the location of contact with the femur. This is provided into order to achieve higher areas of contact as the femur goes into higher ranges of flexion. Therefore, while using the AP data to calculate the motion of the femur with respect to the polyethylene (as obtained from the 2D to 3D registration) the correct femoral and polyethylene radii corresponding to the angle of flexion were used.

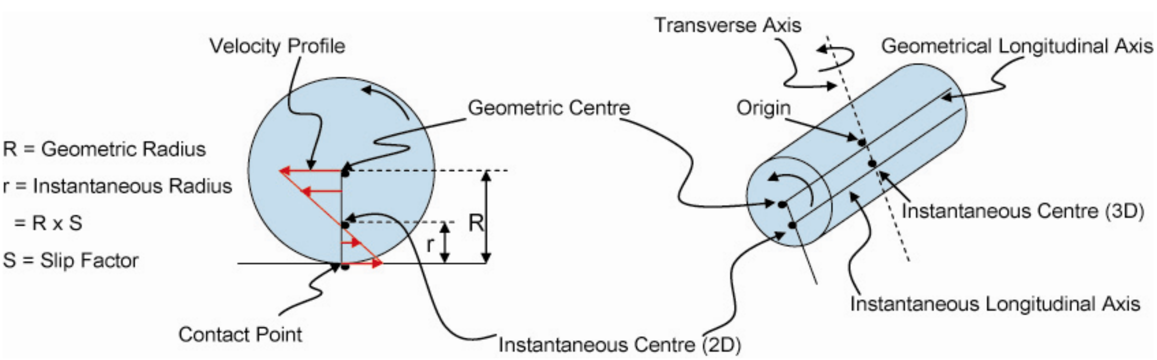

Figure 4-12: Location of the Origin and the Instantaneous Centre for the Femoral Component as used in the Model.

The patella was assumed to be located in the femoral groove and as a result had the same axial rotation as the femur. The patella was assumed to have rotation in the sagittal plane with respect to the femur about a centre passing through the mass centre of the patella. The mass centre of the patella was calculated by the method as outlined in Komistek et. al., 2000 and was considered to be the origin for the patellar coordinate system. Only one point of contact was considered between the femur and the patella and this contact was considered variable based on the contact values directly obtained from the fluoroscopic images using the process described in the referred study.

The surface contacts between the tibia and the polyethylene and between the femur and the polyethylene was modeled as having two contact points corresponding to the medial and lateral condyles. The PS type implants experience and additional contact due to the engagement of the cam-spine mechanism, but this was neglected in this analysis. The femoro-polyethylene and tibio-polyethylene contact forces were included into the system only at the points of contact and were modeled as having two components, one in the direction along the common normal for the surfaces in contact (F_N) and the other in the direction opposite to the direction of relative velocity of the points in contact (frictional force, F_S). A constant frictional co-efficient (C_F) of 0.05 was used for this analysis and the magnitude of the frictional force was obtained as the product of the frictional co-efficient and the normal force (Figure 4-13).

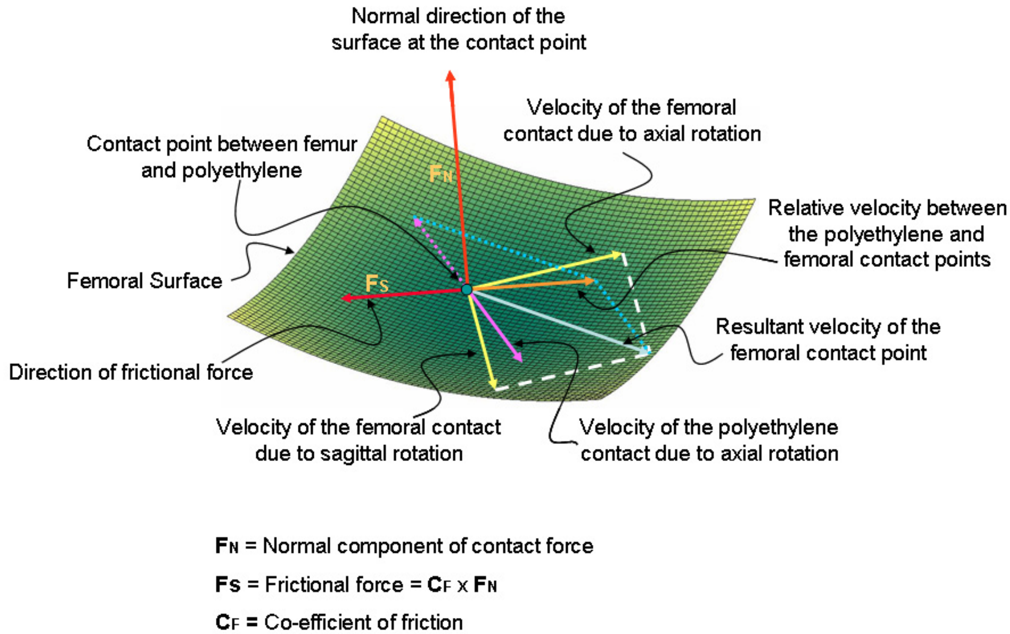

Figure 4-13: The direction of the Femoro-Polyethylene Contact Forces used in the Model.

As the surface curvature of the patellar component was unavailable, the contact forces between the femur and patella were modeled along the three Newtonian unit vector directions.

To keep the system determinate, only the quadriceps and the patellar ligament were entered into the system whose forces were calculated in this model. The quadriceps is a set of four muscles. But in this model it assumed to be a single muscle having its attachment on the greater trochanter of the femur. The patellar ligament and the quadriceps were modeled as mass-less frames (represented as ‘C’ and ‘E’). They were entered into the system as equal and opposite forces acting at their points of attachments and the line of action being the straight line joining their attachment points. Thus though the forces were unknown in magnitude, their direction was known. This helps in reducing the number of unknowns in the system. This method however neglects the effect due to the wrapping of the muscles on the bones.

The model solved for 18 unknowns that included the femoro-polyethylene and tibio-polyethylene contact forces and torques, the patello-femoral contact force, the force in the patellar ligament and quadriceps muscle, and the forces and torques acting at the hip.

4.7 3D CAD Modeling

The in-vivo contact areas were derived by the use of CAD modeling. The CAD models that were provided to us directly from the manufacturer were in 'IGES' format. In this format a 3D object is broken down into surfaces. In order to be able to calculate the interference area Mechanical Desktop^{TM} (Autodesk Inc, San Rafael, CA) requires that the contacting components be solid. Therefore, the surfaces of the femoral and polyethylene components which were supposed to be in contact were converted into solids. This was done by extruding the surfaces in the required direction. Since the cam-spine contact was neglected for this whole study, the structure of the cam on the femur and the spine of the polyethylene were not modified and the contact area between them were not calculated.

4.7.1 Orienting the CAD Models

This process works on the concept of recreating the same scene as that in case of the 2D to 3D registration technique. The CAD models were loaded into the system so that the geometrical centre of the components coincided with the global origin of the software. Using the rotational and translational values obtained from the registration technique, the components were oriented to match in the same way as observed in the registration process. In order to ensure this all rotations for a particular component was applied at the geometrical centre and the order of rotation about the three mutually perpendicular axes was the same as that used in the registration technique. For the mobile bearing TKA only the femur and the polyethylene components were used which were rotated and translated with respect to their geometrical centre. For the fixed bearing TKA, since polyethylene transformation data was unavailable, it was assumed to be rigidly fitted to the tibia. Therefore, the rotation and translation for this component was done with respect to the geometric centre of the tibia, for which it was necessary to fit the polyethylene on the tibia first.

4.7.2 Calculating the Deformation

The compressive stress-strain data for UHMPWE generated by DeHeer and Hillberry (DeHeer, 1992) has been used in several studies, especially FEA studies, for calculation of contact stresses (Walker, 2000b; Halloran, 2005). However, for this study we chose the data from Kurtz et.al. 2002. This study lists the compressive stress strain properties for UHMWPE processed under different radiation levels (unradiated, 30KGy y-N_2, 100KGy 100°C, 100KGy 150°C), tested at different strain rates (0.02/s, 0.05/s, 0.1/s) and temperatures (20°C – 60°C), and tested under uniaxial tension and uniaxial compression. For this study the uniaxial compression data for UHMWPE radiated by 30KGy y-N_2, tested at a strain rate of 0.05/s and a temperature of 37°C was used (Figure 4-14). This data was also compensated for toe-in as per ASTM D695-02a standards.

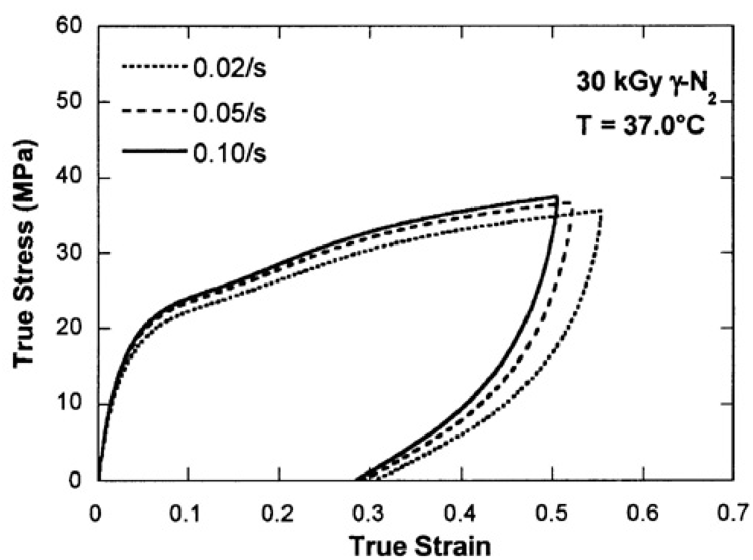

Figure 4-14: Compressive Stress-Strain Nature of UHMWPE (Kurtz, 2002).

The uniaxial compression test data was generated for cylindrical specimens 10mm in diameter and 15mm in height (Kurtz, 2002). From this true stress-strain data, the load versus deformation variation of polyethylene was calculated and used in this study. This was achieved by the following relations:

$Engineering\ Strain, \varepsilon_N = e^{\varepsilon} - 1$ where 'ε' is the true strain and 'e' is the exponent function

$Deformation, \delta = \varepsilon_N x l_0$ where 'l_0' is the original length of the specimen

$Engineering\ Stress, \sigma_N = \dfrac{\sigma}{(1+\varepsilon_N)}$ where 'σ' is the true stress

$Load, P = \sigma_N x A_0$ where 'A_0' is the original area of the specimen

From the load versus deformation variation of the polyethylene, the actual deformation of the polyethylene was calculated using the forces generated by the mathematical model at the femoro-polyethylene contacts. Separate deformation was calculated for the medial and the lateral sides depending upon the forces they experienced.

4.7.3 Generating the Contact Area

In order to generate the contact areas the initially aligned femoro-polyethylene assembly was re-oriented. The polyethylene orientation was unchanged but the model of the femoral component was moved about its superior-inferior axis until it interfered with the polyethylene insert by the deformed amount as calculated previously. Since the medial and the lateral sides in the polyethylene had differing deformation values, with the medial deformation being higher due to higher values of loads acting on the medial side, the final orientation of the femoral component on the polyethylene was achieved in two steps. First, the femoral component was first interfered with the polyethylene component to a thickness equal to that of the predicted medial deformation and then it was rotated along the coronal plane about the medial contact point which was assumed to be the centre of rotation. This ensured the lateral condyle to lift upwards and attain its correct deformation value (Figure 4-15). Once the components were perfectly oriented, the interference area between the two components was obtained and then used as the contact area (Figure 4-16).

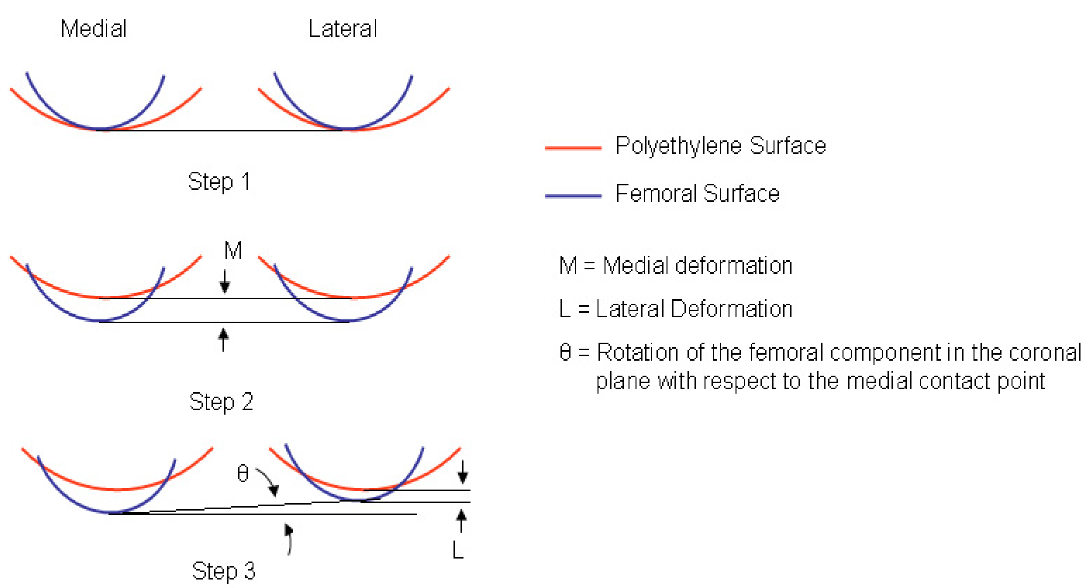

Figure 4-15: Re-orienting the Femoral Component to Interfere with the Polyethylene.

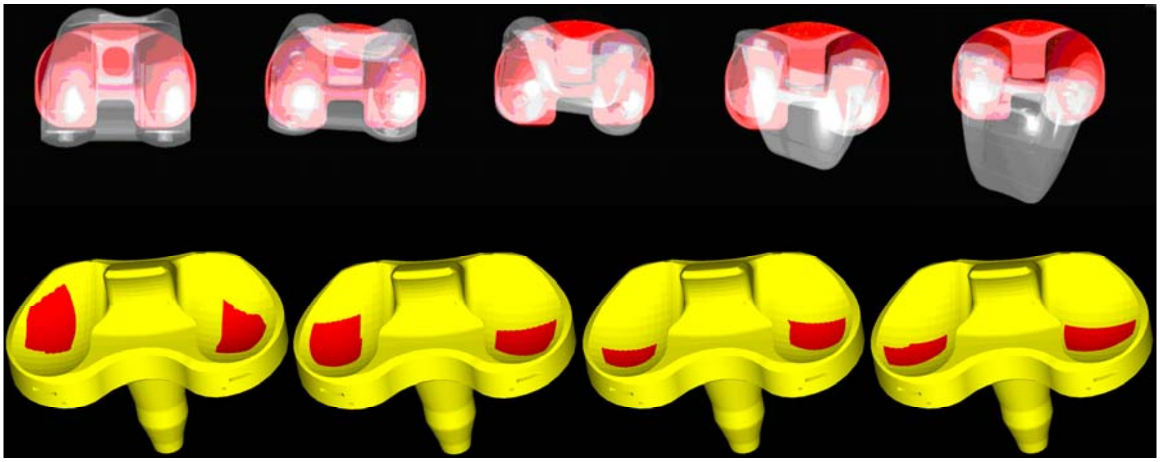

Figure 4-16: (Top) Top view of the final assembled CAD Models. (Bottom) The Interference Area (Contact Area) between the Femur and the Polyethylene.

Chapter 5

Results

This section reports the results obtained for this project. As stated earlier the kinematics used in this project was taken directly from previous studies (Komistek, 2004; Ranawaat, 2004). However, since this project consists of a smaller test group than the original studies the kinematic results described in this section would be different from that published in the literature. The previous studies published data from full extension to 90° of flexion. This study however utilized the data from full extension to maximum flexion.

Since the subjects analyzed in this study experienced various amounts of knee flexion, for comparison purposes, the results obtained were normalized for each subject with respect to their flexion range. This was achieved by converting the motion from full extension to full flexion on a percentage scale with the maximum flexion being denoted as 100%. Also though the calculations of the forces were in Newtons, the final values were scaled with respect to the body weight of each person.

5.1 Kinematics

On average, subjects having a PFC Sigma fixed bearing PS TKA experienced -0.8 mm (range, 2.3 mm to -3.1 mm; SD, 2.1) of posterior motion for the medial condyle and -3.2 mm (range, -0.3 mm to -5.2 mm; SD, 2.1) of posterior motion for the lateral condyle from full extension to maximum knee flexion. Subjects having the mobile bearing PS TKA experienced, on average, an anterior movement of 2.7 mm (range, 0.3 mm to 6.2 mm; SD, 2.8) for the medial condyle and a posterior movement of -1.8 mm (range, 1.2 mm to -4.3 mm; SD, 2.3) for the lateral condyle from full extension to maximum knee flexion. The average amount of internal tibial rotation was 3.1° (range, -3.6° to 5.8°; SD, 3.8) and 5.9° (range, 1.0° to 12.4°; SD, 4.2) for the fixed and mobile bearing PS TKA groups, respectively. The maximum amount of condylar lift-off was 1.3 mm and 1.5 mm for the fixed and mobile PS TKA groups, respectively. Four of five (80%) subjects having a fixed bearing PS TKA and one of five (20%) subjects having a mobile bearing PS TKA experienced greater than 1.0 mm of condylar lift-off at any analyzed increment of flexion. The average weight-bearing range-of-motion for the fixed and mobile bearing PS TKA groups was 112.2° (range, 95° to 130°; SD, 15) and 97.2° (90° to 108°; SD, 8.04), respectively.

5.2 Contact Forces

5.2.1 Mobile Bearing TKA

The contact forces for each subject increased with increasing knee flexion. Subjects having a mobile bearing TKA experienced, on average for the medial condyle, a force at full extension of 0.5BW (range, 0.17 BW to 0.69 BW; SD, 0.22) to a force of 2.7BW (range, 2.68BW to 2.80BW; SD, 0.08) at maximum knee flexion. The lateral contact force remained less than the medial contact force, averaging from 0.34BW (range, 0.25BW to 0.38BW; SD, 0.06) at full extension to 0.91BW (range, 0.88BW to 0.94BW; SD, 0.03) at full knee flexion (Figure 5-1).

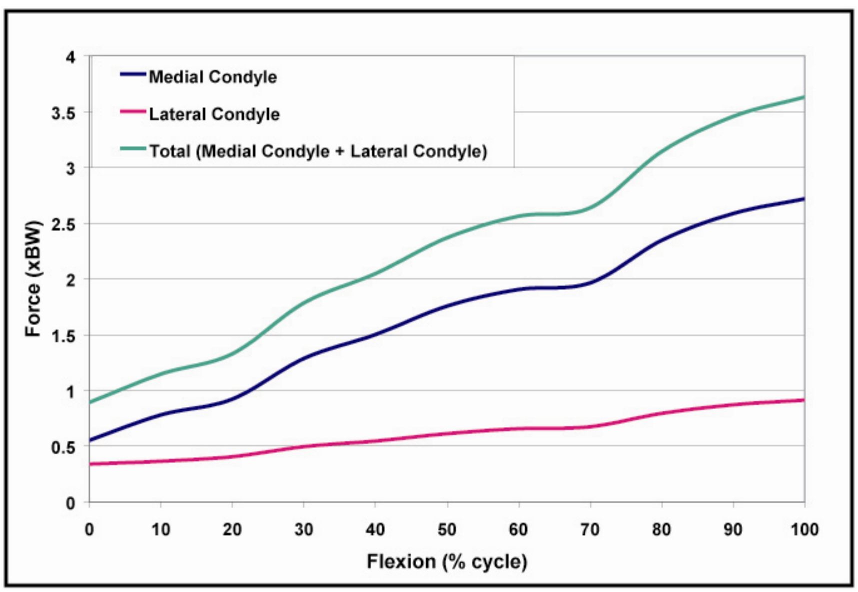

Figure 5-1: The Average Contact Forces in the Mobile Bearing TKA.

The average force in the patellar ligament varied from 0.17BW (range, 0.14Bw to 0.21BW; SD, 0.03) at full extension to 1.5BW (range, 1.47BW to 1.55BW; SD, 0.03) at full knee flexion. The average quadriceps force on the other hand varied from 0.27BW (range, 0.12BW to 0.43BW; SD, 0.15) at full extension to a value of 2.86BW (range, 2.62BW to 3.25BW; SD, 0.28) at full knee flexion. The average patello-femoral contact force had a value of 0.23BW (range, 0.14BW to 0.34BW; SD, 0.09) at full extension, which increased to 2.82BW (range, 2.64BW to 3.00BW; SD, 0.14) at full knee flexion (Figure 4). In summary, all of the subjects experienced a larger patellofemoral force compared to the quadriceps force throughout knee flexion except during early flexion (0-5%) and deep flexion (80-100%) when some subjects experienced larger quadriceps forces that increasingly influenced the group average for this force (Figure 5-2).

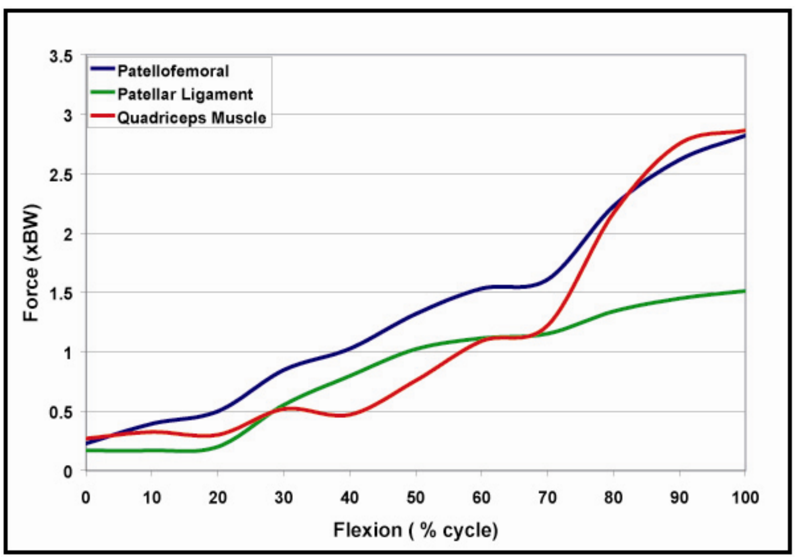

Figure 5-2: The Average Patellofemoral, Patellar Ligament and Quadriceps Force in the Mobile Bearing TKA.

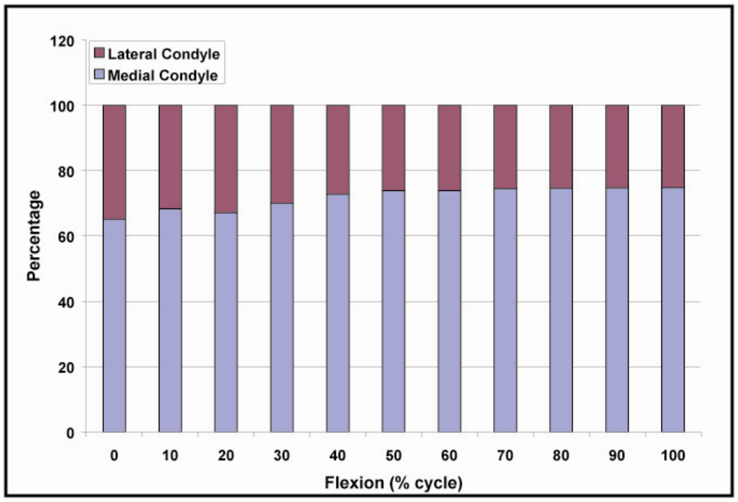

Figure 5-3: Distribution of the Contact Forces in the Mobile Bearing TKA.

The medial-lateral force distribution increased with the increase in flexion and varied from around 65%-35% ratio at full extension to around 73%-27% ratio at maximum knee flexion (Figure 5-3).

5.2.2 Fixed Bearing TKA

Fixed bearing TKA subjects experienced similar force patterns as the mobile bearing TKA subjects where the average forces increased with increasing knee flexion. The average medial force varied from 1.04BW (range, 0.70BW to 1.77BW; SD, 0.42) at full extension to 2.73BW (range, 2.56BW to 2.87BW; SD, 0.12) at full knee flexion. The average lateral force varied from 0.43BW (range, 0.34BW to 0.62BW; SD, 0.11) at full extension to 0.92BW (range, 0.87BW to 0.95BW; SD, 0.03) at full flexion (Figure 5-4).

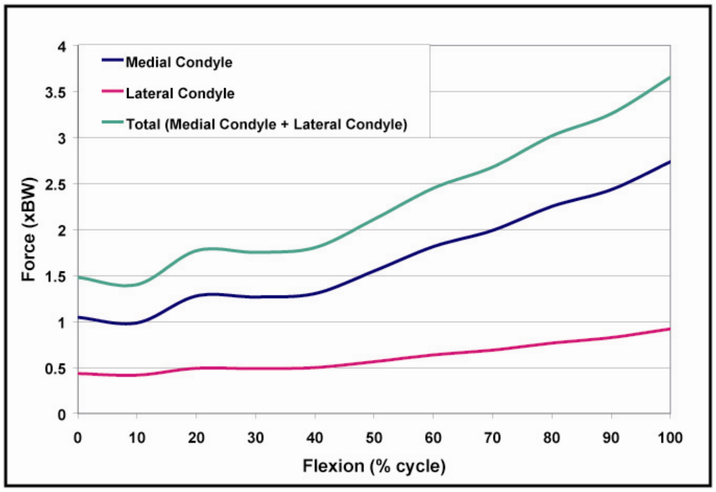

Figure 5-4: The Average Contact Forces in the Fixed Bearing TKA.

The average patellar ligament force varied from 0.27BW (range, 0.06BW to 1.02BW; SD, 0.42) at full extension to 1.54BW (range, 1.48BW to 1.58BW; SD, 0.04BW) at full knee flexion. The average quadriceps force varied from 0.52BW (range, 0.16BW to 1.06BW; SD, 0.32) at full extension to 3.10BW (range, 2.78BW to 3.27BW, SD; 0.19) at full knee flexion. Finally, the average patellofemoral force ranged from 0.62 BW (range 0.24BW to 1.26BW; SD, 0.41) at full extension to 2.92BW (range, 2.72BW to 3.02BW; SD, 0.12) at full knee flexion (Figure 5-5). Unlike the subjects having a mobile bearing TKA, the patellofemoral force remained greater than the quadriceps force, except at the final stage of flexion (90-100%).

The medial-lateral force distribution ranged from 70%-30% at full extension to 72-25% at maximum knee flexion (Figure 5-6).

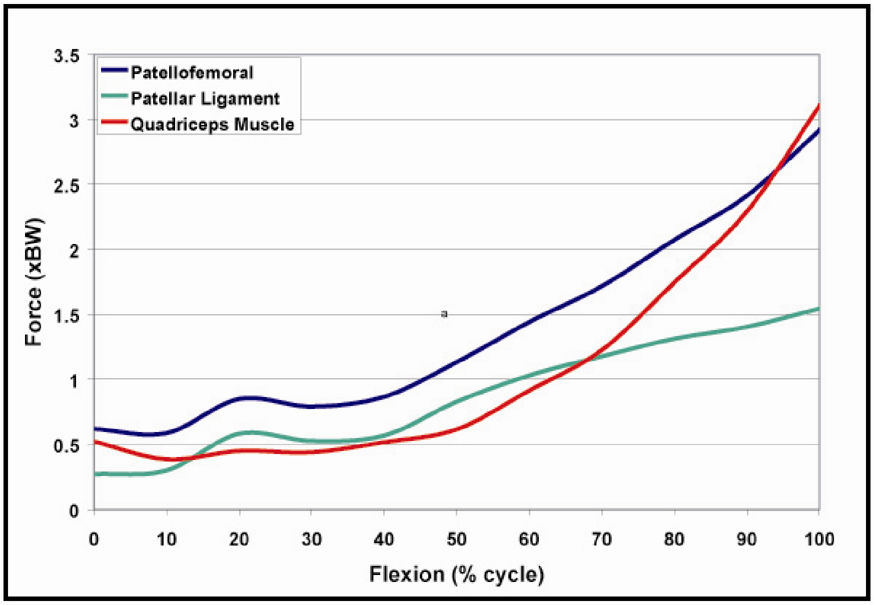

Figure 5-5: The Average Patellofemoral, Patellar Ligament and the Quadriceps Force in the Fixed Bearing TKA.

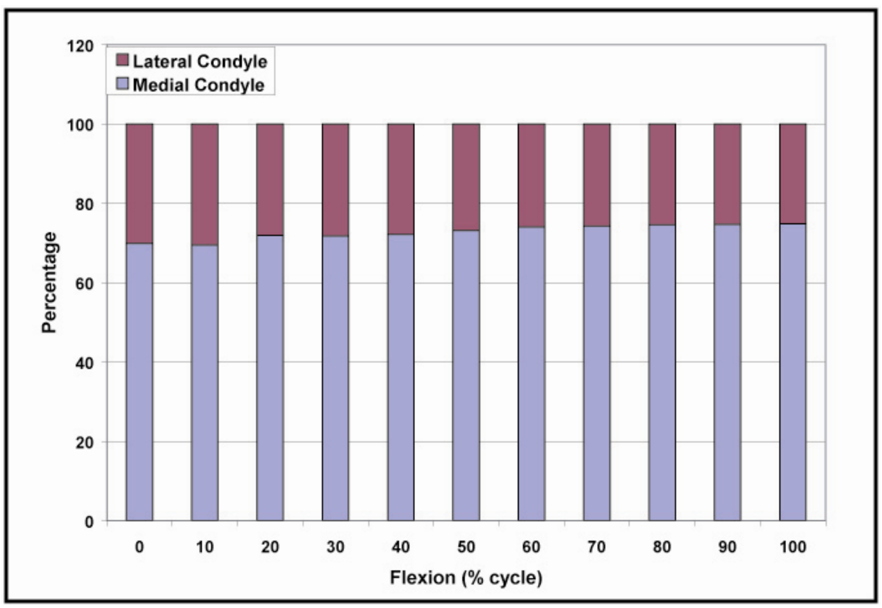

Figure 5-6: Distribution of Contact Forces in the Fixed Bearing TKA.

5.3 Contact Areas

Throughout knee flexion, the medial and lateral condylar contact areas for both TKA types varied considerably. The amount of contact area varied for each subject within a TKA group and, in general, was fairly consistent for the medial side but decreased on the lateral side with increasing knee flexion. The average minimum and maximum contact area values ranged from 50.12 mm^2 to 213.21 mm^2 (Appendix D) for the subjects having mobile bearing TKA (Figure 5-7) and from 59 mm^2 to 160 mm^2 (Appendix D) for the subjects having a fixed bearing TKA (Figure 5-8). For each subject, the analysis revealed that the medial condyle contact area was greater than the lateral condyle contact area. Also, the contact areas for subjects having a mobile bearing TKA were higher than the values for those subjects implanted with a fixed bearing TKA.

Interestingly, for those cases where the relative axial rotation of the femur with respect to the polyethylene was greater than 2.0°, the contact area decreased. This finding seems to suggest that the main factor affecting the contact area is the axial orientation of the femur on the polyethylene. Higher axial rotations cause a mismatch between the components' contour, thus reducing the area of contact between them.

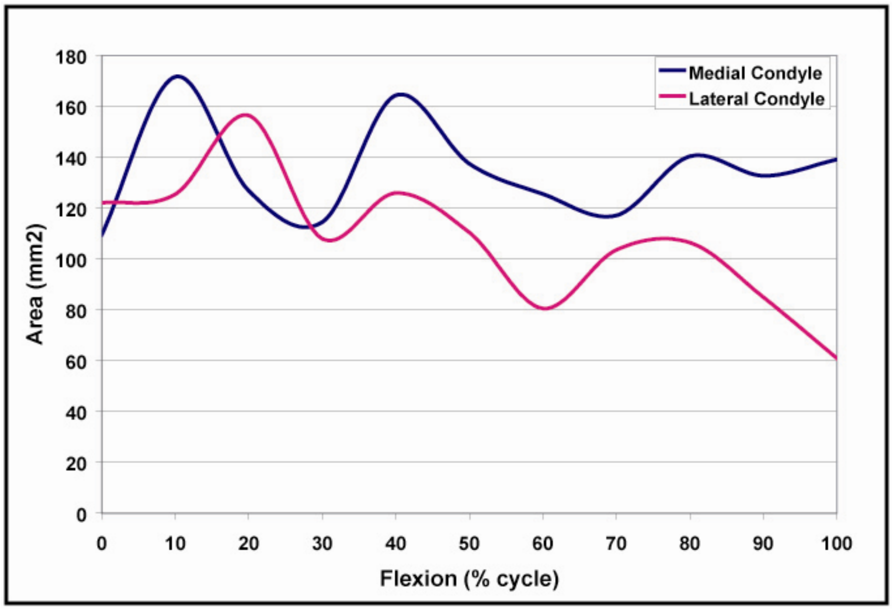

Figure 5-7: The Average Contact Areas in the Mobile Bearing TKA.

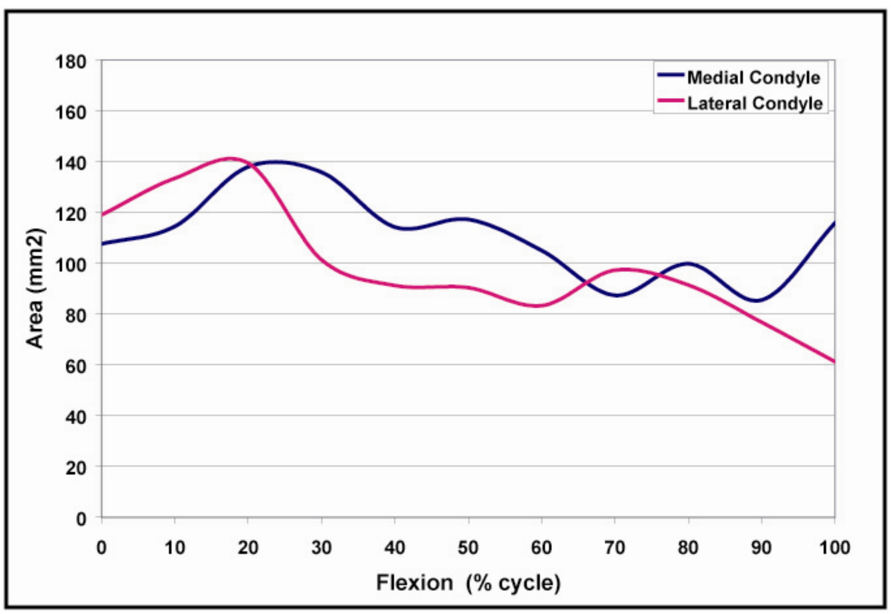

Figure 5-8: The Average Contact Areas in the Fixed Bearing TKA.

5.4 Contact Pressures

The contact pressures for both the mobile and fixed bearing TKA groups increased with the increasing knee flexion. The average maximum medial condylar pressure for the mobile bearing group ranged from 5.49 MPa at 10% of the knee flexion cycle to a maximum value of 25.7 MPa, occurring at maximum knee flexion. The average maximum lateral condylar contact pressure for the mobile bearing group ranged from 3.08 MPa at 20% of the knee flexion cycle to a maximum value of 18.83 MPa, occurring at maximum knee flexion (Figure 5-9).

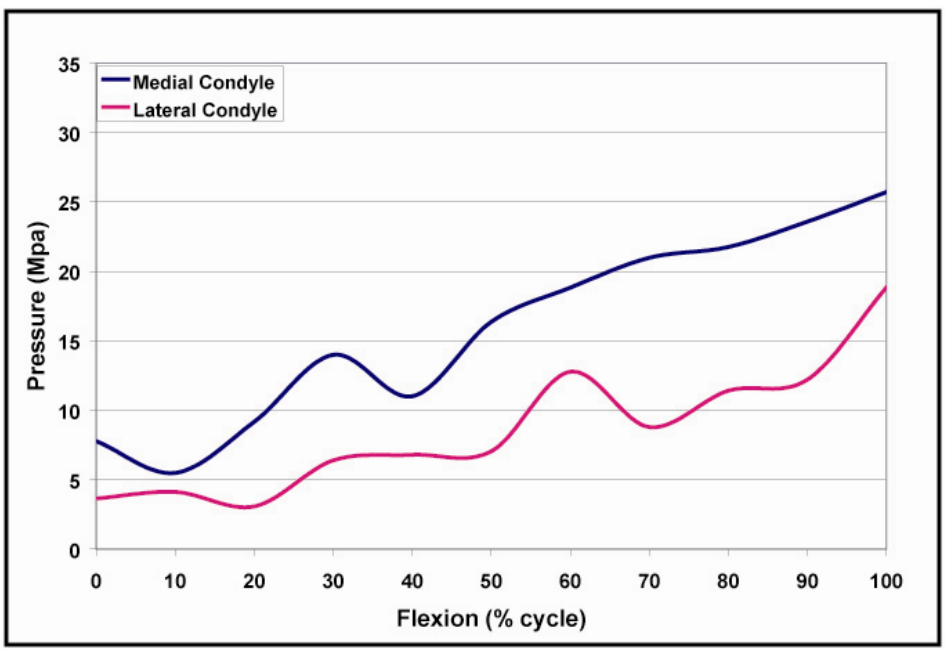

Figure 5-9: The Average Maximum Contact Pressures in the Mobile Bearing TKA.

Although the average maximum lateral condylar contact pressures for the fixed bearing TKA group were similar to the mobile bearing TKA group, ranging from 3.71 MPa at 10% of the knee flexion cycle to 18.36 MPa at maximum knee flexion, the medial condylar contact pressures were greater for the fixed bearing TKA group. The average maximum medial contact pressure for the fixed bearing TKA group started at 12.8 MPa at full extension, increasing rapidly after 40^{o} of knee flexion to a maximum value of 34.38 MPa occurring at 90% of the knee flexion cycle (Figure 5-10).

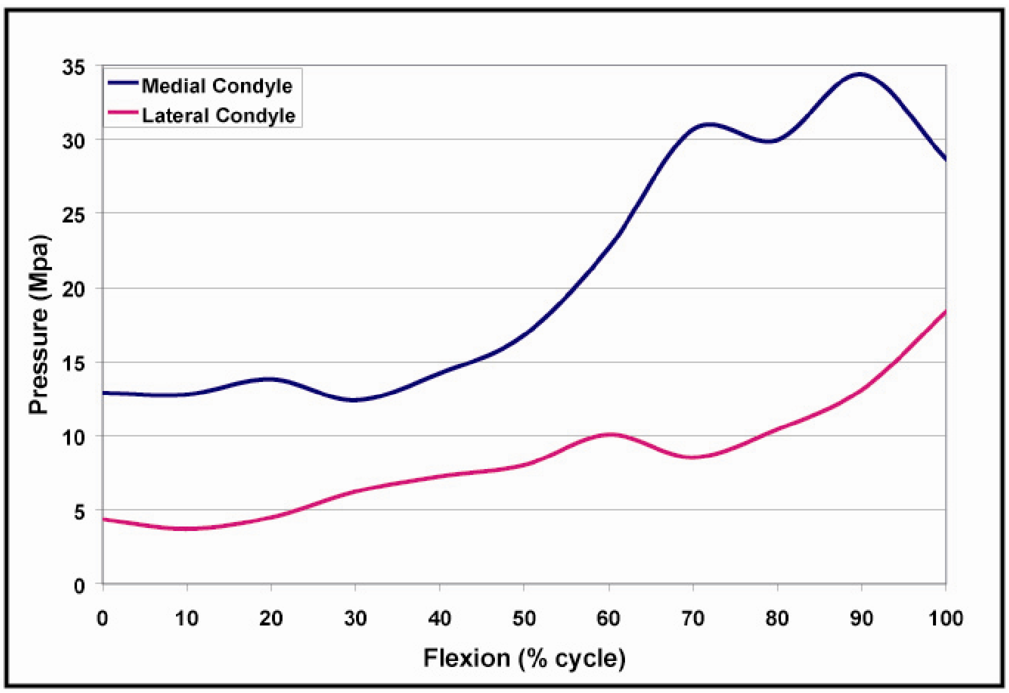

Figure 5-10: The Average Maximum Contact Pressures in the Fixed Bearing TKA.

Chapter 6

Discussion – Analysis of Results

6.1 Introduction

This study describes an in vivo computational method to predict polyethylene contact pressures occurring at the femoro-polyethylene articulation in TKA. This study used the reduction technique of mathematical modeling to calculate in vivo contact forces and solid modeling to calculate in vivo contact areas. This is the first documented study that attempts to model a knee implanted with a TKA and calculates the contact forces on the medial and the lateral sides separately. The overall (sum of medial and lateral) bearing surfaced contact force averaged 3.6BW, which is similar to that obtained in previous studies using telemetry and mathematical modeling (Taylor, 2001; D'Lima, 2005; Komistek, 2005).

6.2 Contact Forces

The bearing surface forces increased with the increase in flexion for all subjects. This is due to the fact that as the knee goes into higher flexion, the forces in the quadriceps increase causing in an increase in the net downward normal force at the femoro-polyethylene interface (Komistek, 2005). The average bearing surface forces on the medial side and the lateral side in the fixed and mobile bearing TKA were similar of similar magnitude. However, the fixed bearing TKA group had slightly higher values, on both the condyles, during the early parts of the flexion cycle (0-25%) compared to the mobile bearing group (Figure 6-1, 6-2). This might be due to the fact that fixed bearing TKA group experienced greater axial rotation during early flexion. Also the similar magnitudes in the forces during higher flexion angles suggest that the additional constraint imposed in the mobile bearing prosthesis, due to its higher conformity in the coronal plane, is offset by the additional rotational degree of freedom it possess. The medial contact force was always higher in magnitude than the lateral contact force. Also, interestingly, for all the subjects (with both fixed and mobile bearing TKA) the contact forces slowly increased at first and then rapidly from round about 40-60% of the flexion cycle (Appendix C). This is the similar range of flexion for which the cam-post mechanism comes in contact and there might be a correlation between the two.

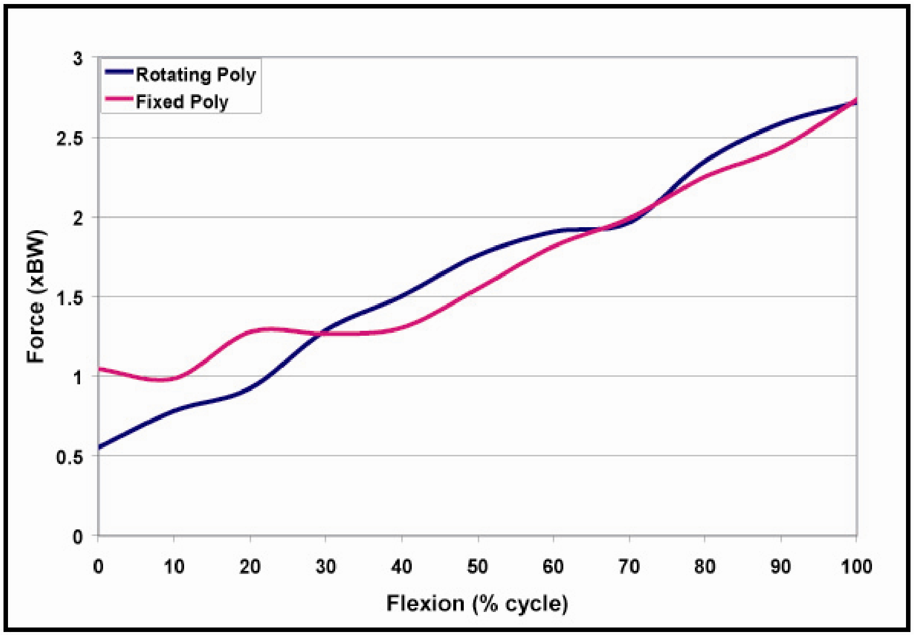

Figure 6-1: Variation of Average Medial Forces with Flexion.

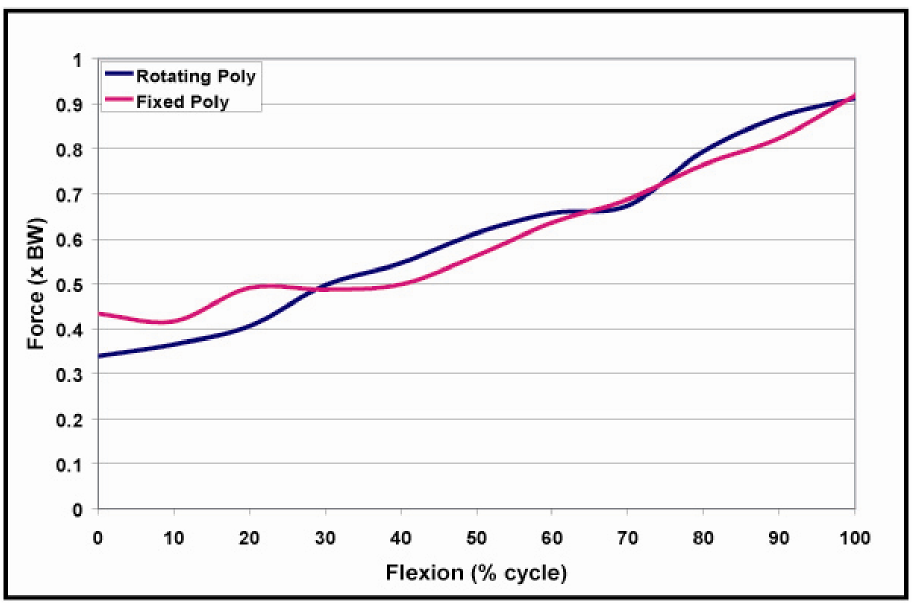

Figure 6-2: Variation of Average Lateral Forces with Flexion.

6.3 Contact Areas

The contact areas for both the implant types demonstrated variable patterns and magnitudes on a subject-to-subject basis (Appendix D). As had been previously hypothesized, the average contact areas, for subjects having a mobile bearing TKA remained higher than those subjects having a fixed bearing TKA, during the majority of the flexion cycle (Figure 6-3, 6-4). This is due to the fact that the mobile bearing has greater conformance than the fixed bearing and this scenario is maintained even throughout flexion due to the ability of the bearing to follow the femoral component in axial rotation. On more interesting fact was that though the medial contact area was pretty consistent throughout flexion, the lateral contact areas decreased with increasing knee flexion and the subjects experienced their lowest contact area value at maximum flexion. As flexion increases, the difference in between the lateral and medial contact forces increases. Since the polyethylene was modeled as viscoelastic, so with increasing flexion the amount of difference in the deformation levels between the medial and the lateral sides also increases. Thus reduction in contact area due to mismatch between the femoral component and the polyethylene gets compensated in the medial side due to higher deformation of the polyethylene but fails to do so in case of the lateral side.

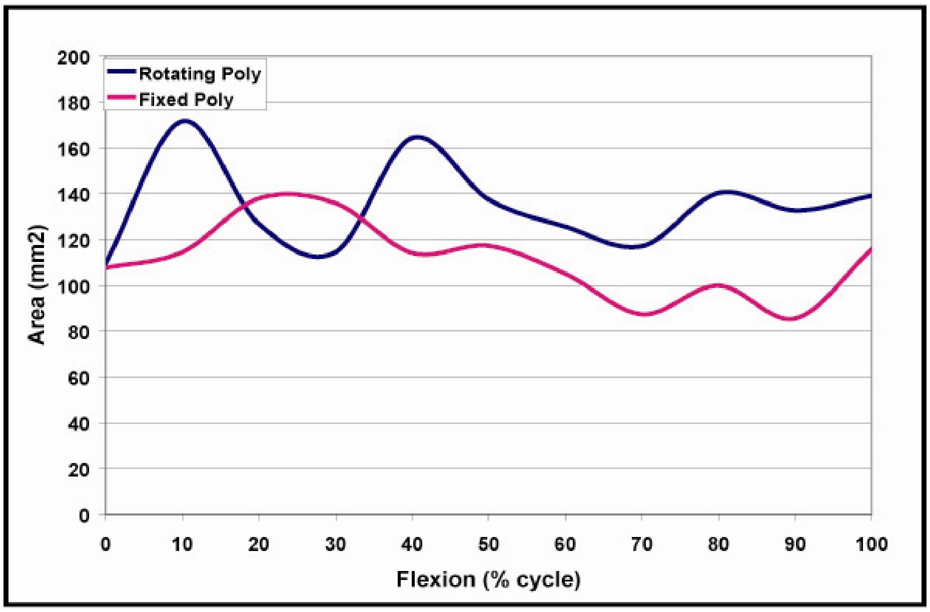

Figure 6-3: Variation of Average Medial Contact Areas with Flexion.

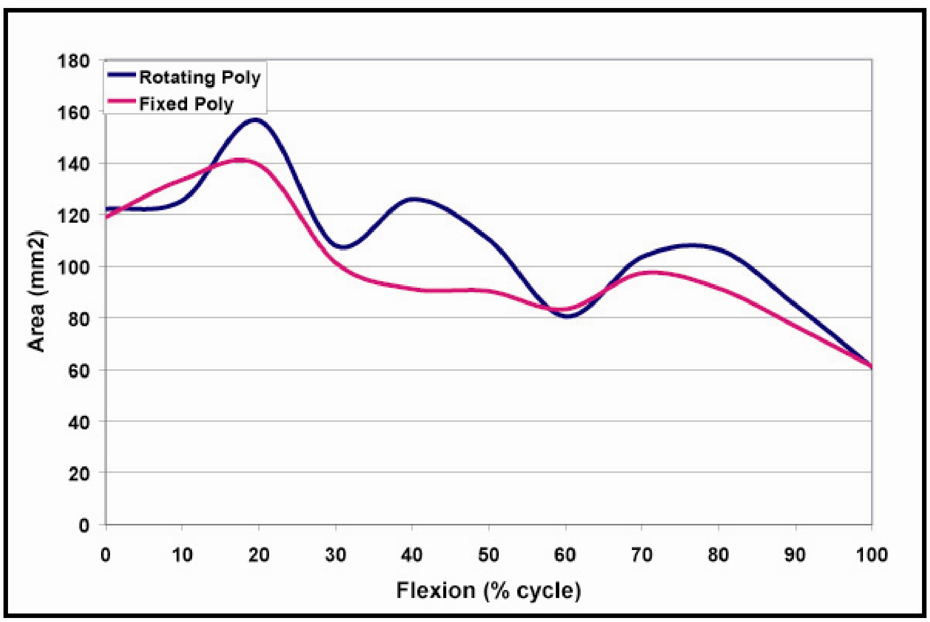

Figure 6-4: Variation of Average Lateral Contact Areas with Flexion.

6.4 Contact Pressures

Both the medial and the lateral average maximum contact pressures increased with the increase in the flexion angle. For the medial side, the average maximum pressure was higher in the fixed bearing than in the mobile bearing (Figure 6-5). This is because the fixed bearing design experienced lesser contact area compared to the mobile bearing while the contact forces in the two were almost similar. Due to similar variation in the lateral contact forces and the lateral contact areas both types of TKA experienced similar maximum average lateral contact pressure (Figure 6-6). Also the medial contact pressure was higher than the lateral contact pressure. This correlates well with the retrieval studies which show that the wear on the medial side is more than the wear on the lateral side (Wasielewski, 1994; Currier, 2005). There were a few cases where the polyethylene contact pressure was more than the yield strength of the polyethylene (generally around 20 – 22 MPa). The highest amount of maximum pressure experienced was about 45 MPa on the medial condyle for a patient implanted with a fixed bearing TKA (Appendix E). This subject also experienced a large amount of axial femoral rotation with respect to the tibia around the same flexion range. This suggests that higher the relative axial rotation of the femur with respect to the polyethylene, higher would be the pressures generated in it. In this regard the mobile bearing design does seem to offer and advantage with respect to the fixed bearing by maintaining a higher area of contact.

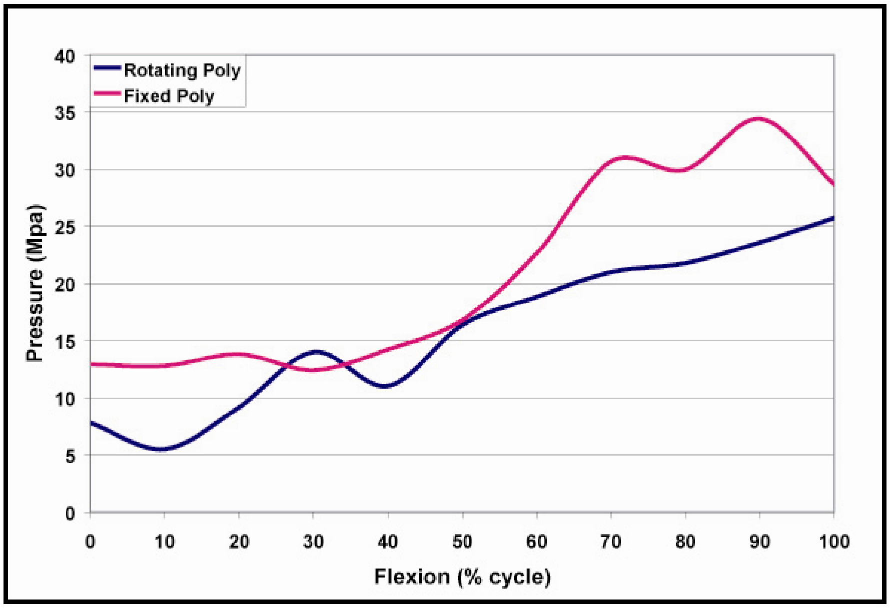

Figure 6-5: Variation of Average Maximum Medial Contact Pressures with Flexion.

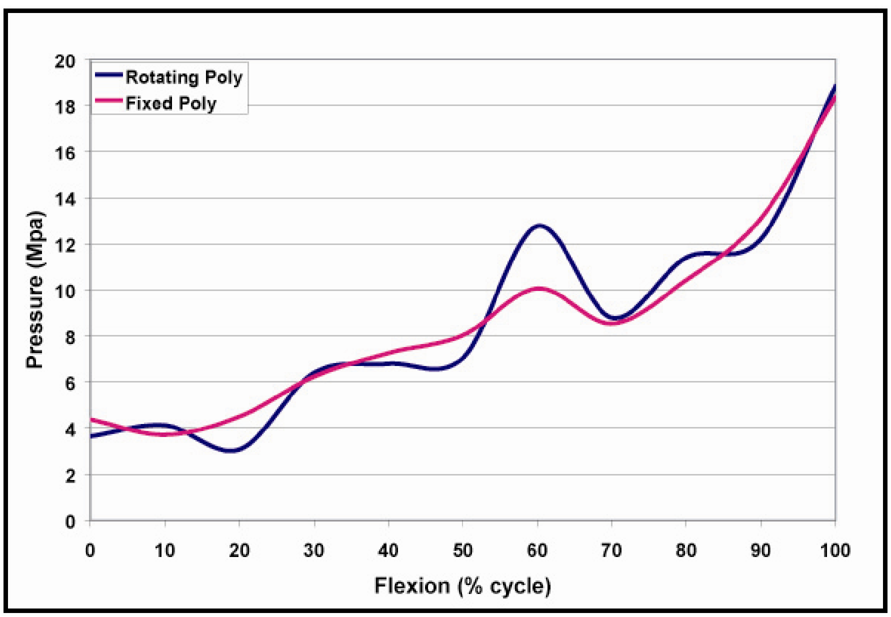

Figure 6-6: Variation of Average Maximum Lateral Contact Pressures with Flexion.

6.5 Conclusions

There exists a great deal of variability in the in-vivo contact forces, contact areas and the contact pressures among all the patients analyzed in this study. This is true even for the patients who had bilateral implants (Appendix C, D, E). This might suggest that in essence no two TKA's are similar and the chief factor to the TKA's performance is the kinematics it experiences. However, there are a few general trends that can be safely concluded from this study:

1. The contact forces (both on the medial and the lateral side) increase with the increase in the flexion, with the medial contact force being higher than the lateral contact force. The difference between the two increases with the increase in flexion.
2. The contact areas are most affected by the relative axial rotation of the femoral component over the polyethylene and the amount of deformation caused in the polyethylene due to the contact forces.
3. The contact pressures also increase with the increase in flexion and the medial contact pressure experienced by the polyethylene is higher than the lateral contact pressure.

Chapter 7

Limitations and Future Work

7.1 Introduction

This was the first computational model that attempted to predict the in-vivo contact forces, contact areas and contact pressures, simultaneously. This original work does have limitations which we intend to eliminate with continuation of work on this project. Some of the limitations in the study include the input parameters used, especially that for the patellar movements and the ground reaction force, some of the assumptions made in the mathematical model to simplify the system, in assuming the interference area as the contact area and finally assuming the maximum contact pressures to be always 1.5 times the average contact pressures.

7.2 Input Collection

The greatest inaccuracy in the input data used in the study was in the use of the ground reaction force data. Since this data was unavailable for each subject, separately collected data for a different subject was used. However, this data was scaled with the individual subject weight and the time they took to complete the activity before being used. Though this results in different magnitudes of the ground reaction force for each subject, however, the nature of variation of the force profile with flexion is similar in all the cases. The ground reaction force depends on the physical characteristics and kinematics, which is unique for each subject, and therefore should not only have differing magnitudes but also have different nature of variations of the profile with the change in flexion. Collecting the force plate data simultaneously while fluoroscoping a subject would be the best way to address this issue.

Another inaccuracy in this study was in the calculation of the patellar motion, which was derived directly from the 2D fluoroscopic images captured in the sagittal plane. The inaccuracy arises from the fact that all these calculations have been based on the projected lengths on the sagittal plane and not the true lengths. Since the patella can rotate in the coronal plane the amount of shortening of the lengths caused by projection also changes. Also due to the axial rotation of the femur and hence the patella, which sits on the femoral groove, the view in the sagittal plane may get obscured. A way to improve the accuracy would be to use biplanar fluoroscopy and derive the true lengths from the projected distances in the two perpendicular planes. However, the use of biplanar fluoroscopy might unacceptably constrain the motion of the patient (Mahfouz, 2003). The best method however would be to use the 3D registration technique on the patella, too. Along with generating correct kinematics, this would also help in correctly determining the contact points of the patella on the femur.

Currently, the lowest point on the femur with respect to an assumed flat tibial surface is used as the contact point. Due to the curvature of the polyethylene insert in both the sagittal and the coronal plane, the actual contact point may not necessarily be the lowest point on the femur. A correlation between the differences caused by this assumption with the actual contact points would help us to address this issue. The best method however, would be to directly modify the algorithm currently used in our 2D to 3D registration technique.

Also instead of relying on previously published anthropometric data, we intend to make use of computed tomography (CT) scans and magnetic resonance imaging (MRI) images to correctly determine the muscle and ligament attachment sites and the size and dimensions of the bones (Komistek, 2005).

7.3 Mathematical Model

One of the greatest simplifications of the model was in neglecting the presence of the cam-spine (cam-post) mechanism which is present in all PS type implants to ensure posterior femoral rollback. In the present study, we determined that these subjects experienced cam-post engagement between 60 and 80 degrees of knee flexion. In our next generation model, we intend to include the effect of the cam-spine mechanism. Inclusion of the cam-spine would necessitate the inclusion of a third point of contact between the femur and the polyethylene and also contact forces associated with it. This would definitely cause a discontinuity in the system which can be easily addressed by breaking up the analysis in two parts – early to mid flexion without the cam-spine contact and mid to late flexion with the cam-spine contact. The future inclusion of cam-post forces should alter both the antero-posterior and medio-lateral forces at the femoro-tibial bearing surface interface.

In order to keep the system determinate, the mathematical model had to neglect muscles and soft tissues and incorporate simplifying assumptions. The quadriceps muscles are the primary extensors in the human body and so would have high amount of force during the flexion of the knee, with values increasing with flexion. This is due to the fact that as the knee flexes, the quadriceps muscle extend more thus causing the force developed in them to increase. The opposite case exists with the knee flexors (hamstring muscles act as the primary flexors while the gastrocnemius muscles help in small amounts). As the flexion angle increases, the tension in them decreases as they start to reduce from their stretched lengths. Thus they should have an effect on the kinetics and the kinematics of the knee, especially during the early part of the flexion, with their effect progressively decreasing with increase in the flexion angle. In our future model, along with the quadriceps, we would like to incorporate the knee flexors (especially, the hamstrings) too.

Moreover, in this model in order to reduce the number of unknowns, we assumed the quadriceps as a single set of muscle having its superior attachment site on the femur. In reality quadriceps is a set of four muscles, three of which attach on the femur and one attaches on the pelvis. So in our future models while incorporating any muscle group we intend to use the individual muscle attachment sites. This would necessitate modeling of the whole leg from the pelvis to the foot. The reduction method that we use, calculates six kinematic terms associated with each rigid body. So the inclusion of more rigid bodies in the form of the pelvis, the fibula and the foot would help us in increasing the number of unknowns we can calculate.

We would also like to incorporate them medial and the lateral collateral ligaments, and the anterior and posterior cruciate ligaments (when present). These soft tissues act as the secondary stabilizers to the knee and so forms an integral part of the system. We want to incorporate them as known quantities instead of unknowns. We intend to do this by modeling them as extensions springs (Mommersteeg, 1997; Abdel-Rahman, 1998). This can be done by studying their visco-elastic behavior and deriving the value of the spring constant from their stress-strain relationship. By measuring the distances of their attachment sites we can obtain their passive lengths and the strain developed in them, which we can use to calculate the forces generated in them. Another important factor that we intend to take into account is the wrapping of muscles and ligaments around the bones. Wrapping not only causes the effective length of the soft tissues to decrease and change the line of action of the forces generated in them but also results in additional forces acting on the bones at the region where they wrap.

Finally, we intend to incorporate the rotation of the femur in the coronal plane which this current model neglects. The femur has been found to rotate in the coronal plane causing one of the condyles to lift off (Dennis, 2003; Komistek, 2004). Lift off causes the contact forces to increase dramatically as the whole contact force acts on one condyle instead of two. This creates the same problem of discontinuity as exists with the cam spine contact. This is because the number of contact points would vary with time depending on whether there is lift off or not. We intend to address this issue by introducing additional conditional statements in the code for the mathematical model.

7.4 Deformation Model

This current study used uniaxial compression data to determine the deformation of the polyethylene. Also the interference areas between the polyethylene insert and the femoral component, derived from the assembly of the 3D CAD models, was used to determine the contact areas. Finally the average pressure was multiplied by a factor of 1.5 to calculate the peak contact pressure (Similar to the peak Hertzian stress calculation). Though simple to implement, this method does not take into account the multiaxial behavior of polyethylene and the effect of deformation of one point on the adjacent points. Moreover, this method might not correctly estimate the contact area. These factors might add up to affect the final values of the contact pressures and stresses which we intend to address by the use of finite element analysis. In our future efforts, we plan to incorporate a more exact deformation model of polyethylene that will utilize more parameters. In order to simulate the mechanical behavior of UHWMPE used in orthopedic implants models like the Arruda-Boyce model, Hasan-Boyce model, Bergstrom-Boyce model and Hybrid models have been developed. It has been found that the Hybrid model performs the best in predicting the visco-elastic behavior of modern cross linked UHMWPE (Bergstrom, 2004). We would like to extend this model and also would like to incorporate the factors like creep, deterioration due to shelf life and the aging of the polyethylene due to its operation within the human body.

7.5 Conclusion

Once this current system is perfected we intend to integrate all the individual elements to work in a seamless manner with minimal human interaction. This will not only result in the generation of faster results but will also reduce the errors associated with the human interaction. Finally, by incorporating a wear model which takes into account factors like kinematics, kinetics and material properties, we intend to extend the capability of this system in order to serve as a reliable predictor of wear in polyethylene implants

REFERENCES

References – Websites

1. Ahlfeld Sports Medicine Orthopaedic Centre website.” *Patient Education – Knee Joint Anatomy*”. Visited on 03-14-2005.
   Link :- http://yoursportsdoc.com/pages-subsections/ht_k_anat.html

2. New York Online Access to Health (NAOH) website. “*Total Knee Replacement – The Surgery*”. Link to BUPA foundation. Visited on 03-14-2005.
   Link to NAOH :- http://www.noah-health.org/en/bjm/knee/care/tkr/
   Link to BUPA :-
   http://www.bupa.co.uk/health_information/pdfs/healthy_living/physical/knee/knee_brochure.pdf

3. New York Online Access to Health website. “*Total Knee Replacement – The Surgery*”. Link to AAOS. Visited on 03-14-2005.
   Link to NAOH :- http://www.noah-health.org/en/bjm/knee/care/tkr/
   Link to AAOS :-
   http://orthoinfo.aaos.org/fact/thr_report.cfm?Thread_ID=279&topcategory=Knee

4. American Academy of Family Physicians website. “*Acute Knee Injuries: Use of decision rules for selective radiograph ordering*”. Visited 03-16-2005.
   Link :-http://www.aafp.org/afp/991201ap/2599.html

5. SEER’s Training website. “*Planes of the Body*”. Visited 03-14-2005.
   Link :- http://training.seer.cancer.gov/module_anatomy/unit1_3_terminology2_planes.html

References – Publications

1. Abdel-Rahman EM, Hefzy MS, 1998: "*Three-Dimensional Dynamic Behaviour of the Human Knee Joint under Impact Loading*". Medical Engineering Physics 20, 276-290.
2. Ahmed AM, Burke DL, 1983: "*In Vitro Measurement of Static Pressure Distribution in Synovial Joints – Part I: Tibial Surface of the Knee*". Journal of Biomechanical Engineering 105, 216-225.
3. Alexander EJ, Andriacchi TP, 2001: "*Correcting for Deformation in Skin-Based Marker Systems*". Journal of Biomechanics 34, 355-361.
4. Anderson FC, Pandy MG, 2001: "*Dynamic Optimization of Human Walking*". Journal of Biomechanical Engineering 123, 381-190.
5. Andriacchi TP, Alexander EJ, 2000: "*Studies of Human Locomotion: Past Present and Future*." Journal of Biomechanics 33, 1217-1224.
6. Andriacchi TP, Alexander EJ, Toney MK, Dyrby CO, Sum JA, 1998: "*A Point Cluster Technique Method for In Vivo Motion Analysis: Applied to a Study of Knee Kinematics*". Journal of Biomechanical Engineering 120, 743-749.
7. Antonsson EK, Mann RW, 1989: "*Automated 6-DOF Kinematic Trajectory Acquisitions and Analysis*". ASME Journal of Dynamic Systems Measurement and Control 111, 31-39.
8. ASTM D695-02a, 2002: "*Standard Test Method for Compressive Properties of Rigid Plastics*". West Conshohocken, PA. American society for testing and materials.

9. Ateshian GA, Kwak SD, Soslowsky LJ, Mow VC, 1994: "*A Stereophotogrammetric Method for Determining In Situ Contact Areas in Diarthrodial Joints, a Comparison with Other Methods*". Journal of Biomechanics 27, 111-124.

10. Baker DA, Hastings RA, Pruitt L, 2000: "*Compression and Tension Fatigue Resistance of Medical Grade Ultra-High Molecular Weight Polyethylene: The Effect of Morphology, Sterilization, Aging and Temperature*". Polymer 41(2), 795-808.

11. Banks SA, Hodge WA, 1996: "*Accurate Measurement of Three-Dimensional Knee Replacement Kinematics using Single Plane Fluoroscopy*". IEEE Transactions on Biomedical Engineering 43(6), 638-649.

12. Bankston AB, Keating EM, Ranawat CS, Faris PM, Ritter MA, 1995: "*Comparison of Polyethylene Wear in Machined versus Moulded Polyethylene*". Clinical Orthopaedics and Related Research 317, 37-43.

13. Bartel DL, Bicknell VL, Ithaca, Wright TM, 1986: "*The Effect of Conformity, Thickness and Material on Stresses in Ultra-High Molecular Weight Components for Total Joint Replacement*". Journal of Bone and Joint Surgery (Am) 68-A(7), 1041-1051.

14. Bartel DL, Burstein AH, Toda MD, Edwards Dl, 1985: "*The Effect of Conformity and Plastic Thickness on Contact Stresses in Metal Backed Plastic Implants*". Journal of Biomechanical Engineering 107, 193-199.

15. Bartel DL, Rawlinson JJ, Burstein AH, Ranawat CS, Flynn WF, 1995: "Stresses in Polyethylene Components of Contemporary Total Knee Replacements". Clinical Orthopaedics and Related Research 317, 76-82.

16. Bell CJ, McEwen HMJ, Barnett PI, Farrar R, Stone M, Fisher J, 2003: "*Comparison of Wear in Fixed and Mobile Bearing Knee Designs*". Transactions 49th Orthopaedic Research Society, New Orleans, 1403.

17. Bellare A, Cohen RE, 1996: "*Morphology of Rod Stock and Compression Moulded Sheets of Ultra-High Molecular Weight Polyethylene used in Orthopaedic Implants*". Biomaterials 17, 2325-2333.

18. Bergstrom JS, Rimnac CM, Kurtz SM, 2004: "*An Augmented Hybrid Model for Simulation of Unloading and Cyclic Loading Behavior of Conventional and Highly Crosslinked UHMWPE*". Biomaterials 25, 2171-2178.

19. Black JD, Matejczyk MB, Greenwald AS, 1981: "*Reversible Cartilage Staining Technique for Defining Articular Weight Bearing Surfaces*". Clin Orthop 159, 265-267.

20. Blunn GW, Walker PS, Joshi A, Hardinge K, 1991: "*The Dominance of Cyclic Sliding in Producing Wear in Total Knee Replacements*". Clinical Orthopaedics and Related Research 273, 253-260.

21. Brand RA, Crowninshield RD, Wittock CE, Pedersen DR, Clark CR, Vankrieken FM, 1982: "*A Model of Lower Extremity Muscular Anatomy*". Journal of Biomechanics 104(4), 304-310.

22. Buechel FF, Pappas MJ, Makris G, 1991: "*Evaluation of Contact Stress in Metal Backed Patellar Replacements*". Clinical Orthopaedics and Related Research 273: 190-197.

23. Bull AMJ, Amis AA, 1998: "*Knee Joint Motion: Description and Measurement*". Proceedings of Institution of Mechanical Engineers 212(H), 357-371.

24. Burny F, Donkerwolcke M, Moulart F, Bourgois R, Puers R, Van Schuylenberg K, Barbosa M, Paiva O, Rodes F, Beguert JB, Lawes P, 2000: "*Concept Design and Fabrication of Smart Orthopedic Implants*". Medical Engineering Physics 22, 469-479.

25. Cappozzo A, Catani F, Della CU, Leardini A, 1993 : "*Calibrated Anatomical Systems Technique in 3-D Motion Analysis Assessment of Artifacts*". Proceedings of the International Symposium on 3D Analysis of Human Movement. Poiters, France, Jul 1, 45-52.

26. Chao EYS, 1980: "*Justification of Triaxial Goniometry for the Measurement of Joint Rotation*". Journal of Biomechanics 13, 989-1006.

27. Collier JP, Mayor MB, McNamara JL, 1991: "*Analysis of the Failure of 122 Polyethylene Inserts from Uncemented Tibial Knee Components*". Clinical Orthopaedics and Related Research 273, 232-242.

28. Colwell CW Jr., Patil S, Steklov N, Slamin J, Pulido P, D'Lima DD, 2005: "*An Electronic Knee Prosthesis: Measurements of Tibial Forces In Vivo*". Scientific Exhibit SE082, 47th AAOS conference, Washington DC.

29. Conditt MA, Thompson MT, Usrey MM, Ismaily SK, Noble PC, 2005: "*Backside Wear of Polyethylene Tibial Inserts: Mechanism and Magnitude of Material Loss*". Journal of Bone and Joint Surgery 87, 326-331.

30. Currier JH, Bill MA, Mayor MB, 2005: "*Analysis of Wear Asymmetry in a Series of 94 Retrieved Polyethylene Tibial Bearing*". Journal of Biomechanics 38, 367-375.

31. D'Lima DD, Chen PC, Colwell CW, 2001: "*Polyethylene Contact Stresses, Articular Congruity and Knee Alignment*". Clinical Orthopaedics and Related Research 393, 232-238.

32. D'Lima DD, Townsend CP, Arms SW, Morris BA, Colwell CW Jr., 2005: "*An Implantable Telemetry Device to Measure Intra-Articular Tibial Forces*". Journal of Biomechanics 38, 299-304.

33. DeHeer DC, Hillberry BM, 1992: "*The Effect of Thickness and Nonlinear Material Behavior on Contact Stresses in Polyethylene Tibial Components*". Transactions of the 38th Annual Meeting, Orthopaedic Research Society.

34. deLeva P, 1996: "*Adjustments to Zatsiorski-Sleluyanov's Segment Inertial Parameters*". Journal of Biomechanics 29, 1223-1230.

35. Dennis DA, Komistek RD, Mahfouz MR, 2003: "*In Vivo Fluoroscopic Analysis of Fixed Bearing Total Knee Replacements*". Clinical Orthopaedics 410, 114-130.

36. Dennis DA, Komistek RD, Mahfouz MR, Walker SA, Haas BD, 2005b: *In Vivo Determination of Axial Rotation: A Multicentre Analysis of 1027 Knees*". Scientific Exhibit SE048, 47th AAOS Conference, Washington DC.

37. Dennis DA, Mahfouz MR. Komistek RD, Hoff W, 2005a: "*In Vivo Determination of Normal and Anterior Cruciate Ligament Deficient Knee Kinematics*". Journal of Biomechanics 38, 241-253.

38. DesJardins JD, Walker PS, Haider H, Perry J, 2000: "*The use of a Force-Controlled Dynamic Knee Simulator to Quantify the Mechanical Performance of Total Knee Replacement Designs during Functional Activity*". Journal of Biomechanics 33, 1231-1242.

39. Fehring TK, Odum S, Griffin WL, Mason JB, Naduad M, 2001: "*Early Failures in Total Knee Arthroplasty*". Clinical Orthopaedics and Related Research 392, 315-318.

40. Fehring TK, Valadie AL, 1994: "*Knee Instability after Total Knee Arthroplasty*". Clinical Orthopedics 299, 157-162.

41. Fisher J, Dowson D, 1991: "*Tribology of Total Artificial Joints*". Proceedings of the Institution of Mechanical Engineers Part H 205, 73-79.

42. Fregly BJ, Sawyer WG, Harman MK, Banks SA, 2005: "*Computational Wear Prediction of a Total Knee Replacement from In Vivo Kinematics*". Journal of Biomechanics 38, 305-314.

43. Gebhard JS, Kilgus DJ, 1990: "*Dislocation of a Posterior Stabilized Total Knee Prosthesis: A report of Two Cases*". Clinical Orthopedics 254, 225-228.

44. Godest AC, Beaugonin M, Haug E, Taylor M, Gregson PJ, 2002: "*Simulation of a Knee Joint Replacement during Gait Cycle using Explicit Finite Element Analysis*". Journal of Biomechanics 35, 267-275.

45. Godest AC, deCloke S, et.al., 2000: "*A Computational Model for the Prediction of Total Knee Replacement Kinematics in the Sagittal Plane*". Journal of Biomechanics 33, 435-442.

46. Goodfellow J, O'Connor J, 1978: "*The Mechanics of the Knee and Prosthesis Design*". Journal of Bone and Joint Surgery (Br) 60-B(3), 358-369.

47. Greenwald AS, O'Connor JJ, 1971: "*The Transmission of Load through the Hip Joint*". Journal of Biomechanics 4, 507-528.

48. Haider H, Walker PS, 2005: “*Measurements of Constraint of Total Knee Replacement*”. Journal of Biomechanics 38, 341-348.

49. Halloran JP, Petrella AJ, Rullkoetter PJ, 2005: “*Explicit Finite Element Modeling of Total Knee Replacement Mechanics*”. Journal of Biomechanics 38, 323-331.

50. Harman M, DesJardins J, Banks S, Benson L, LaBerge M, Hodge W, 2001: “*Damage Patterns on Polyethylene Inserts After Retrieval and After Wear Simulation*”. Proceedings 47th Orthopaedic Research Society, 1003.

51. Harris ML, Morberg P, Bruce WJM, Walsh WR, 1999: “*An Improved Method for Measuring Tibiofemoral Contact Areas in Total Knee Arthroplasty: A Comparison of K-scan sensor and Fuji film*”. Journal of Biomechanics 32, 951-958.

52. Heim CS, Postak PD, Greenwald AS, 1996: “*Chapter 34: Factors Influencing the Longevity of UHMWPE Tibial Components*”. AAOS Instructional Course Lectures 45, 303-312.

53. Heim CS, Postak PD, Plaxion NA, Greenwald AS, 2001: “*Classification of Mobile Bearing Knee Designs: Mobility and Constraint*”. Journal of Bone and Joint Surgery 83-A, 22-32.

54. Heimke G, Leyen S, Willmann G, 2002: “*Knee Arthroplasty: Recently Developed Ceramics Offer New Solution*”. Biomaterials 23, 1539-1551.

55. Hertz H, 1881: “*Uebes die Beruehrung fester elastische Koerper (On the Contact of Elastic Solids)*”. J. fues. Reine und angewandte Mathematik 92, 156-171.

56. Hoff WA, Komistek RD, Dennis DA, Gabriel SM, Walker SA, 1998: “*Three-Dimensional Determination of Femoral-Tibial Contact Positions under In Vivo Conditions using Fluoroscopy*”. Clinical Biomechanics 13, 455-472.

57. Holden JP, Orsini JA, Holden SJ, 1994: “*Estimates of Skeletal Motion – Movement of Surface Mounted Targets Relative to Bone during Gait*”. Proceedings of the Thirteenth Southern Biomedical Engineering Conference, Washington DC, April 16.

58. Holden JP, Orsini JA, Siegel KL, Kepple TM, Gerber LH, Stanhope SJ, 1997: "*Surface Movement Errors in Shank Kinematics and Knee Kinetics during Gait*". Gait and Posture 3, 217-227.

59. Hood RW, Wright TM, Burstein AH, 1983: "*Retrieval Analysis of Total Knee Prostheses: A Method and its Application to 48 Total Condylar Prostheses*". Journal of Biomedical Materials Research 17, 829-842.

60. Howling GI, Barnett PI, Tipper JL, Stone MH, Fisher J, Ingham E, 2001. "*Quantitative Characterization of Polyethylene Debris Isolated from Periprosthetic Tissue in Early Failure Knee Implants and Early and Late Failure of Charnley Hip Implants*". Journal of Biomedical Materials Research 58, 415-420.

61. Huang CH, Ma HM, Liau JJ, Ho FY, Cheng CK, 2002a: "*Late Dislocation of Rotating Platform in New Jersey Low Contact Stress Prosthesis*". Clinical Orthopaedics 405, 189-194.

62. Huang CH, Ma HM, Liau JJ, Ho FY, Cheng CK, 2002b: "*Osteolysis in Failed Total Knee Arthroplasty: A Comparison of Mobile Bearing and Fixed Bearing Knees*". Journal of Bone and Joint Surgery (Am) 84, 2224-2229.

63. Huston RL, 1990: "*Multibody Dynamics*". Butterworth-Heinemann, Stoneham, MA, USA.

64. Insall JN, Dorr LD, Scott RD, Scott WN, 1989: "*Rationale of the Knee Society Clinical Rating System*". Clinical Orthopaedics and Related Research 248, 13-14.

65. Jacobs JJ, Shanbhag A, Glant TT, Black J, Galante JO, 1994: "*Wear Debris in Total Knee Replacements*". Journal of the American Academy of Orthopaedic Surgeons 2, 212-220.

66. Kane, T.R. and Levinson D.A, 1985: "*Dynamics: Theory and applications*". McGraw-Hill, New York, USA.

67. Karrholm J, 1989: "*Roentgen Stereophotogrammetry, Review of Orthopaedic applications*". Acta Orhtopaedics Scandinavica 60(4), 491-503.

68. Kauffman KR, Kovacevic N, Irby SE, Colwell CW, 1996: "*Instrumented Implant for Measuring Tibiofemoral Forces*". Journal of Biomechanics 29, 667-671.

69. Kennedy FE, Currier JH, PLumet S, Duda JL, Gestwick DP, Collier JP, Currier BH, DuBourg MC, 2000: "*Contact Fatigue Failure of UHMWPE Bearing Components of Knee Prosthesis*". ASME Journal of Tribology 122, 332-339.

70. Komistek RD, Dennis DA, Mabe JA, Walker SA, 2000: "*An In Vivo Determination of Patellofemoral Contact Positions*". Clinical Biomechanics 15, 29-36.

71. Komistek RD, Dennis DA, Mahfouz MR, Walker SA, Outten J, 2004: "*In Vivo Polyethylene Bearing Mobility is Maintained in Posterior Stabilized Total Knee Arthroplasty*". Clinical Orthopaedics and Related Research 428, 207-213.

72. Komistek RD, Kane TR, Mahfouz MR, Ochoa JA, Dennis DA, 2005: "*Knee Mechanics: A Review of Past and Present Techniques to Determine In Vivo Loads*". Journal of Biomechanics 38, 215-228.

73. Komistek RD, Stiehl JB, Dennis DA, 1998: "*Mathematical Model of the Lower Extremity Joint Reaction Forces using Kane's Method of Dynamics*". Journal of Biomechanics 31, 185-189.

74. Kurosawa H, Fukubayashi T, Nakajima H, 1980: "*Load Bearing Mode of the Knee Joint: Physical Behavior of the Knee Joint with or without the Menisci*". Clinical Orthopaedics 149, 283-290.

75. Kurtz SM, Villarraga ML, Herr MP, Bergstrom JS, Rimnac CM, Edidin AA, 2002: "*Thermomechanical Behavior of Virgin and Highly Crosslinked Ultra-High Molecular Weight Polyethylene used in Total Joint Replacements*". Biomaterials 23, 3681-3697.

76. Kuster MS, Stachowaik GW, 2002: "*Factors Affecting Polyethylene Wear in Total Knee Arthroplasty*". Orthopedics 25(2), 235-247.

77. LaFortune MA, Cavanagh PR, Sommer HJ, Kalenak A, 1992: "*Three-Dimensional Kinematics of the Human Leg During Walking*". Journal of Biomechanics 25, 347-357.

78. Laurent MP, Johnson TS, Yao JQ, Blanchard CR, Crownshield RD, 2003: "*In Vitro Lateral versus Medial Wear of a Knee Prosthesis*". Proceedings 49th Orthopaedic Research Society, New Orleans, 1321.

79. Lewis G, 1998: "Contact Stress at Articular Surfaces in Total Joint Replacements: Analytical and Numerical Methods". Journal of Biomedical Materials.

80. Li S, Burnstein AH, 1994: "*Ultra-High Molecular Weight Polyethylene: The Material and its use in Total Joint Implants*". Journal of Bone and Joint Surgery 76-A, 1080-1090.

81. Liau JJ, Cheng CK, Huang CH, Lo WH, 2002: "*The Effect of Malalignment on Stresses in Polyethylene Component of Total Knee Prostheses – A Finite Element Analysis*". Clinical Biomechanics 17, 140-146.

82. Lu TW, O'Connor JJ, 1999: "*Bone Position Estimation from Skin Marker Coordinates using Global Optimization with Joint Constraints*". Journal of Biomechanics 32, 129-134.

83. Lu TW, O'Connor JJ, Taylor SJG, Walker PS, 1998: "*Validation of a Lower Limb Model with In Vivo Femoral Forces Telemetered from Two Subjects*". Journal of Biomechanics 31, 63-69.

84. Lu TW, Taylor SJG, O'Connor JJ, Walker PS, 1997: "*Influence of Muscle Activity on the Forces in the Femur: An In Vivo Study*". Journal of Biomechanics 30, 1101-1106.

85. Lucchetti L, Cappozzo A, Capello A, Della CU, 1998: "*Skin Movement Artifact Assessment and Compensation in the Estimation of Knee Joint Kinematics*". Journal of Biomechanics 31, 977-984.

86. Machan S, 2004: "*Finite Element Analysis of Polyethylene Stresses in Total Knee Replacements*". PhD Dissertation, University of Sydney, Sydney, Australia.

87. Mahfouz MR, Hoff WA, Komistek RD, Dennis DA, 2003: "*A Robust Method for Registration of Three-Dimensional Knee Implant Models to Two-Dimensional Fluoroscopy Images*". IEEE Transactions on Medical Imaging 22(12), 1561-1574.

88. Matthews LS, Goldstein SAA, Kaufer H, 1985: "*Experiences with Three Distinct Types of Total Knee Arthroplasty*". Clinical Orthopedics 192, 97-107.

89. McEwen HMJ, Barnett PI, Bell CJ, Farrar R, Auger DD, Stone MH, Fisher J, 2005: "*The Influence of Design, Materials and Kinematics on the In Vitro Wear of Total Knee Replacements*". Journal of Biomechanics 38, 357-365.

90. McKellop H, Shen FW, Lu B, Campbell P, Salovey R, 1999: "*Development of an Extremely Wear Resistant Ultra High Molecular Weight for Total Hip Implants*". Journal of Orthopaedic Research 17, 157-167.

91. Mikosz RP, Andriacchi TP, Andersson GB, 1988: "*Model Analysis of Factors Influencing the Prediction of Muscle Forces at the Knee*". Journal of Orthopaedic Research 6, 205-214.

92. Mommersteeg TJA, Huiskes R, Blankevoort L, Kooloos JGM, Kauer JMG, 1997: "*An Inverse Dynamics Modeling Approach to Determine the Restraining Function of the Human Knee Bundles*". Journal of Biomechanics 30(2), 139-146.

93. Moreland JR, 1988: "*Mechanisms of Failure in Total Knee Arthroplasty*". Clinical Orthopaedics and Related Research 226, 49-64.

94. Morra E, Postak B, Greenwald AS, 1998: "*The Influence of Mobile Bearing Knee Geometry on the Wear of UHMWPE Tibial Inserts: A finite element study*". AAOS.

95. Morris BA, D'Lima DD, Slamin J, Kovacevic N, Arms SW, Townshed CP, Colwell CW, 2001: "*e-knee: Evolution of the Electronic Knee Prosthesis*". Journal of Bone and Joint Surgery 83A (suppl 2 part 2), 62-66.

96. Muratoglu OK, Perinchief RS, Bragdon CR, O'Connor DO, Konrad R, Harris WH, 2003: "*Metrology to Quantify Wear and Creep of Polyethylene Tibial Knee Inserts*". Clinical Orthopaedics 410, 155-164.

97. Murphy MA, 1990: "*Geometry and the Kinematics of the Normal Human Knee*". PhD Dissertation, MIT, Cambridge. MA.

98. Nilsson KG, Karrholm J, Linder L, 1995: "*Femoral Component Migration in Total Knee Arthroplasty: Randomized Study Comparing Cemented and Uncemented Fixation of the Miller-Galante Design*". Journal of Orthopaedic Research 13(3), 347-356.

99. Nordin M, Frankel VH, 2001: "*Basic Biomechanics of the Musculoskeletal System*". Lippincott Wiliams and Wilkins, Philadelphia, 2nd Edition, Chapter 7, 177-201.

100. Oakeshott R, Stiehl BJ, Komistek RA, Anderson DT, Haas BD, 2003: "*Kinematic Analysis of a Posterior Cruciate Retaining Mobile-Bearing Total Knee Arthroplasty*". Journal of Arthroplasty 18, 1029-1037.

101. Ochoa JA, Sommerich RE, Zalenski EB, 1993: "*Application of an Innovative Experimental Method to Characterize Contact Mechanics of Total Joint Replacements*". Proceedings 39th Annual Orthopaedic Research Society, San Francisco, California.

102. Paul JP, 1965: "*Bio-engineering Studies of the Forces Transmitted by Joints. Engineering Analysis*". In: Kenedi, R.M. (ed.), Biomechanics and Related Bio-Engineering Topics. Pergamon Press, Oxford, 369-380.

103. Paul JP, 1976: "*Approaches to Design: Force Actions Transmitted by Joints in the Human Body*". Proceedings of the Royal Society of London 192, 163-172.

104. Piazza SJ, Delp SL, 2001: "*Three-Dimensional Dynamic Simulation of Total Knee Replacement Motion during a Step-Up Task*". Journal of Biomechanical Engineering 123, 599-606.

105. Pugh JW, Rose RM, Radin EL, 1973: "*A Structural Model for the Mechanical Behavior of Trabecular Bone*". Journal of Biomechanics 6, 657-670.

106. Ranawat CS, Komistek R, Dennis DA, 2004: "*In Vivo Kinematics for Fixed and Mobile Bearing Posterior Stabilized Knee Prosthesis*". Clinical Orthopaedics 418: 184-190.

107. Rand JA, Trousdale RT, Ilstrup DM, Harmsen WS, 2003: "*Factors Affecting the Durability of Primary Total Knee Prosthesis*". Journal of Bone and Joint Surgery (Am) 85-A (2), 259-265.

108. Rao AR, Engh GA, Collier et.al, 2002.: "*Tibial Interface Wear in Retrieved Total Knee Components and Correlation with Modular Insert Motion*". Journal of Bone and Joint Surgery (Am) 84, 1849-1855.

109. Rawlinson J, Furman B, Li S, Bartel D, 2001: "*Kinematics, Stresses and Damage from a TKR Simulator and a Finite Element Model*". Transactions of the 47th Annual Meeting of the Orthopaedic Research Society.

110. Rullkoetter PJ, Gabriel SM, Colleran DP, et.al., 1999: "*The Relationship between Contact Stress and Contact Area with Implications for TKR Evaluation and Design*". Program and Abstracts from the 45th Annual meeting of the Orthopaedic Research Society, Anaheim, California.

111. Sathasivam S, Walker PS, 1998: "*A Computer Model to Predict Subsurface Damage in Tibial inserts on Total knees*". Journal of Orthopaedic Research 16, 564-571.

112. Sathasivam S, Walker PS, Campbell PA, Rayner K, 2001: "*The Effect of Contact Area on Wear Relation to Fixed Bearing and Mobile Bearing Replacements*". Journal of Biomedical Materials Research 58, 282-290.

113. Sati M, deGuise JA, Larouche S, Drouin G., 1996: "*Quantitative Assessment of Skin-Bone Movement at the Knee*". The Knee 3, 121-138.

114. Scuderi GR, Insall JN, Windsor RE, Moran MC, 1989: "*Survivorship of Cemented Knee Replacements*". Journal of Bone and Joint Surgery (Br) 71, 798-803.

115. Seireg A, Arvikar RJ, 1973: "*The Prediction of Muscular Load Sharing and Joint Forces in the Lower Extremities during Walking*". Journal of Biomechanics 6, 89-102.

116. Sharkley PF, Hozack WJ, Rothman RH, Shastri S, Jacoby SM, 2002: "*Why are Total Knee Arthroplasties Failing Today ?*" Clinical Orthopaedics and Related Research 404, 7-13.

117. Spoor CW, Veldpas FE, 1988: "*Rigid Body Motion Calculated from Spatial Coordinates of Markers*". Journal of Biomechanics 13, 391-393.

118. Stewart T, Jin ZM, Shaw D, Auger DD, Stone M, Fisher J, 1995: "*Experimental and Theoretical Study of the Contact Mechanics of Five Total Knee Joint Replacements*". Proceedings of the Institution of Mech Eng [H] 209, 255-231.

119. Tanner MG, Whiteside La, white Se, 1995: "*Effect of Polyethylene Quality on Wear in Total Knee Arthroplasty*". Clinical Orthopaedics and Related Research 317, 83-88.

120. Taylor SJG, Walker PS, 2001: "*Forces and Moments Telemetered from Two Distal Femoral Replacements during Various Activities*". Journal of Biomechanics 34, 839-848.

121. Taylor SJG, Walker PS, Perry JS, Cannon SR, Woledge R, 1998: "*The Forces in the Distal Femur and the Knee during Walking and other Activities Measured by Telemetry*". Journal of Arthroplasty 13, 428-437.

122. Thatcher JC, Zhou XM, Walker PS, 1987: "*Inherent Laxity in Total Knee Prosthesis*". Journal of Arthroplasty 2, 199-207.

123. Thompson MT, 2001: "*Design of a Cyclic Sliding, Dynamically Loaded Wear Testing Device for the Evaluation of Total Knee Replacement Materials*". Master's Thesis, Virginia Polytechnic Institute and State University, Blacksburg, Virginia.

124. Valstar ER, deJong FW, Vrooman HA, Rozing PM, Reiber JHC, 2001: "*Model Based Roentgen Stereophotogrammetry of Orthopaedic Implants*". Journal of Biomechanics 34, 715-722.

125. Walker PS, Blunn GW, Joshi A and Sathasivam S, 1993: "*Modulation of Delamination by Surface Wear in Total Knees*". Proceedings 39th Annual Meeting of Orthopaedic Research Society, San Francisco, California.

126. Walker PS, Blunn GW, Lilley PA, 1996: "*Wear Testing of Materials and Surfaces for Total Knee Replacements*". Journal of Biomedical Material Research 33, 159-175.

127. Walker PS, Blunn GW, Perry J, 2000a: "*Methodology for Long-Term Wear Testing of Total Knee Replacements*". Clinical Orthopaedics and Related Research 372, 290-301.

128. Walker PS, et.al., 1988: “Bearing Surface Design in Total Knee Arthroplasty”. Engineering Medicine, 149-154.

129. Walker PS, Sathasiviam S, 1999. “*The Design of Guide Surfaces for Fixed Bearing and Mobile Bearing Knee Replacements*”. Journal of Biomechanics 32(1), 27-34.

130. Walker SA, 2000b: “*Determination of TKA Contact Mechanics from In Vivo Kinematic Data*”. Master’s Thesis, Colorado School of Mines, Denver, Colorado.

131. Wang A, Essner A, Polineni VK, 1998: “*Lubrication and Wear of Ultra-High Molecular Weight Polyethylene in Total Joint Replacements*”. Tribology International 31, 17-33.

132. Wang A, Essner A, Stark C, Dumbleton JH, 1999: “*A Biaxial Line Contact Wear Machine for the Evaluation of Implant Bearing Materials for Total Joint Replacement*”. Wear 225-229 (2), 701-707.

133. Wasielewski RC, Galante JO, et.al., 1994: “*Wear Patterns on Retrieved Polyethylene Tibial Inserts and Their Relationship to Technical Considerations during Total Knee Arthroplasty*”. Clinical Orthopaedics and Related Research 299, 31-43.

134. Wasielewski RC, Parks N, Williams I, et.al, 1997: “*Tibial Insert Undersurface as a Contributing Source of Polyethylene Wear Debris*”. Clinical Orthopaedics 345, 53-59.

135. White SC, Yack HJ, Winter DA, 1989: “*A Three-Dimensional Musculoskeletal Model for Gait Analysis. Anatomical Variability Estimates*”. Journal of Biomechanics 22, 885-893.

136. White SE, Paxson RD, Tanner MG, Whiteside LA, 1996: “*Effects of Sterilization on Wear in Total Knee Arthroplasty*”. Clinical Orthopaedics and related Research 331, 164-171.

137. Williams IR, Mayor MB, Collier JP, 1998: “*The Impact of Sterilization Method on Wear in Knee Arthroplasty*”. Clinical Orthopaedics and Related Research 356, 170-180.

138. Wimmer MA, Andriacchi TP, 1997: "*Tractive Forces during Rolling Motion of the Knee Implications for Wear in Total Knee Replacement*". Journal of Biomechanics 30, 131-137.

139. Windsor RE, Scuderi GR, Moran MC, Insall JN, 1989: "*Mechanisms of Failure of the Femoral and Tibial Components in Total Knee Arthroplasty*". Clinical Orthopedics 248, 15-20.

140. Wright TM, Burstein AH, Bartel DL, 1985: "*Retrieval Analysis of Total Joint Replacement Components: A Six Year Experience*". AC Fraker and CD Griffin Corrosion and Degradation of Implant Materials: Second Symposium. American Society for Testing and Materials, Philadelphia ASTM STP 859, 415-428.

141. Wroblewski BM, Siney PD, Fleming PA, 1999: "*Low Friction Arthroplasty of the Hip using Alumina Ceramic and Crosslinked Polyethylene – a Ten Year Follow Up Report*". Journal of Bone and Joint Surgery 81-B, 54-55.

142. Wrona M, Mayor MB, Collier JP, Jensen RE, 1994: "*The Correlation between Fusion Defects and Damage in Tibial Polyethylene Bearings*". Clinical Orthopaedics and Related Research 299, 92-103.

143. Yamaguchi GT, 2001: "*Dynamic Modeling of the Musculoskeletal Motion: "A Vectorized Approach for Biomechanical Analysis in Three Dimensions*". Kluwer Academic Publishers, Norwell, MA, USA.

144. Yao JQ, Seedhom BB, 1991: "*A New Technique for Measuring Contact Areas in Human Joint – the '3S technique'*". Proceedings of the Institution of Mech. Engg. [H] 205: 69-72.

145. Zatsiorski V, Seluyanov V, 1983: "*The Mass and Inertial Characteristics of the Main Segments of the Human Body*". Biomechanics VIII-B. H. Matsui and K. Kobayashi. Human Kinetics, Champaign, IL, pp 1152-1159.

146. Zdero R, Fenton PV, Rudan J, Bryant JT, 2001: "*Fuji film and Ultrasound Measurement of Total Knee Arthroplasties Contact Areas*". Journal of Arthroplasty 16(3), 369-375.

APPENDIXES

Appendix A - Referencing Terminology

The following directions and planes are used in the medical field and also in the field to biomechanics to describe the locations on the human body:

- Superior or Cranial – direction towards the head or the upper part of the body (above).
- Inferior or Caudal – direction away from the head and towards the lower part of the body (below).
- Medial – direction towards the midline of the body (inner side).
- Lateral – direction away from the midline of the body (outer side).
- Anterior or Ventral – direction towards the front of the body (front).
- Posterior or Dorsal – direction towards the back of the body (back).
- Proximal –direction towards or nearest the trunk or the point of origin of a body part (closer).
- Distal – direction away or farthest from the trunk or the point of origin of a body part (farther).
- Superficial – direction towards the surface of the body (external).

- Profundum – direction away from the surface of the body (internal).
- Sagittal or Lateral – plane perpendicular to the ground in the antero-posterior direction dividing the body into right and left. A sagittal plane which divides the body into two equal halves is also known as the Medial Plane.
- Coronal or Frontal – plane perpendicular to the ground in the medio-lateral direction dividing the body into front and back.
- Transverse or Horizontal– plane parallel to the ground dividing the body into upper and lower.

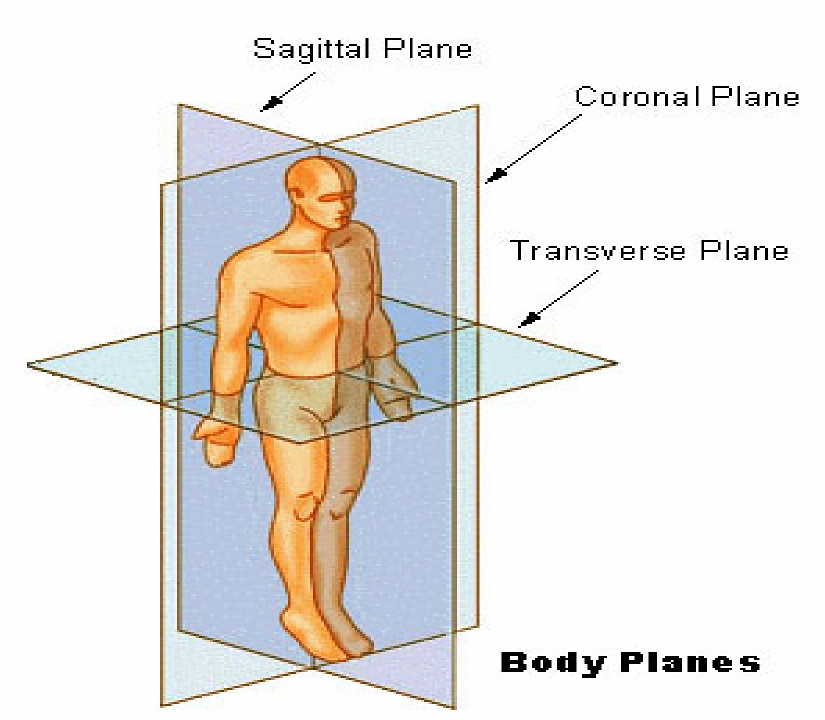

Figure A-1: The Anatomical Planes defined in the Human Body (SEER, 2005).

Appendix B – Kane’s Dynamics

Kane’s method combines the advantages of both Newton-Euler methods and the Lagrangian method (Huston, 1990). By using generalized forces, this method avoids the incorporation of non-contributing interactive and constraint forces between the bodies. Also this method avoids the use of energy functions. Finally, in this method differentiation needed to compute velocities and accelerations are obtained through the use of vector products.

The governing equation for Kane’s method is that the sum of the generalized active forces and the generalized reactive forces should be zero. The key component while conducting an analysis with the Kane’s method lies in development and the use of “partial velocities” and “partial angular velocities”.

Calculating the partial velocities:

Generalized coordinates, $\boldsymbol{q_r}$ – These are defined as time varying translations and rotations selected to define the position of all points and the orientation of rigid bodies.

$$q_r \qquad (r = 1, \dots\dots\dots, n)$$

Where $'n'$ is the number of degrees of freedom.

Generalized speeds, $\boldsymbol{u_r}$ – These are defined as time varying linear functions of $\dot{q}_r$'s (derivative with respect to time) selected so as to simplify expressions for velocities of points and angular velocities of rigid bodies.

$$u_r = \sum_{s=1}^{n} Y_{rs}\, \dot{q}_s + Z_r \qquad (r = 1, \dots\dots, n)$$

Where $'Y_{rs}'$ and $'Z_r'$ are functions of $'q_1, \dots\dots, q_n'$ and time $'t'$.

Partial angular velocities, $\boldsymbol{\omega_r}$, **and partial velocities**, $\boldsymbol{v_r}$ – These are time varying linear functions of u_r's, determined by inspection, which greatly facilitate the formulation of the equations of motion.

$$\omega = \sum_{r=1}^{n} \omega_r u_r + \omega_t$$
$$\nu = \sum_{r=1}^{n} \nu_r u_r + \nu_t$$

Where $'\omega'$ is the angular velocity of the rigid body, $'\nu'$ is the velocity of a point, and, $'\omega_r', '\nu_r', '\omega_t'$ and $'\nu_t'$ are the functions of $'q_1, ..., q_n'$ and $'t'$. In principle, partial angular velocities need only be formed for those rigid bodies subjected to applied torques and possessing inertia, while partial velocities need only be forces for those points subjected to applied forces or possessing mass.

Using the partial velocities:

Generalized active forces, $\boldsymbol{F_r}$ – These are the quantities formed by taking the dot products of partial velocities and active (i.e. applied) forces and dot products of partial angular velocities and active torques. For each point $'P_i'$ subjected to an applied force,

$$(F_r)_{P_i} = \nu_r^{P_i} \bullet R_{P_i} \qquad (r = 1, ..., n)$$

Where $'v_r^{P_i}'$ is the r^{th} partial velocity of $'P_i'$ and $'R_{P_i}'$ is the resultant of all contact and distance forces acting on $'P_i'$. Similarly, for each rigid body $'B_j'$ subjected to an applied torque,

$$(F_r)_{B_j} = \omega_r^{B_j} \bullet T_{B_j} \qquad (r = 1, \ldots\ldots\ldots, n)$$

Where $'\omega_r^{B_j}'$ is the r^{th} partial velocity of $'B_j'$ and $'\mathrm{T}_{B_j}'$ is the resultant of all couples acting on $'B_j'$. The r^{th} generalized active force $'F_r'$ can then be determined by summing the results over all points $'P_i'$ and all rigid bodies $'B_j'$:

$$F_r = \sum_{i=1}^{\kappa} (F_r)_{P_i} + \sum_{j=1}^{\lambda} (F_r)_{B_j} \qquad (r = 1, \ldots\ldots\ldots, n)$$

Where $'\kappa'$ is the number of points subjected to applied forces and $'\lambda'$ is the number of rigid bodies subjected to applied torques.

Generalized inertia forces, $\boldsymbol{F_r^*}$ - These are the quantities formed by taking the dot products of partial velocities and inertia forces and dot products of partial angular velocities and inertia torques. For each point $'P_i'$ possessing mass,

$$(F_r^*)_{P_i} = v_r^{P_i} \bullet R_{P_i}^* \qquad (r = 1, \ldots\ldots., n)$$

Where '$v_r^{P_i}$' is the r^{th} partial velocity of 'P_i' and '$R_{P_i}^*$' is the inertia force for 'P_i' and is defined as

$$R_{P_i}^* = -m_{P_i} a^{P_i}$$

Where 'm_{P_i}' is the mass of 'P_i' and 'a^{P_i}' is the acceleration of 'P_i'.Similarly, for each rigid body 'B_j' possessing inertia,

$$(F_r^*)_{B_j} = \omega_r^{B_j} \bullet T_{B_j}^* \qquad (r = 1, \ldots\ldots.., n)$$

Where '$\omega_r^{B_j}$' is the r^{th} partial velocity of 'B_j' and '$\mathrm{T}_{B_j}^*$' is the inertia torque for 'B_j' and is defined as

$$T_{B_j}^* = -\alpha^{B_j} \bullet I^{B_j/B_j*} - \omega^{B_j} \times I^{B_j/B_j*} \bullet \omega^{B_j}$$

Where $'I^{B_j/B_j*}'$ is the inertia dyadic of $'B_j'$ about its mass centre $'B_j^*'$, $'\omega^{B_j}'$ is the angular velocity of $'B_j'$ and $'\alpha^{B_j}'$ is the angular acceleration of $'B_j'$.

The r^{th} generalized active force $'F_r^*'$ can then be determined by summing the results over all points $'P_i'$ and all rigid bodies $'B_j'$:

$$F_r^* = \sum_{i=1}^{\mu}(F_r^*)_{P_i} + \sum_{j=1}^{\eta}(F_r^*)_{B_j} \qquad (r = 1, \ldots\ldots\ldots, n)$$

Where $'\mu'$ is the number of points possessing mass and $'\eta'$ is the number of rigid bodies possessing inertia.

Equations of motion:

The equations of motion can be generated by adding all the generalized active forces and the generalized reactive forces and then equating the results to zero.

$$F_r + F_r^* = 0 \qquad (r = 1, \ldots\ldots\ldots, n)$$

In this method statics problems can be solved by considering $F_r = 0$.

Appendix C – Contact Forces in the Patients

For the mobile bearing TKA, patient 1 and patient 2 refer to the same person. This is the person who had received bilateral implants.

For the fixed bearing TKA patient 4 and patient 5 is the same person having bilateral implants.

Mobile Bearing TKA:

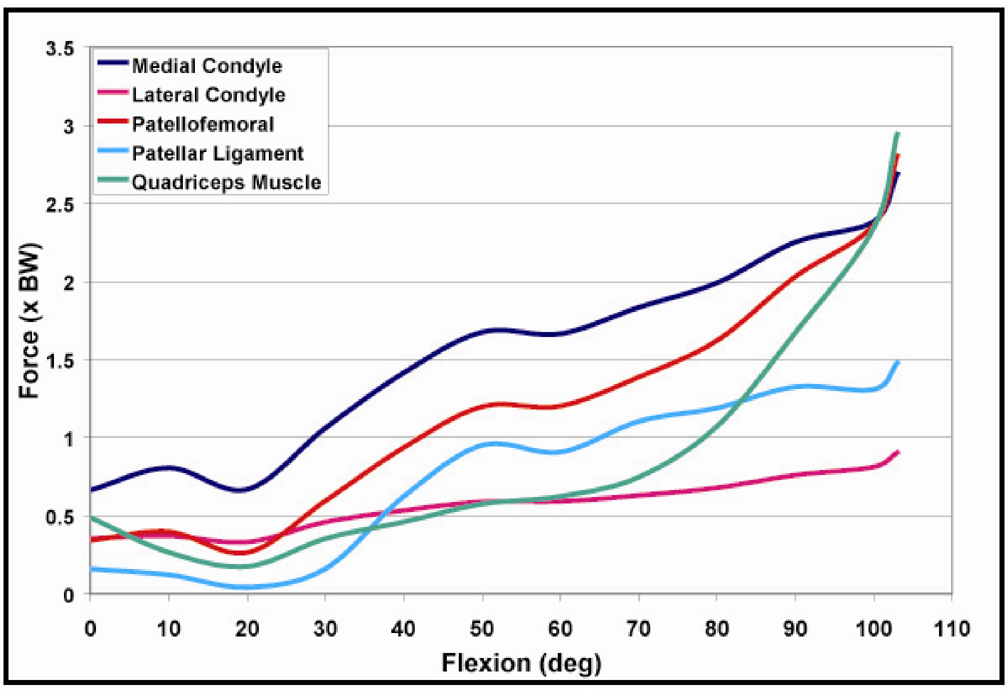

Figure C-1: Contact Forces in Patient 1 with a Mobile Bearing TKA

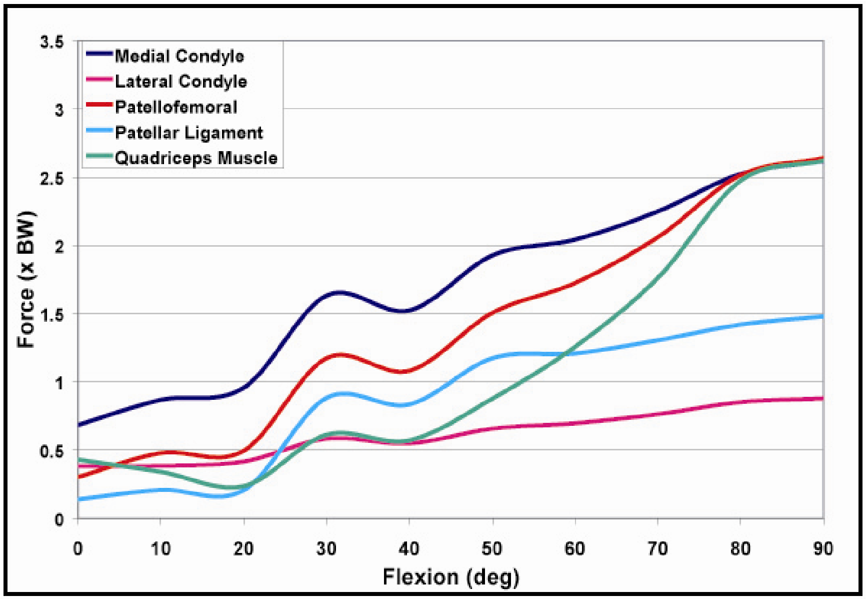

Figure C-2: Contact Forces in Patient 2 with a Mobile Bearing TKA

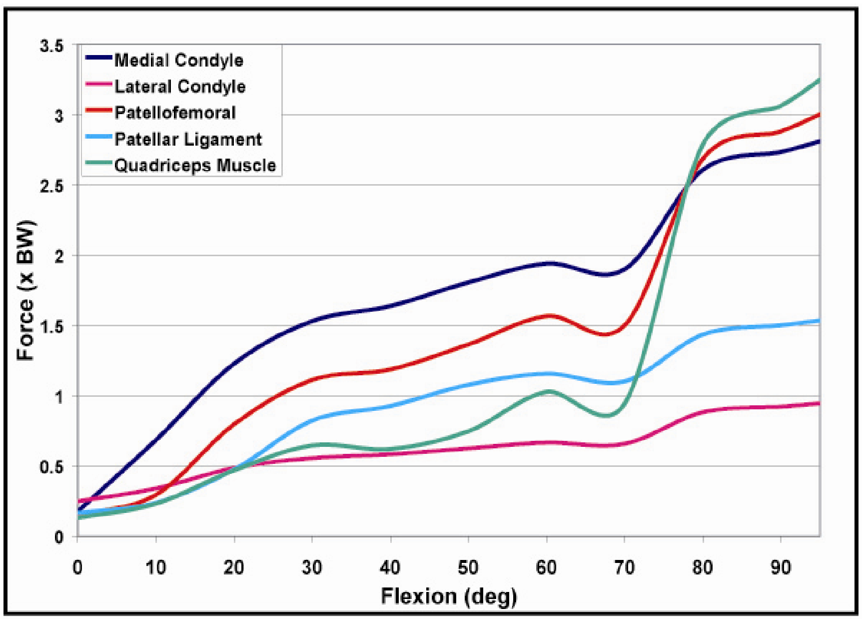

Figure C-3: Contact Forces in Patient 3 with a Mobile Bearing TKA

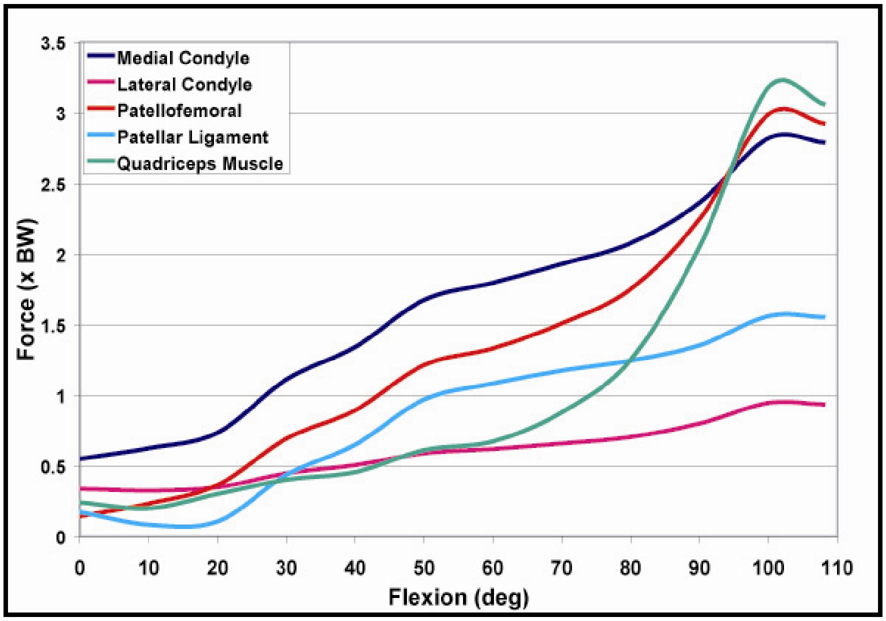

Figure C-4: Contact Forces in Patient 4 with a Mobile Bearing TKA

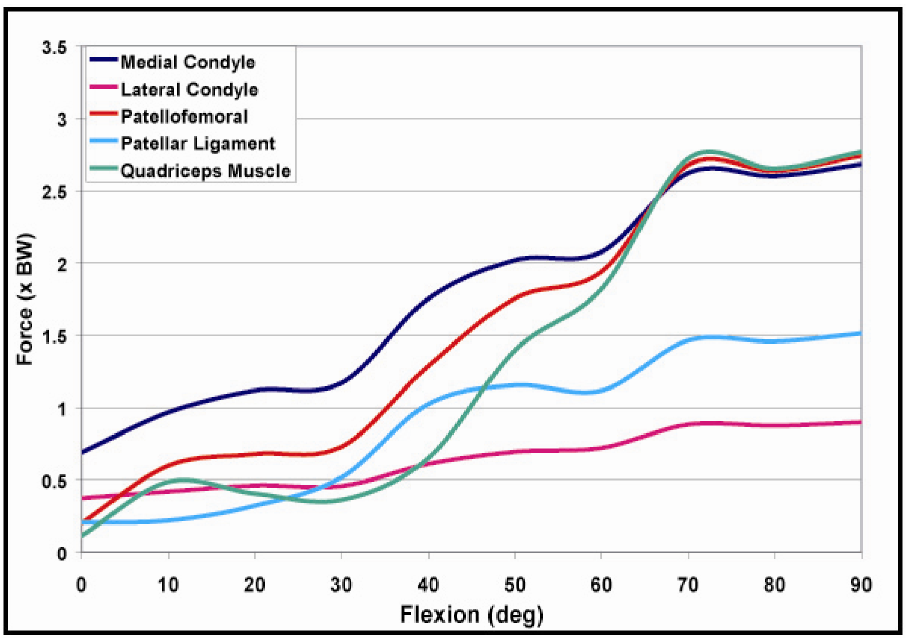

Figure C-5: Contact Forces in Patient 5 with a Mobile Bearing TKA

Fixed Bearing TKA:

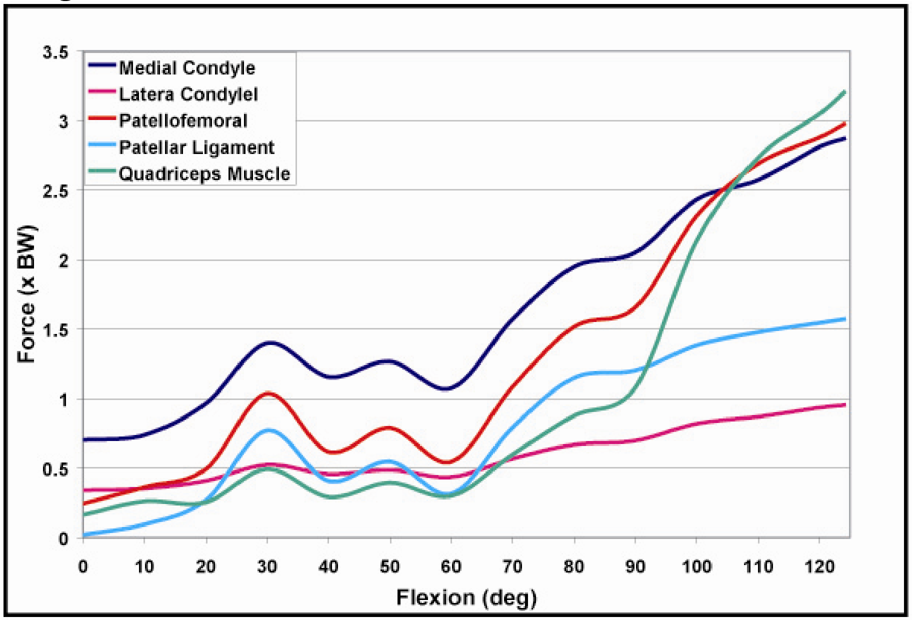

Figure C-6: Contact Forces in Patient 1 with a Fixed Bearing TKA

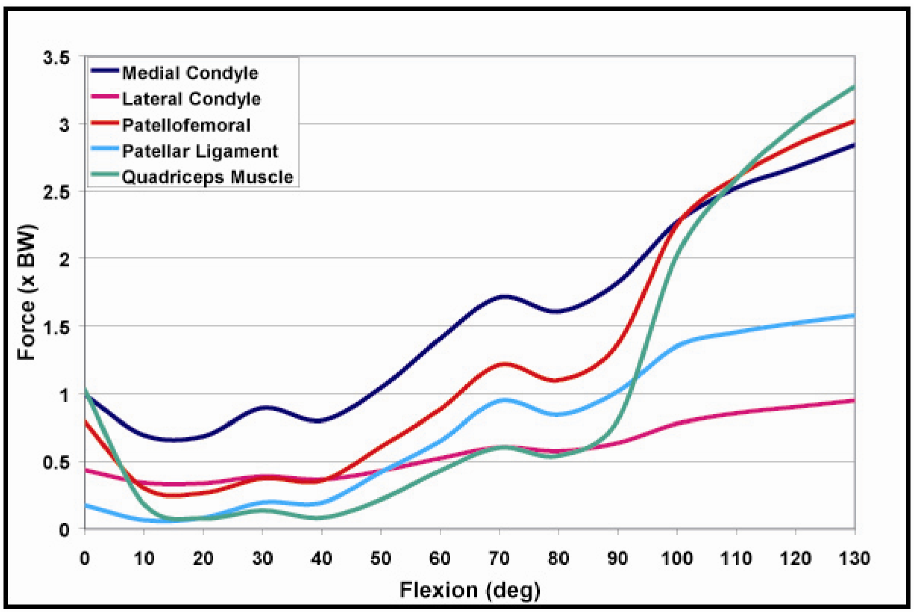

Figure C-7: Contact Forces in Patient 2 with a Fixed Bearing TKA

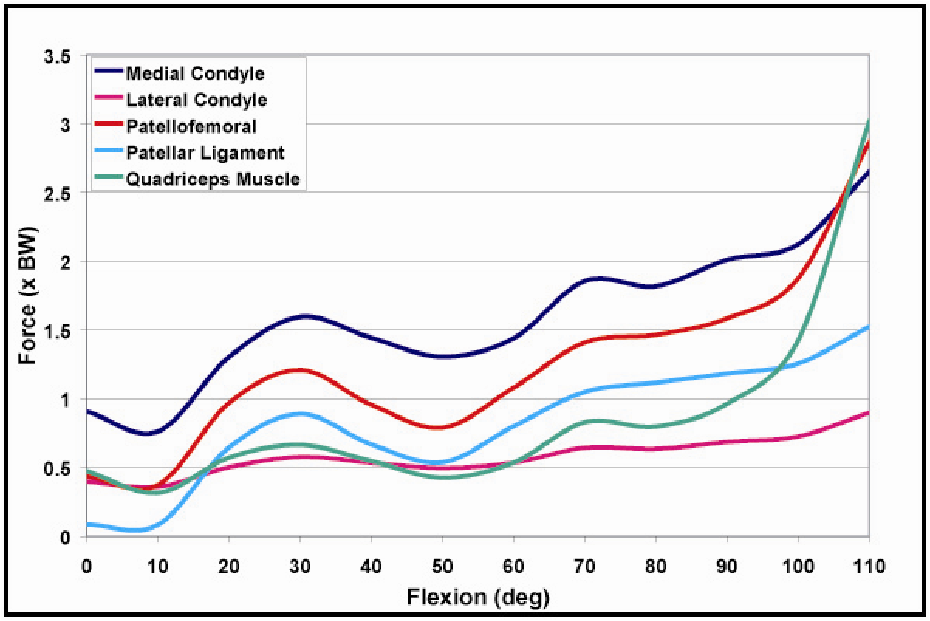

Figure C-8: Contact Forces in Patient 3 with a Fixed Bearing TKA

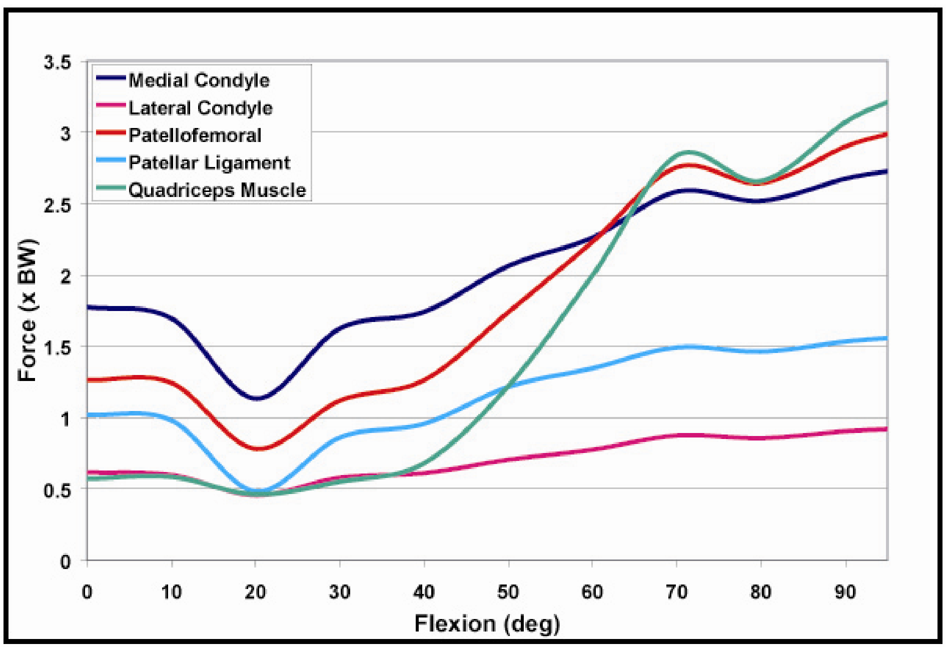

Figure C-9: Contact Forces in Patient 4 with a Fixed Bearing TKA

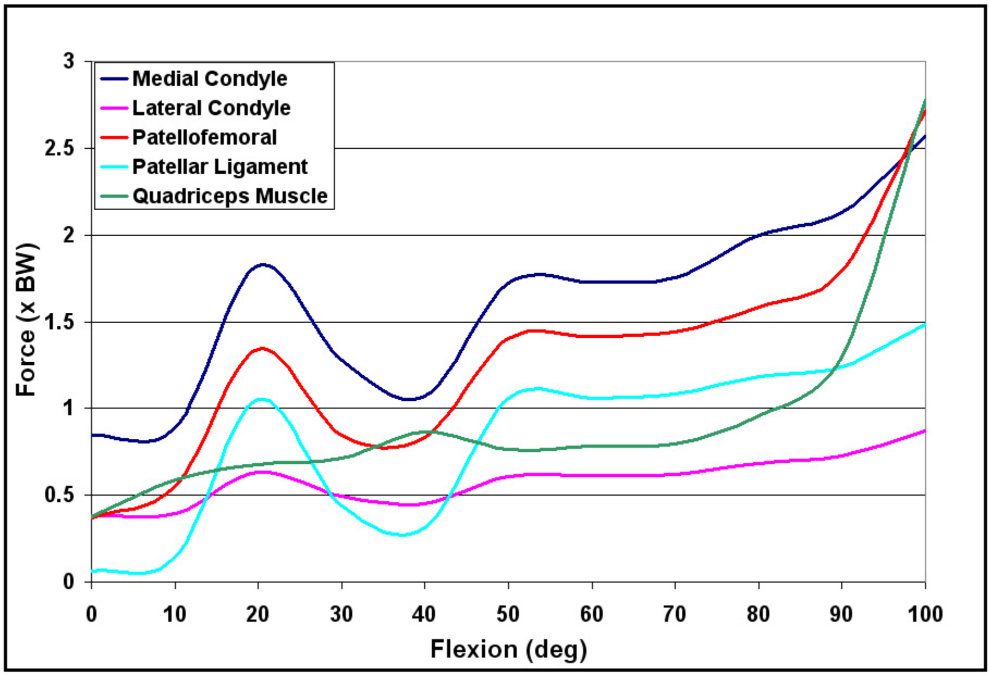

Figure C-10: Contact Forces in Patient 5 with a Fixed Bearing TKA

Appendix D – Contact Areas in the Patients

For the mobile bearing TKA, patient 1 and patient 2 refer to the same person. This is the person who had received bilateral implants.

For the fixed bearing TKA patient 4 and patient 5 is the same person having bilateral implants.

Mobile Bearing TKA:

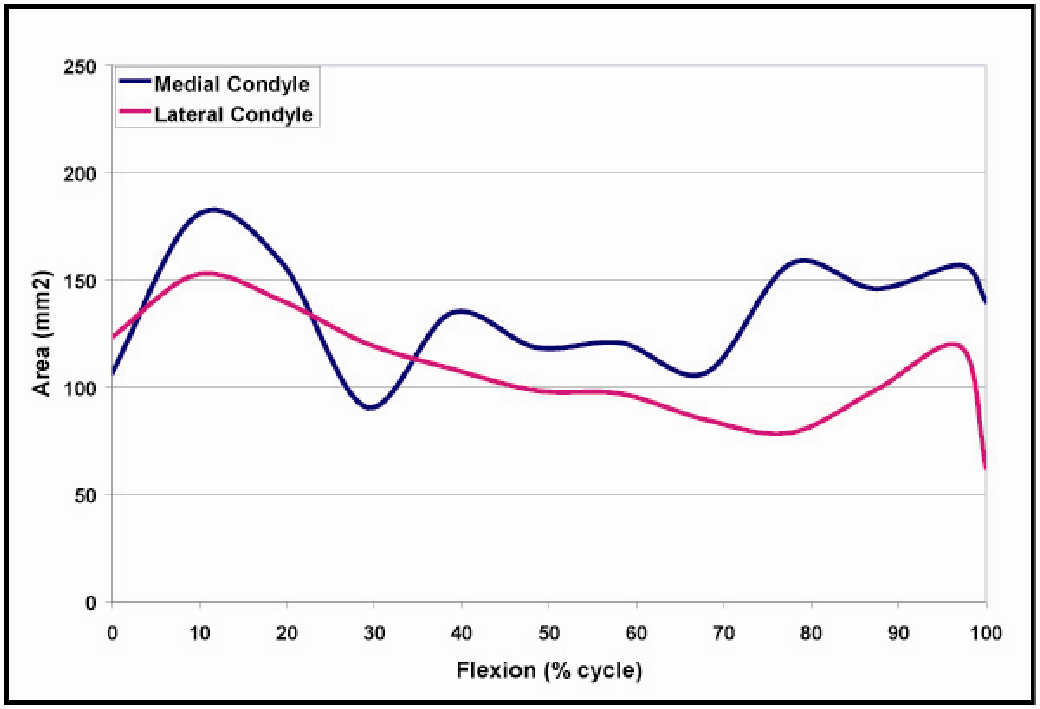

Figure D-1: Contact Areas in Patient 1 with a Mobile Bearing TKA

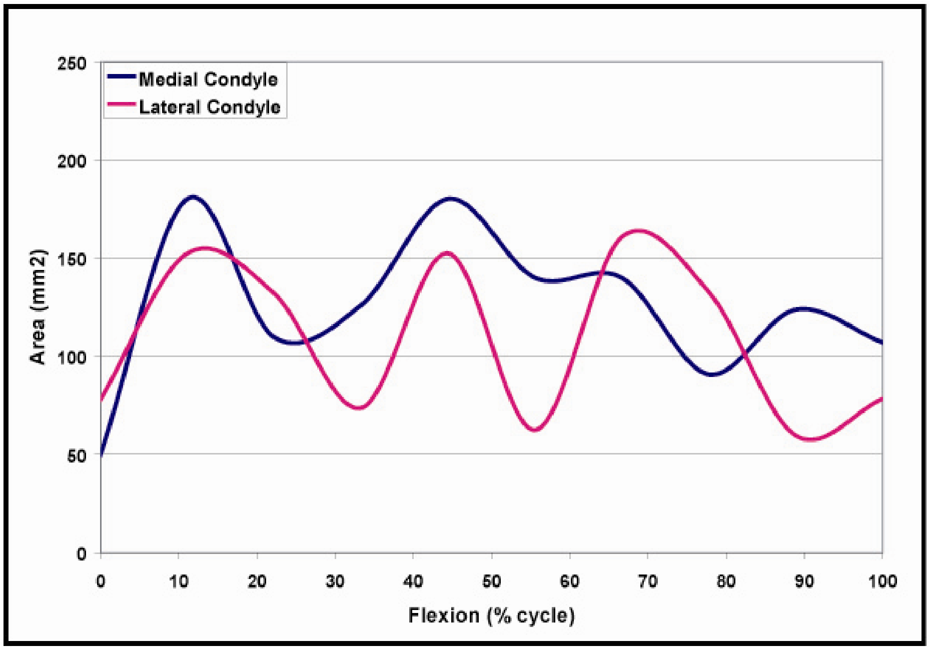

Figure D-2: Contact Areas in Patient 2 with a Mobile Bearing TKA

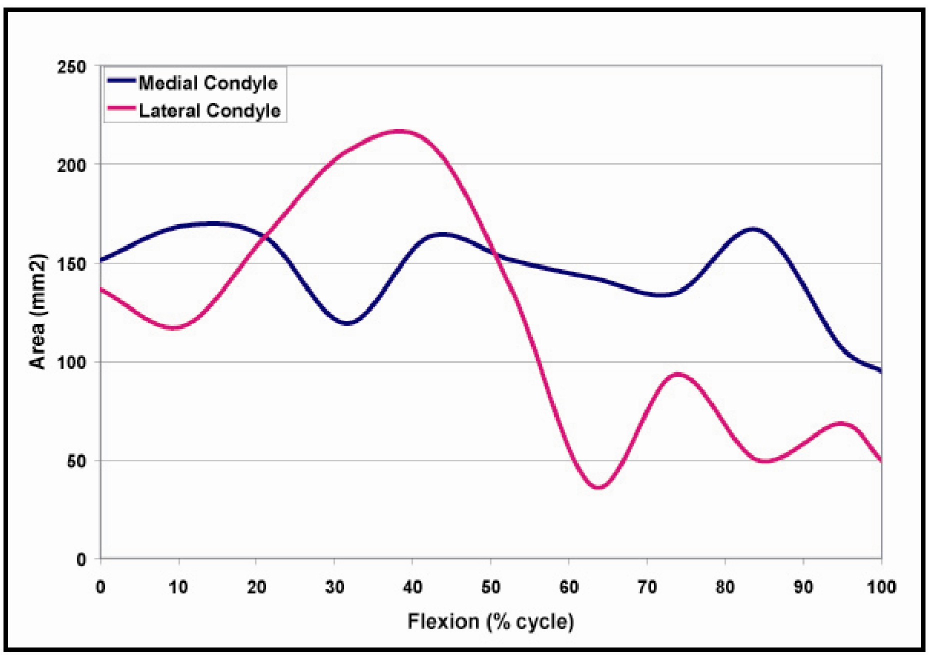

Figure D-3: Contact Areas in Patient 3 with a Mobile Bearing TKA

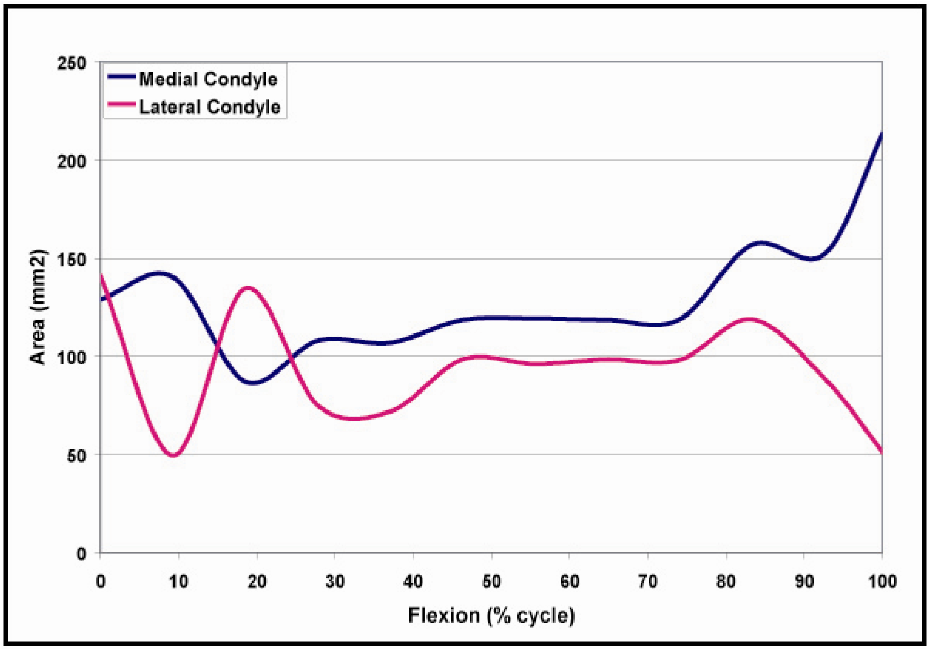

Figure D-4: Contact Areas in Patient 4 with a Mobile Bearing TKA

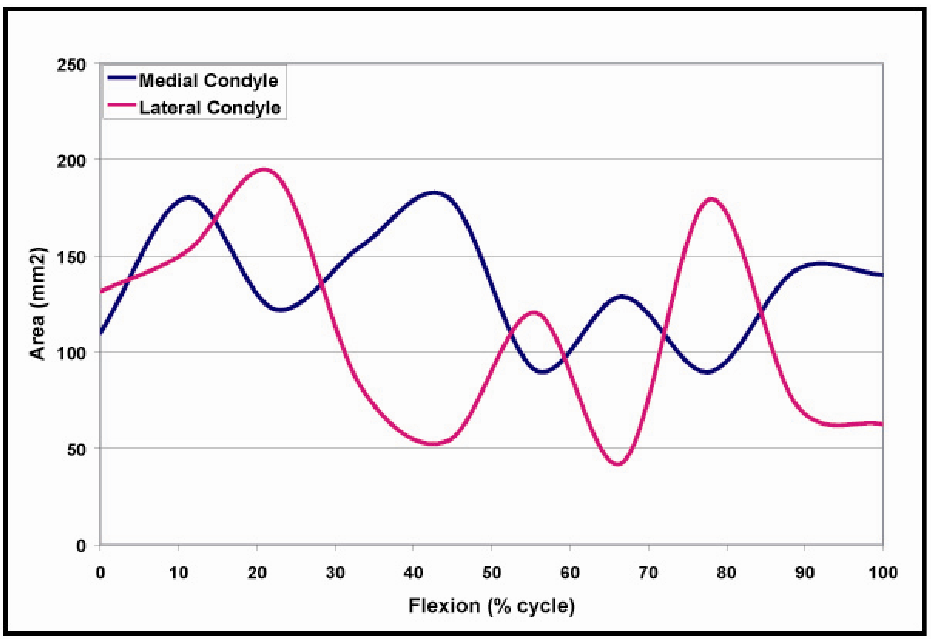

Figure D-5: Contact Areas in Patient 5 with a Mobile Bearing TKA

Fixed Bearing TKA:

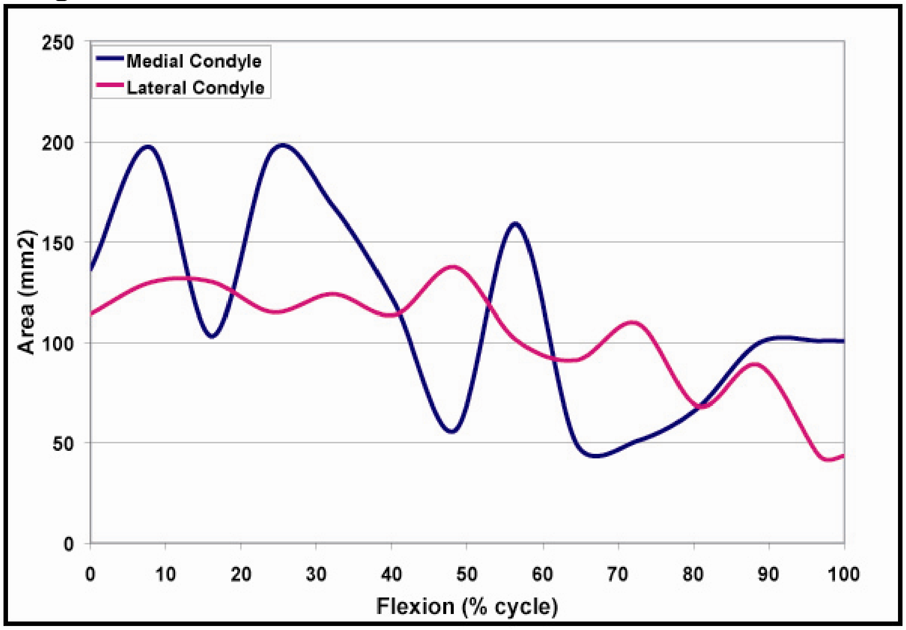

Figure D-6: Contact Areas in Patient 1 with a Fixed Bearing TKA

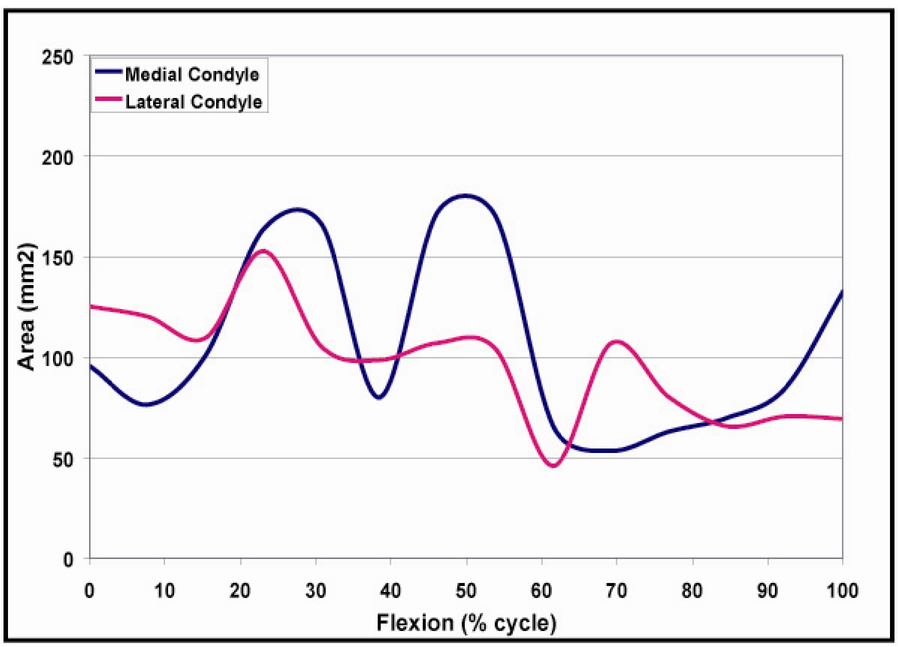

Figure D-7: Contact Areas in Patient 2 with a Fixed Bearing TKA

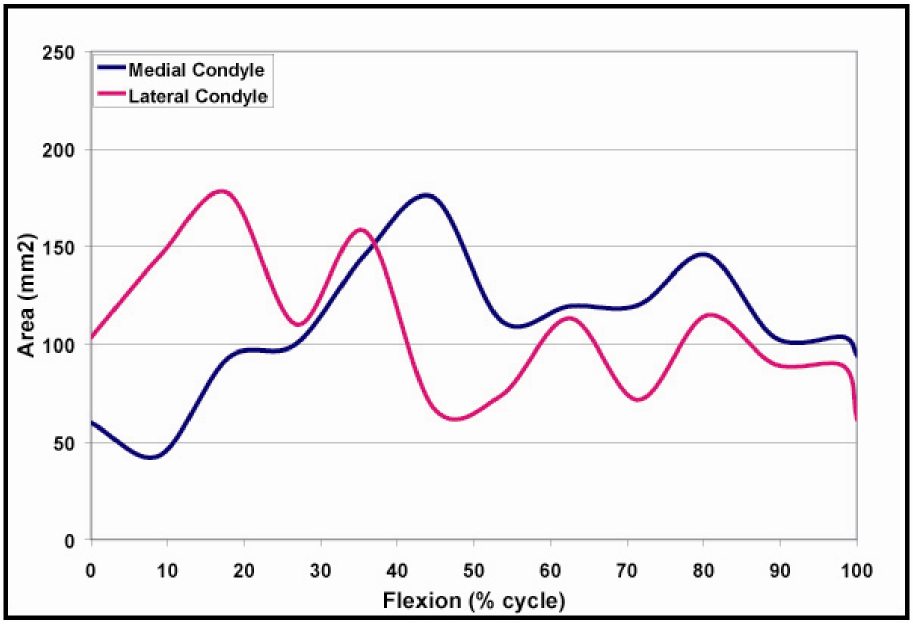

Figure D-8: Contact Areas in Patient 3 with a Fixed Bearing TKA

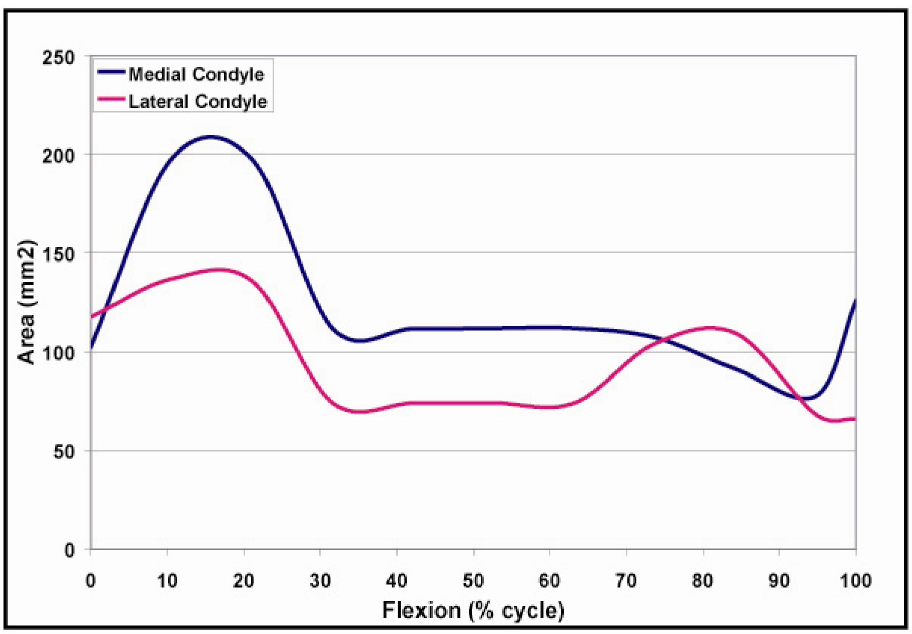

Figure D-9: Contact Areas in Patient 4 with a Fixed Bearing TKA

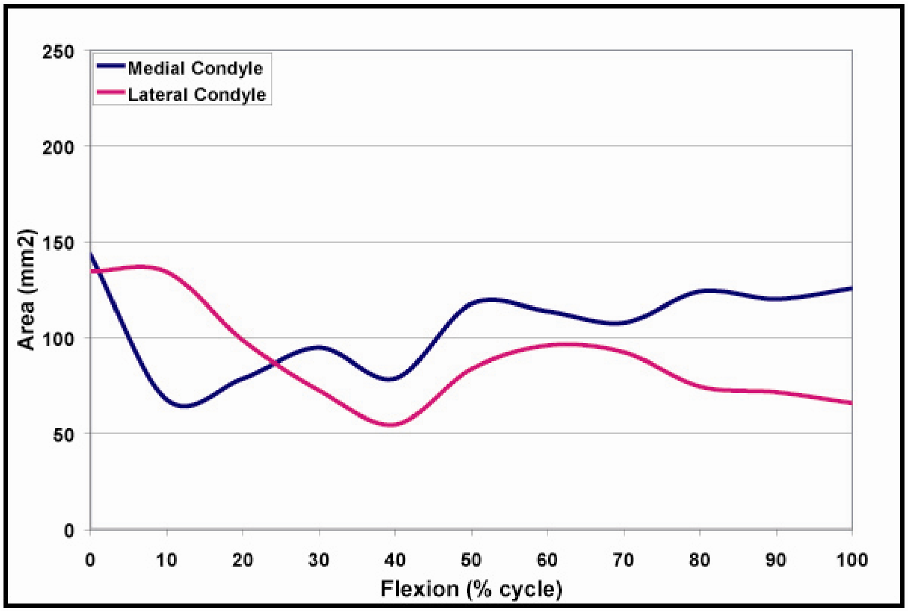

Figure D-10: Contact Areas in Patient 5 with a Fixed Bearing TKA

Appendix E – Contact Pressures in the Patients

For the mobile bearing TKA, patient 1 and patient 2 refer to the same person. This is the person who had received bilateral implants.

For the fixed bearing TKA patient 4 and patient 5 is the same person having bilateral implants.

Mobile Bearing TKA:

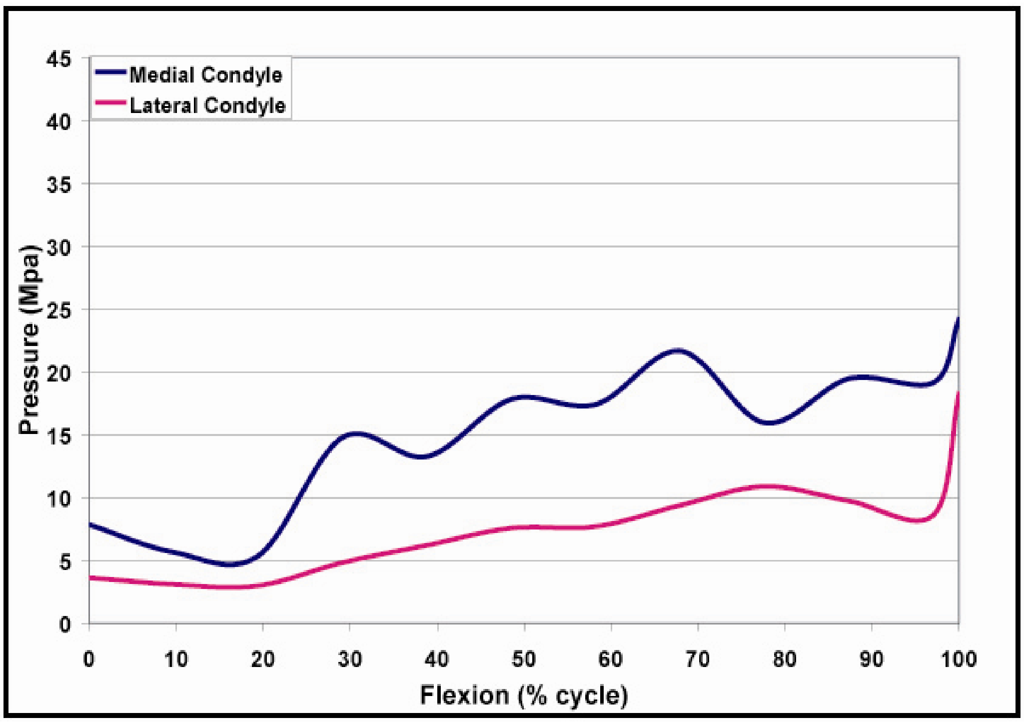

Figure E-1: Contact Pressures in Patient 1 with a Mobile Bearing TKA

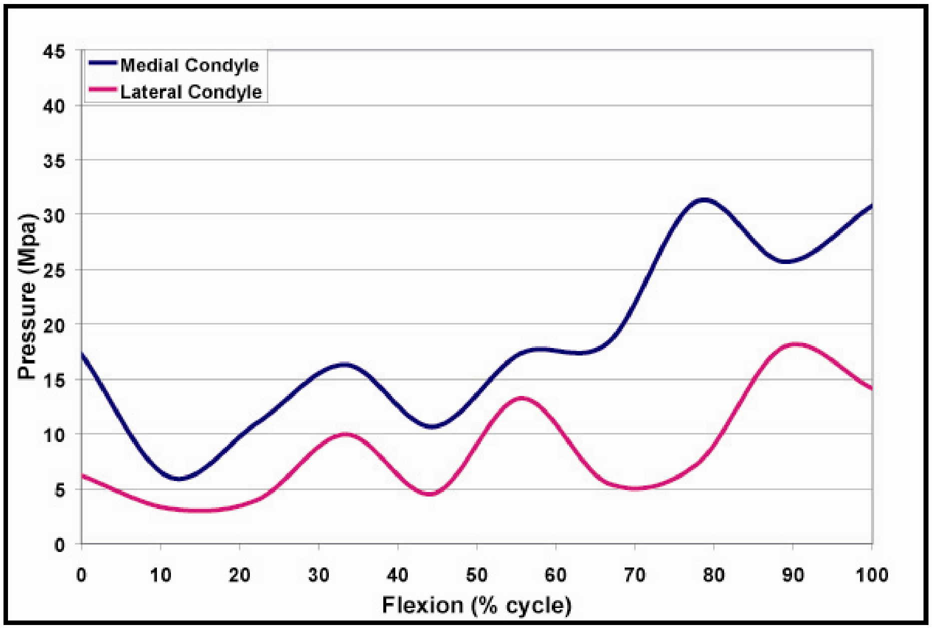

Figure E-2: Contact Pressures in Patient 2 with a Mobile Bearing TKA

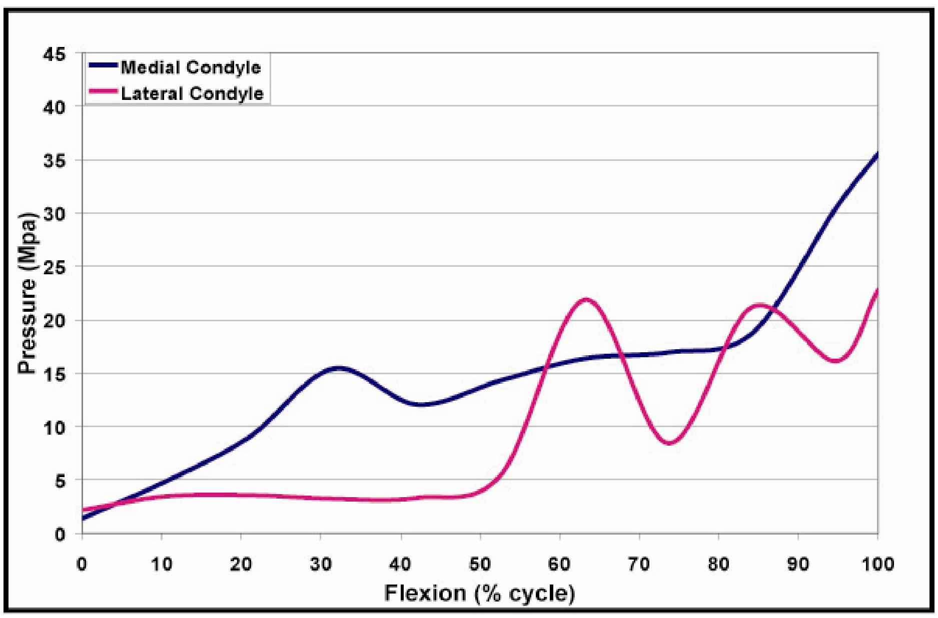

Figure E-3: Contact Pressures in Patient 3 with a Mobile Bearing TKA

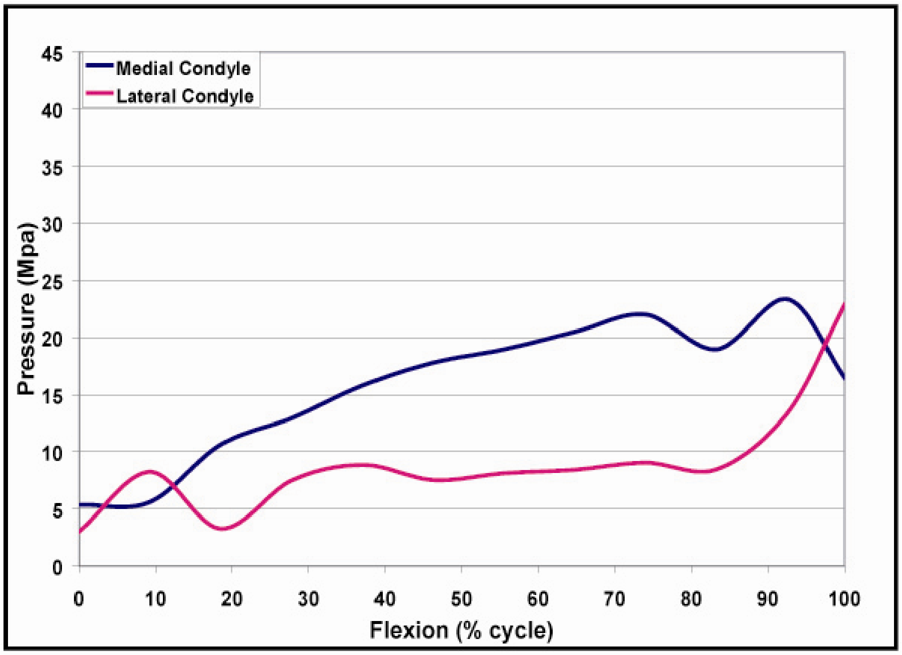

Figure E-4: Contact Pressures in Patient 4 with a Mobile Bearing TKA

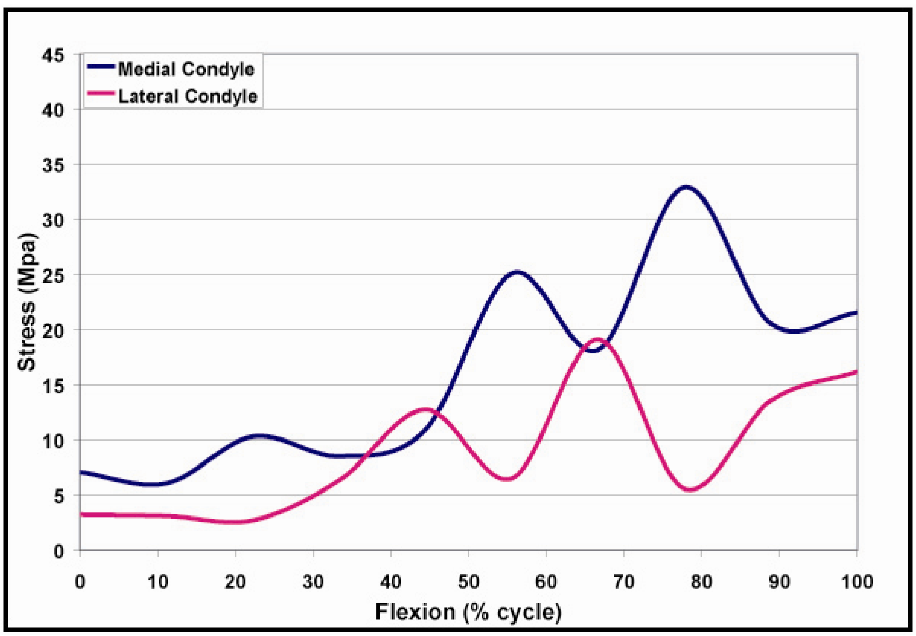

Figure E-5: Contact Pressures in Patient 5 with a Mobile Bearing TKA

Fixed Bearing TKA:

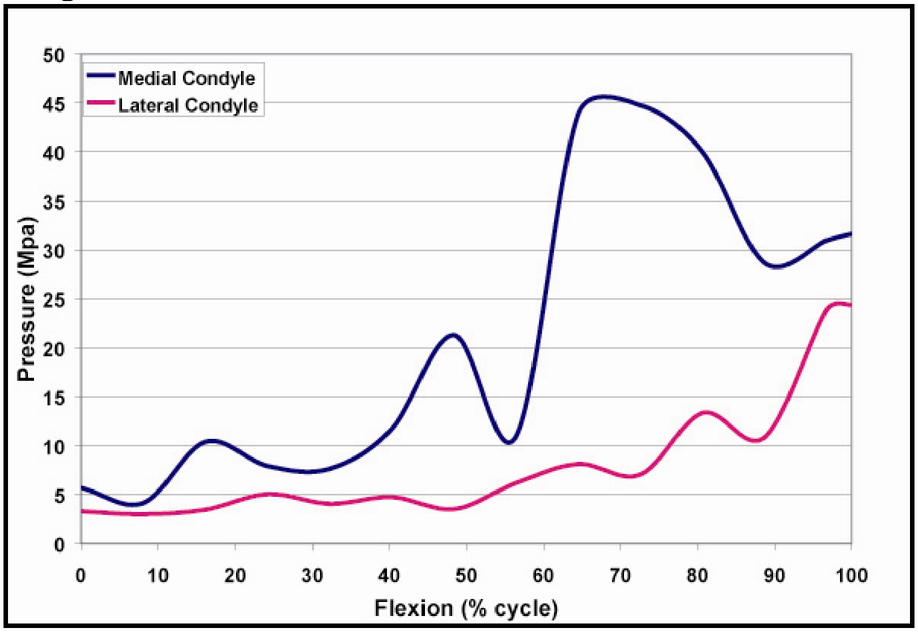

Figure E-6: Contact Pressures in Patient 1 with a Fixed Bearing TKA

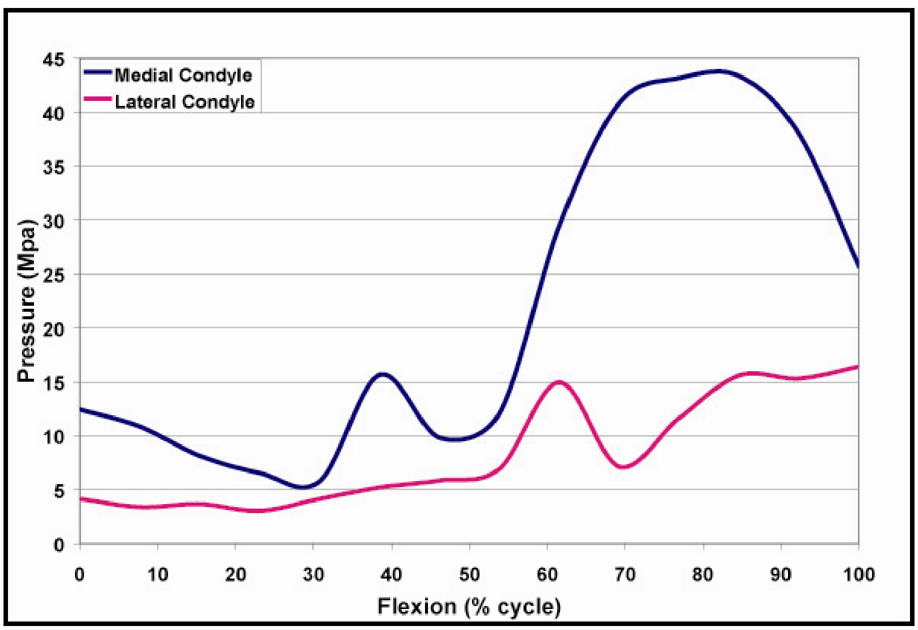

Figure E-7: Contact Pressures in Patient 2 with a Fixed Bearing TKA

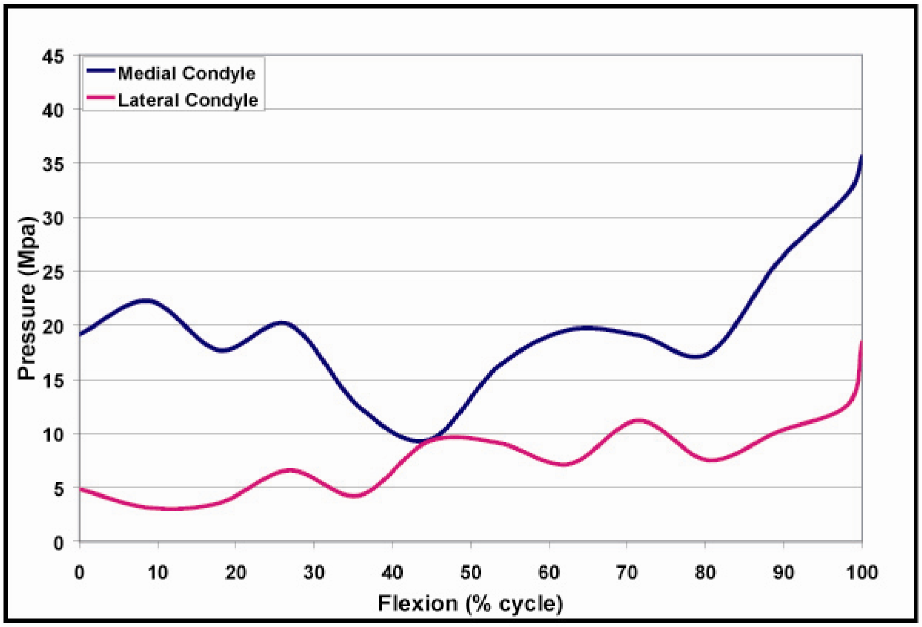

Figure E-8: Contact Pressures in Patient 3 with a Fixed Bearing TKA

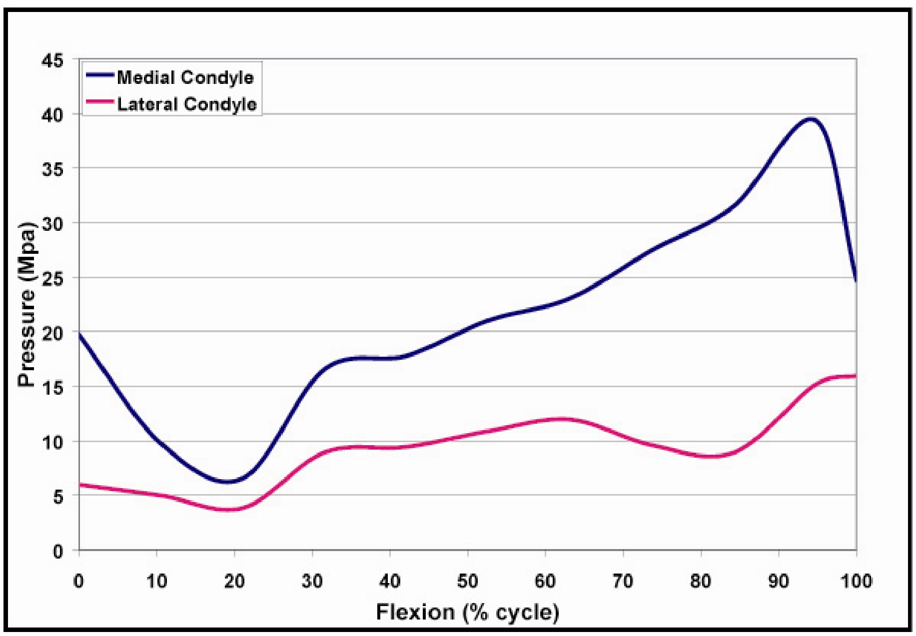

Figure E-9: Contact Pressures in Patient 4 with a Fixed Bearing TKA

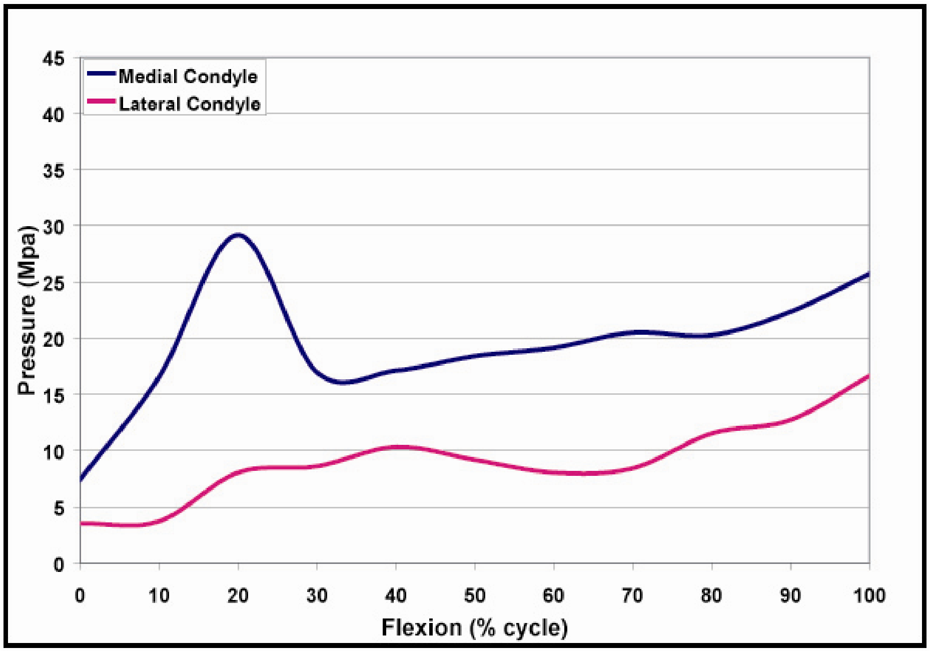

Figure E-10: Contact Pressures in Patient 5 with a Fixed Bearing TKA

Vita

Adrija Sharma was born in Calcutta, India on the 7th of June 1977. His wanderlust, his interest in interacting with different people and cultures, and his love for the sea always motivated him to become a marine engineer. He pursued Bachelors of Mechanical Engineering, from Jadavpur University, Calcutta, India. During this time he was also the recipient of the coveted National Talent Search Scholarships. Not surprisingly enough, he joined the merchant navy after graduation. He worked for three years. However, influenced by the suffering of his beloved grandmothers due to arthritis, and with a vision to improve the quality of life of millions of people worldwide suffering from this disease, he started his post graduate studies in biomechanics in the Fall of 2003. After his Masters he intends to work on his PhD from the same university.